Synthesis of Ag/ZnO/Bentonite Nanocomposite Using *Hagenia Abyssinica* Plant Leaf Extract for Antibacterial Studies

Adisu Girma Zewudie

A Thesis Submitted to

The department of Chemistry

School of Applied Natural Science

Presented in Partial Fulfillment of the Requirement for the Degree of Master's of Science in Applied Chemistry (In Inorganic Chemistry)

Office of Graduate Studies

Adama Science and Technology University

September, 2022

Adama, Ethiopia

Synthesis of Ag/ZnO/Bentonite Nanocomposite Using *Hagenia Abyssinica* Plant Leaf Extract for Antibacterial Studies

Adisu Girma Zewudie

Advisor: Eneyew Amare (PhD)

Co-advisor: Teshome Abdo (PhD)

A Thesis Submitted to

The department of Chemistry

School of Applied Natural Science

Presented in Partial Fulfillment of the Requirement for the Degree of Master's of Science in Applied Chemistry (In Inorganic Chemistry)

Office of Graduate Studies

Adama Science and Technology University

September, 2022

Adama, Ethiopia

Declaration

I hereby declare that this Master Thesis entitled "Synthesis of Ag/ZnO/Bentonite Nanocomposite Using *Hagenia Abyssinica* Plant Leaf Extract for Antibacterial Studies" is my original work. That is, it has not been submitted for the award of any academic degree, diploma or certificate in any other university. All sources of materials that are used for this thesis have been duly acknowledged through citation

_____	_____	_____
Name of the student	Signature	Date

Recommendation

We, the advisor(s) of this thesis, hereby certify that we have read the revised version of the thesis entitled "Synthesis of Ag/ZnO/Bentonite Nanocomposite Using *Hagenia Abyssinica* Plant Leaf Extract for Antibacterial Studies" prepared under our guidance by Adisu Girma submitted in partial fulfillment of the requirements for the degree of Mater's of Science in chemistry (In Inorganic chemistry). Therefore, we recommend the submission of revised version of the thesis to the department following the applicable procedures.

_____	_____	_____
Major Advisor	Signature	Date
_____	_____	_____
Co-advisor	Signature	Date

Approval Page

We, the advisors of the thesis entitled "Synthesis of Ag/ZnO/Bentonite Nanocomposite Using *Hagenia Abyssinica* Plant Leaf Extract for Antibacterial Studies" and developed by Adisu Girma; hereby certify that the recommendation and suggestions made by the board of examiners are appropriately incorporated into the final version of the thesis.

Major Advisor	Signature	Date
Co-advisor	Signature	Date

We, the undersigned, members of the Board of Examiners of the thesis by Adisu Girma have read and evaluated the thesis entitled "Synthesis of Ag/ZnO/Bentonite Nanocomposite Using *Hagenia Abyssinica* Plant Leaf Extract for Antibacterial Studies" and examined the candidate during open defense. This is, therefore, to certify that the thesis is accepted for partial fulfillment of the requirement of the degree of Master of Science in Inorganic Chemistry.

Chairperson	Signature	Date
Internal Examiner	Signature	Date
External Examiner	Signature	Date

Final approval and acceptance of the thesis is contingent upon submission of its final copy to the Office of Postgraduate Studies (OPGS) through the Department Graduate Council (DGC) and School Graduate Committee (SGC).

Department Head	Signature	Date
School Dean	Signature	Date
Office of Postgraduate Studies, Dean	Signature	Date

ACKNOWLEDGEMENT

My profound gratitude goes to God Almighty, for the strength, wisdom, provisions, and guidance for the success of this thesis work. To Him alone, I ascribe all the glory.

I sincerely acknowledge my hard-working advisor: Dr. Eneyew Amare for his constructive support, expert advice, technical assistance, and patience throughout my study period. I appreciate his tremendous encouragement, understanding, and arranging of research facilities. Sir, I appreciate the time you devoted to this work; and your experience. It is a great privilege and honor for me to be advised by him. Moreover, my heartfelt appreciation goes to my Co-Advisor Dr. Teshome Abdo for his constructive feedback and suggestions that have been extremely valuable.

Last but most importantly, I would like to extend my most profound gratitude to all my family members for their sincere love, help, and encouragement during the entire study period.

Finally, I would like to express my sincere gratitude to; Adama Science and Technology University for budget support, providing the necessary knowledge, assistance and facilities to conduct my research work and Adama Public Health Research and Referral Laboratory Center for assistance and facilities to conduct my research work in their lab.

TABLES OF CONTENTS

Contents **Page**

LIST OF TABLES

LIST OF FIGURES

LIST OF ABBREVIATION

Ag NPs.....	Silver nanoparticles
APHRRLC.....	Adama Public Health Research and Referral Laboratory Center
ATCC.....	American Type Culture Collection
CEC ……..	Cation exchange capacity
CFU.....	Colony forming unit
DMSO.....	Dimethyl sulfoxide
DNA.....	Deoxyribonucleic acid
EDX……	Energy Dispersive Spectrometry
FT-IR……...	Fourier Transmission Infra-red
H. abyssinica ……..	*Hagenia abyssinica*
HRTEM.....	High Resolution Transmission electron microscopy
FWHM.....	Full width half maximum
JPCDS.....	The Joint Committee on Powder Diffraction Standards
MIC……	Minimum Inhibitory Concentration
MBC……	Minimum Bactericidal Concentration
MMT.....	Montmorillonite
Na-AB……..…	Sodium Activated Bentonite
NCs……..	Nanocomposites
NPs…….	Nanoparticles
PB……	Purified bentonite
RNA.....	Ribonucleic acid
ROS.....	Reactive oxygen species
SAED…….....	Selected Area Electron Diffraction
TEM……	Transmission electron microscopy
UV-Vis-DRS …….	X-Ray Diffraction
XRD……	UV-Visible-Diffuse reflectance spectroscopy

ABSTRACT

In 2017, the World Health Organization (WHO) estimated that by 2050, multibacterial infections, which are caused by two or more bacterial species, will cause more deaths than cancer due to the antimicrobial resistance. This implies the need to identify and assess new antibacterial agents. The aim of this study was to synthesize environmentally friendly Ag/ZnO/Bentonite NCs for antibacterial studies by a green method. The Ag/ZnO/Bentonite NC was synthesized successfully using H. abyssinica plant leaf extract as reducing and capping agents. Ag NPs, ZnO NPs, Ag/Bentonite NCs, ZnO/Bentonite NCs were also synthesized to compare their antibacterial activity with that of Ag/ZnO/Bentonite NCs. The synthesized materials were characterized by UV-Vis-DRS, XRD, FTIR, HR-TEM, and SEM. UV-Vis-DRS results confirmed the formation of NPs and NCs with the optical band gap (Eg) of Ag NPs, ZnO NPs, Ag/Bentonite NCs, ZnO/Bentonite NCs, and Ag/ZnO/Bentonite NCs 2.5, 3.07, 2.9, 3.2, and 3.3 eV respectively. The XRD pattern of Ag and ZnO showed peaks of Ag and ZnO NPs, confirming the formation of the silver (fcc) and hexagonal phase (wurtzite structure) ZnO. The XRD patterns of the binary and ternary nanocomposites also confirmed the formation of Ag/Bentonite, ZnO/Bentonite and Ag/ZnO/Bentonite NCs. The average crystalline sizes (D) of Ag NPs and ZnO NPs were estimated at about 7.4 nm and 9.4 nm respectively, from the XRD pattern of Ag/ZnO/Bentonite NCs. FTIR spectra confirmed the presence of hydroxyl, carbonyl, alkyl, amide, and other functional groups on the surface of NPs and NCs. TEM analysis revealed the formation of Ag and ZnO NPs, with an average particle size of 10.8 nm and 18.5 nm respectively, which agreed with XRD results analysis. The antibacterial activities of the composites were evaluated against Gram-negative E. coli ATCC 25922 and Gram-positive S. aureus ATCC 25923 by the disk diffusion and broth dilution methods. Better antibacterial activity with maximum values of 14.3 $\pm$ 0.3 and 17 mm at 10 mg/mL dosage toward E. coli and S. aureus respectively for the ternary (Ag/ZnO/Bentonite) NCs was observed. The MIC and MBC observed for Ag/ZnO/Bentonite NCs were 156.25 μgmL^{-1}, and 312.5 μgmL^{-1} for E. coli and 78.125 μgmL^{-1}, 156.25 for S. aureus, respectively. The results revealed that the Ag/ZnO/Bentonite composite is a promising bactericide that can be used as an antibacterial agent.

Key words: *Antibacterial activity, Bentonite, Disk diffusion, Green synthesis, Nanoparticles, Nanocomposite.*

CHAPTER ONE
INTRODUCTION

1.1.Background of the study

The number of Multidrug-resistant (MDR) pathogenic bacteria has substantially increased currently. This intimidating trend implies the need to identify and assess new antibacterial agents. Multidrug-resistant (MDR) bacteria are defined as bacteria that are resistant to at least one antimicrobial agent from three or more antimicrobial classes by in vitro susceptibility testing (Farzana et al., 2013). Beginning with Alexander Fleming's discovery of penicillin in 1928 and throughout the present period, antimicrobial resistance (AMR) has been recognized as an ancient biological phenomenon, even as new antimicrobial agents were discovered and manufactured (Xiao et al., 2011).

The World Health Organization (WHO) has identified AMR as one of the three most important problems facing human well-being globally. Increasingly frequent isolation of MDR pathogens both from the hospital and community-acquired infections over the past decades has further intensified the problem of AMR. MDR bacteria may affect people at any stage of life, as well as the health care, veterinary, and agriculture industries, making it one of the world's most urgent global problems (Alemayehu, 2021). In 2017, the World Health Organization (WHO) estimated that, by 2050, multibacterial infections, which are caused by two or more bacterial species, will cause more deaths than cancer (Cândido et al., 2019). The lack of proper antimicrobial supply and improper or unnecessary use of antibiotics in developing countries like Africa make the condition more serious (Ayukekbong et al., 2017).

Bacteria have a diversity of resistance mechanisms to cover themselves from the biological effects of antimicrobial agents. Among these mechanisms are: limiting or changing the cell wall structure; using molecular efflux pumps to eliminate drugs; production of enzymes that change the chemical structure of the drug; and altering the target sites for antimicrobial action. Many of these resistance mechanisms are encoded on extra chromosomal elements called plasmids that may be transmitted from one bacterium to another within the same species and sometimes across bacterial families (Alemayehu, 2021)

The increasingly pronounced occurrence of conventional antibiotic-resistant bacteria leads to considerable efforts to be made over the past decade to develop new classes of materials with antibacterial that can address this public health problem. The basic idea is to use properties of certain metals such as intrinsic antibacterial (Saravanakkumar et al., 2018), especially silver nanoparticles. Indeed, the latter are widely applied as an antibacterial agent thanks to the numerous advantages compared to the conventional antimicrobial (Franci et al., 2015), such as chemical stability, safety for the user, a prolonged period, and excellent antibacterial activity because of their high reactivity due to the large surface area to volume ratio. It has been observed that nanoscale nanomaterials exhibit significantly different properties compared to the bulk properties of the same material and that the properties of the nanoscale materials depend on size and shape (Alavi & Varma, 2021). However, used alone, silver nanoparticles have disadvantages related to leaching and aggregation phenomena that can generate environmental problems and limit its application. Also, the ionic form of Ag is toxic to most microorganisms; it can damage the mammalian cells if loaded at high concentrations. To avoid these limitations and maintain their antibacterial activity for a prolonged time as possible, Ag nanoparticles are frequently used to make nanocomposites (Motshekga et al., 2013; Tobaldi et al., 2014). A broad spectrum of materials including metal oxides e.g., copper oxide (CuO), zinc oxide (ZnO) (Lungu et al., 2016), and titanium oxide (TiO_2) (Muflikhun et al., 2019), nanoparticles have been used as supporting material for Ag nanoparticles.

Motshekga et al., (2013) reported that a combination of Ag and ZnO nanoparticles is likely to possess potent antibacterial activity against a broad spectrum of bacteria and is effective against both gram-negative and gram-positive bacteria. Metal/oxide nanoparticles have been studied over the past two decades. They have large surface areas, a wide range of physicochemical properties, and strong antibacterial properties against a wide range of bacteria compared to their counterparts in large quantities. Composites of nanoparticles on substrates such as clay, carbon nanotubes, and activated carbon have been envisaged as alternative materials for inactivating bacterial. Such composites avoid the leaching of the nanoparticles into the water (Motshekga et al., 2015).

In order to utilize the nanoparticle as an antibacterial agent, it must be applied on the substrates such as graphite, zeolite, carbon nanotubes, and clays or polymer materials. Clays are excellent and expandable aluminum silicate material. Clays such as bentonite,

montmorillonite (MMT), kaolinite, halloysites, and palygorskite are commonly used as supporting substrates for nanoparticles. Bentonite contains more than 75% MMT and has been attracted by researchers because of its abundance, non-toxic, inexpensive, and eco-friendly. Also, it possesses excellent adsorption and antibacterial effects. The charge imbalance is offset by exchangeable cations to interlayer sites, such as potassium (K), sodium (Na), and calcium (Ca) at the bentonite surface. This property renders them suitable for the incorporation of various positively (cationic) charged inorganic compounds such as Ag/TiO_2 nanoparticles among the layers, generating the so called intercalation (Krishnan & Mahalingam, 2017a). In order to obtain hybrid materials with better antibacterial properties; in this context Ag and ZnO NPs were combined with clay material.

The size, shape, stability, and physicochemical properties of the nanocomposites can be strongly influenced by experimental factors, the interaction of metal precursor ions with reducing agents, and the interface of the capping agent with metal nanoparticles (Katas et al., 2018; Yunusov et al., 2021). In contrast to bulk material, the corresponding nanoparticles have high surface energy values due to their small size and therefore often accumulate. Hence, the selection of a suitable capping agent is often a prerequisite for the stabilization of nanoparticles.

Capping agents appear to work using a variety of mechanisms, including electrostatic stabilization, steric stabilization, stabilization by hydration forces, depletion stabilization, and stabilization using van der Waals forces, and a combination of some of these mechanisms may be at work for certain capping agents. Aside from their main role in stabilizing nanoparticles, some capping agents (e.g. citrate) are able to play the additional role of reducing metal ions (e.g. silver ions) to metal nanoparticles. Therefore, the selection of the capping agent plays a crucial role in the synthesis process of nanoparticles, and capping agents also affect the properties of nanoparticles(Ajitha et al., 2016).

There are a lot of work was reported by the different researcher including metal and metal oxide supported on clay materials as antibacterial agents through different chemical methods, but no reported on green synthesis of Ag/ZnO/Bentonite nanocomposites. In this study, a low-cost and environmentally friendly alternative to chemical and physical methods, *Hagenia*

abyssinica plant leaf extract were used as a capping and reducing agent for the synthesis of Ag/ZnO/bentonite nanocomposite for antibacterial study.

The *Hagenia abyssinica* plant is a member of the rose family and is a species of flowering plant native to the high-altitude Afromontane regions of central and eastern Africa from Sudan and Ethiopia. It is known in English as African Redwood and East African rosewood and in the Amharic language as Kosso and in the Oromo language as Hexo. Hagenia abyssinica is a slender tree up to 20 m tall with a short trunk and thick branches ((Kifle, Debeb, et al., 2021; Kifle, Kidanu, et al., 2021). Generally, this study addressed advanced materials with a particular focus on synthesis of Ag/ZnO/bentonite nanocomposite materials for antibacterial study.

Figure 1: *Hagenia abyssinica* plant tree and its leaf

1.2.Statement of the problem

Several epidemiological analyzes have shown that microbial contamination has always been associated with an increased risk of infectious disease transmission. Many pathogens like bacteria are involved in various diseases. Therefore, the use of antimicrobials to destroy harmful microorganisms is important for human health. Resistance bacteria to various antibacterial agents are a common problem. Recently, treatment of microbial infection has become more complex since bacteria have the ability to conform themselves against antibiotics. Thus, they can rapidly and easily mutate their genes, making their elimination difficult. For instance, *Staphylococcus aureus* (*S. aureus*) is one of bacterium that commonly

colonizes human skin and mucosa, and can cause serious illnesses if the bacteria come into the body, such as in wound infections, endocarditis, pneumonia, blood stream infection and so forth. *Escherichia coli (E. coli)* are another bacterium commonly found in the gut of warm-blooded organisms. Most strains of *E. coli* are not harmful but are part of the healthful bacterial flora in the human gut. However, some types can cause illness in humans, including diarrhea, abdominal pain, fever, and sometimes vomiting. Other types of E. coli infection can lead to urinary tract infections, respiratory illness, pneumonia, and meningitis (Díez-Pascual & Luceño-Sánchez, 2021). Therefore it is important to develop an efficient, environmentally friendly, inexpensive, and robust method to disinfect those Pathogenic bacteria. Several reports have suggested that the synergetic effect of composites of nanoparticles is efficient and cheap materials used for antibacterial activities. However, a nanoparticle is toxic to most microorganisms; it can damage mammalian cells when loaded in high concentrations and small particle sizes are caused to aggregate rapidly, tending to reduce its stability and bioactivity for long-term applications. To overcome this problem, supporting nanoparticles on carrier clay are a solution. Therefore, the current studies focused on the synthesis of Ag/ZnO/Bentonite nanocomposites using *Hagenia abyssinica* plant leaf extract as a capping agent to stabilize and reduce the toxicity of these nanocomposites for effective bacterial disinfection.

1.3.Objective of the study

1.3.1. General objective

The overall objective of this study was to; Synthesis characterizes and study antibacterial activity of Ag/ZnO/Bentonite nanocomposite.

1.3.2. Specific objective

The specific objectives of studies were to;

i. Synthesis of Ag NPs, ZnO NPs and Ag/Bentonite, ZnO/Bentonite and Ag/ZnO/Bentonite Nanocomposites using *Hagenia abyssinica* plant leaf extract
ii. Characterization of Bentonite, Ag NPs, ZnO NPs, Ag/Bentonite and ZnO/Bentonite Ag/ZnO/Bentonite NCs through different techniques like UV-vis-DRS, FTIR, XRD, SEM, and TEM.
iii. Evaluate performance of the synthesized materials against gram-positive *(Staphylococcus aureus)* and gram-negative (*Escherichia coli*) bacterial species

1.4.Significance of study

This study gives information for the scientific community about synthesis and antibacterial activities of Ag/ZnO/Bentonite nanocomposites.

1.5.Scope of the study

This research works was limited to synthesis, characterization of the synthesized nanocomposite using UV-Vis-DRS, XRD, FTIR, TEM, HRTEM, SAED and SEM-EDX technique. As well as study their application as antibacterial agent on *Staphylococcus aureus* and *Escherichia coli* bacteria.

CHAPTER TWO
LITERATURE REVIEW

2.1. Nanotechnology

Nanoscience and technology is an exciting and rapidly evolving branch of science and technology that works at the atomic, molecular and macromolecular levels. Nanotechnology deals with manipulation and uses various nanoscale tools and functional materials. The concept of nanotechnology was first proposed in 1959 by American Nobel Prize winner Richard Feynman. However, the basic idea of definition and popularization was studied much further in the 1980s (Prasad et al., 2021). The focus on the nano regime relates to the convenience of a standard definition that can be used both to categorize nanotechnology, nanoscience and nanoproducts and to act as a bridge between quantum mechanical effects and area effects. Nanoscience is not merely about size; it is about the unique physical, chemical, biological, and optical properties that emerge naturally at the nanoscale, while nanotechnology is related to the ability to manipulate and engineer such effects.

In today's competitive market, the implementation of nanotechnology is imperative due to several potential benefits for food, textile, and biomedical applications. Indeed, modern technologies and current materials such as nanostructures have some crucial advantages that increase the efficiency, stability and improvement of food and biomedical products in case of quality and safety problems, overcoming future economic conditions (Bagheri et al., 2019; de Dicastillo et al., 2020). Accordingly, general orientations on nanotechnology should be taken into account at an early stage of technological progress (Roig, 2018b).

2.2. Nanoparticles (NPs)

The prefix “nano” has found in last decade an ever-increasing application to different fields of the knowledge. Nanoscience, nanotechnology, nanomaterials or nanochemistry are only a few of the new nano-containing terms that occur frequently in scientific reports, in popular books as well as in newspapers and that have become familiar to a wide public, even of non-experts. The prefix comes from the ancient Greek with meaning literally very small. Within the convention of International System of Units (SI) it is used to indicate a reduction factor of 10^9 times. So, the nanosized world is typically measured in nanometers (1nm corresponding to 10^{-9} m) and it encompasses systems whose size is above molecular dimensions and below

macroscopic ones (generally > 1 nm and < 100 nm) (Konwar & Ahmed, 2016).

The use of nanoparticles in different fields like molecular biology, physics, organic and inorganic chemistry, medicine and material science is unexpectedly augmented nowadays (Sánchez-López et al., 2020). Decrease in particle size to nano-size demonstrates peculiar and improved properties such as particle size distribution and morphology, which is not showed by larger particles of bulk material (Jamkhande et al., 2019). Nanoparticles have both solute and separate particle phase properties. The surface to volume ratio of nanoparticle is 35–45% times higher as compared to large particle or atom. This unique extrinsic property of specific surface area of nanoparticle is a contributory factor for its high value and also influences different intrinsic properties such as strong surface reactivity which is size dependent (Gharpure et al., 2019). Overall, these exclusive features of nanoparticles are responsible for its multifunctional properties and developing interest for its application in various fields like energy, medicines and nutrition. Metallic nanoparticles or metal nanoparticles, a new terminology has been originated in the field of nanoparticles in recent few years. The noble metal like gold, silver, and platinum having beneficial effects on health are utilized for the synthesis of nanoparticles and designated as metallic nanoparticles (Hamad et al., 2020). Nowadays researchers are focusing on metal nanoparticles, composite like polymer preparations, disease diagnosis and treatment, and sensor technology (Jamkhande et al., 2019).

2.2.1. Synthesis of Nanoparticles

The selection of preparation method of metallic and metal oxide nanoparticle is equally important because during nanoparticle synthesis processes such as kinetics of interaction of metal ions with reducing agent, adsorption process of stabilizing agent with metal nanoparticles and various experimental techniques produces strong influence on its morphology (structure and size) stability and physicochemical properties (Vijayakumar et al., 2013).

Synthesis of NPs as shown in Fig 2, has two major approaches, one is top-down, in which the size of larger molecules makes smaller to nanoscale and the other is a bottom-up approach, in which small molecules or atoms are combined to produce nanomaterials (Ahmed et al., 2016). These approaches involve several synthesis methods and four major categories like chemical, physical, mechanical, and biological. Generally, the top-down approach involves methods like

high-energy ball milling, severe plastic deformation, etching, mechanical alloying, lithography, reactive milling, and micromachining methods. Whereas, bottom-up includes molecular self-assembly, sol-gel, electron (or ion) beams, metal-organic chemical vapor deposition, vacuum arc deposition, inert gas condensation, electrodeposition, physical/chemical vapor deposition, and ultrasonic dispersion (Ahmed et al., 2016; Alarcon, 2015).

Biological synthesis of nanoparticles is a green chemistry approach that interconnects nanotechnology and biotechnology. The advancement of green syntheses over chemical and physical methods is: environment friendly, cost effective and easily scaled up for large scale syntheses of nanoparticles, furthermore there is no need to use high temperature, pressure, energy and toxic chemicals(Ahmed et al., 2016; Rane et al., 2018).

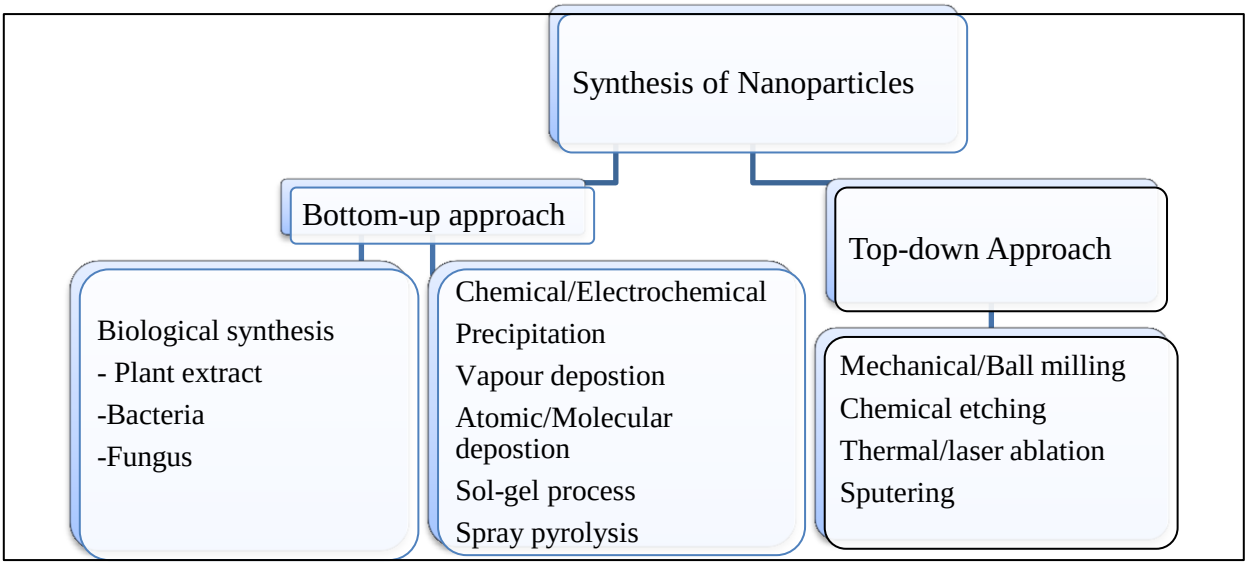

Figure 2: Different approaches for synthesis of nanoparticles

2.2.2. Silver Nanoparticles (Ag NPs)

Silver nanoparticles have tunable physical and chemical properties, so it has been studied widely to improve its applicability. The antimicrobial properties of Ag NPs are finding their application in enhancing the activity of drugs and composite scaffolds for controlled release of drugs and targeted delivery of drugs due to their low toxicity and biocompatibility (Hamad et al., 2020; Sánchez-López et al., 2020). Similarly, their surface plasmon resonance property

makes Ag NPs a top-notch material for developing (bio) sensors, for instance, in surface-enhanced Raman spectroscopy, for detecting biomarkers, diseases, pollutants, and higher catalytic activity in photochemical reactions. Besides these, highly conducting Ag NPs are used in wearable and flexible sensors to generate electrocardiographs. Physicochemical or biological approaches are used to prepare Ag NPs; however, each method has its pros and cons. The prohibitive cost and use of hazardous chemicals hinder the application of physicochemical synthesis. Likewise, biological synthesis is not always reproducible for extensive use but can be a suitable candidate for therapeutic activities like cancer therapy. Excess use of Ag NPs is cytotoxic, and their unregulated discharge in the environment may have effects on both aquatic and terrestrial biota. The research in Ag NPs has always been driven by the need to develop a technology with potential benefits and minimal risk to environmental and human health (Dawadi et al., 2021).

Silver (Ag) nanoparticles (NP) and nanocomposites are the most widely used antimicrobial nanomaterials in the food industry (Araújo et al., 2020). Ag NPs display biocidal activity against a broad range of Gram-positive and Gram-negative (Duffy et al., 2018). Thi Lan Huong & Nguyen, also reported that the green synthesized AgNPs exhibited effective antibacterial activities against both gram-positive (*Staphylococcus aureus*) and gram-negative (*Pseudomonas aeruginosa*) microorganisms(Thi Lan Huong & Nguyen, 2019). Silver nanoparticles have been emerged as one of the best agents for the disinfection of water as it does not produce any by-products in drinking water. Synthesis and development of silver NPs is still a point of discussion among the scientific community owing to its oligodynamic nature that can kill antibiotic resistant microbes (Bhardwaj et al., 2021).

One of the limitations of using Ag NPs is its toxicity. The toxicity of silver nanoparticles (AgNPs) has been shown in many publications. The silver ion fraction of AgNPs suspensions, contribute to the toxicity of AgNPs in lung cells. Cell viability assays revealed that AgNP suspensions were more toxic when the initial silver ion fraction was higher. While the antibacterial effect of silver nanoparticles (AgNPs) on environmentally beneficial microbes has drawn considerable attention, the stability and microbial toxicity of AgNPs in a system (R. K. Rajendran & Lin, 2021).

2.2.3. Zinc Oxide Nanoparticles (ZnO NPs)

Transition metal oxides are one among the different class of nanomaterials which are heavily studied. These oxides are of particular interest because of their varied metal to oxygen ratio and large number of phases with different structures, properties, and application. Zinc oxide (ZnO), which belongs to II-VI transition metal oxides, is one of the most widely studied oxides as a result of its interesting physicochemical, optoelectronic properties and hence its application in many areas including in catalysis, sensors, medicine, personal care products, paints, batteries, solar cells, memory devices, electronic and spintronics, and in agriculture to control crop disease and as bio fertilizer. In particular, by virtue of its chemical stability, biocompatibility and biodegradability nature, it has been extensively used as antibacterial agent in antifouling application and also in the radiation–assisted degradation of organic contaminants in wastewater treatment (Chaudhuri & Malodia, 2017; Mankad et al., 2016). Nowadays, access to clean water is becoming an increasing demand.

ZnO NPs is the most common use of nanomaterials in cosmetics in skincare products, and particularly, in sunscreens to act as UV filters. It is reported that nanoscale ZnO show great advantages over many products at larger than nano-dimensions. Micro-ZnO is used as ingredients in sunscreens due to UV absorption capabilities. A nanoparticle of ZnO is also widely used in sunscreens as UV filters starting at the size of 20 nm. It show better dispersion and leave a better cosmetic result (Fytianos et al., 2020).

There are different methods for synthesis of ZnO NPs those are; physical (Physical vapor deposition, Laser ablation, Ball milling, Etching), chemical (Solvothermal, Sol-gel, Microemulsion, Precipitation, Pyrolysis and Chemical reduction), biological (Microorganisms and Plants extracts), and hybrid Bio hydrothermal , Electrochemical , Chemical Vapor Deposition , Particle Arresting in glass polymer or zeolite) methods for different application including antibacterial activity and photocatalytic activity (Weldegebrieal, 2020). He conclude that, Nowadays, the biological synthesis method has gained tremendous interest among researchers due to its advantages such as environmental benignity, low cost, low toxicity, simple procedures and instrumentation involved during the preparation process over chemical methods.

However, it has drawbacks such as difficulty of control over particle size and shape of the

biosynthesized ZnO NPs, which is predetermined by phytochemical compounds available in the plant extract, and also purifying the NPs synthesized from the plant material is a challenge. So in this work both chemical and biological methods have been used.

ZnO nanoparticles has different application from that one of promising application of ZnO NPs is as antibacterial agent for preventing bacterial growth in medicine and food packaging. It is sensitive to both Gram-positive and Gram-negative bacteria. One of its limitation is that its inhibiting efficacy depends on factors such as particle size, its concentration in suspension, the type of bacteria under investigation, presence of surface modifiers, availability of light, and in general on the synthesis method employed. The antibacterial mechanism of action of ZnO NPs has been proposed to be due to physical interaction of ZnO NPs with bacterial surface, that is, deposition of NPs on surface, damaging cell envelope and cytoplasm via abrasion or blocking ion diffusion channels, and chemical interaction and then leads death of the bacteria (Weldegebrieal, 2020). To overcome those limitations of NPs related with toxicity and efficacy recent studies on antibacterial activities of clay-based materials are mainly focused on immobilization of inorganic cations and oxide such as silver (Ag^{+}), zinc(Zn^{2+}) and zinc oxide(ZnO) on to clay minerals (Abed et al., 2020).

2.3. Clays

Clays are considered as widely attractive an appealing substrate for immobilization of a variety of nanoparticles than other fillers because of its being inexpensive, non-hazardous, flexible, high specific surface area, high chemical stability, excellent binder, eco-friendly supporting materials, high swelling, adsorption and ion exchange properties and very promising supports for the design and preparation of biocompatible nanocomposite material and widely available. Bentonite (Aguiar et al., 2020), kaolinite (Chen et al., 2020), and zeolite (Roshanfekr Rad & Anbia, 2021) are some of clays used as stable and solid support in synthesis of metal oxide/clay nanocomposites.

2.3.1. Bentonite Clay

From old times, the human kind has used clays, externally or internally, for maintaining body health or treating some diseases. Bentonite clay is one of the available clays in nature, used as traditional habits, and remedies in many cultures. Bentonite is absorbent aluminium phyllosilicate clay. It is named after Fort Benton, Wyoming where its largest sources are

found. Its other name, Montmorillonite clay, stems from the region of France called Montmorillon, where it was first found. It has been used and eaten from ancient time till now as human believes in its therapeutic benefits (Nones et al., 2015).

2.3.2. Structure, Properties and Application of Bentonite

Bentonite is natural clay composed mainly of montmorillonite with other associated minerals such as feldspar, calcite and quartz (Srasra & Bekri-Abbes, 2020). Dry bentonite, or more correctly its main component montmorillonite, is built up by layers approximately 1 nm thick, each consisting of two tetrahedral and one octahedral unit. The latter consists of Al (III), coordinated with oxygen, and is surrounded by the two tetrahedral sheets consisting of oxygen coordinating Si (IV). In bentonite one aluminum atom shares oxygen atoms with the two silica sheets, which gives the unit cell formula, $[Al_2\ (OH)_{\ 2}\ (Si_2O_5)_2]$. The bentonite layers are charged due to exchange of Al (III) with for example Mg (II) and/or Fe (II) yielding an excess of negative charges. To obtain electro neutrality bentonite clay holds, most commonly, sodium or calcium ions as counterions (Al-Hammood et al., 2021a).

There are two types of bentonite are found swelling type bentonite or sodium bentonite and non-swelling type bentonite or calcium bentonite. Most of the bentonite found worldwide is of calcium type (Asad, 2013; A. Kumar & Lingfa, 2020). Sodium bentonite is canonicalized compound, the bond donor count of hydrogen and bond acceptor of hydrogen count is 1 and 13 respectively. The type of bentonite is determined based on the dominant smectite in it, for example, calcium bentonite contains calcium montmorillonite as a major mineral, and sodium bentonite contains sodium montmorillonite as a major mineral, and so on. The general chemical formula of montmorillonite is: $(Na,Ca)_{0.3}(Al,\ Mg\ )_2(Si_4O_{10})(OH)_2.nH_2O$ (Al-Hammood et al., 2021a, 2021b)

Bentonite is in the form of an aluminum phyllosilicate developed frequently from the conversion of volcanic ash, principally consists of smectite minerals, mainly montmorillonite (80–90% by weight). When montmorillonite comes in contact with water can expand several times by its original volume. In addition to the predominant montmorillonite mineral, bentonite rocks contain clay minerals such as kaolinite, illite and palygorskite, and also contain non-clay minerals such as gypsum, quartz and calcite (Al-Hammood et al., 2021a, 2021b).

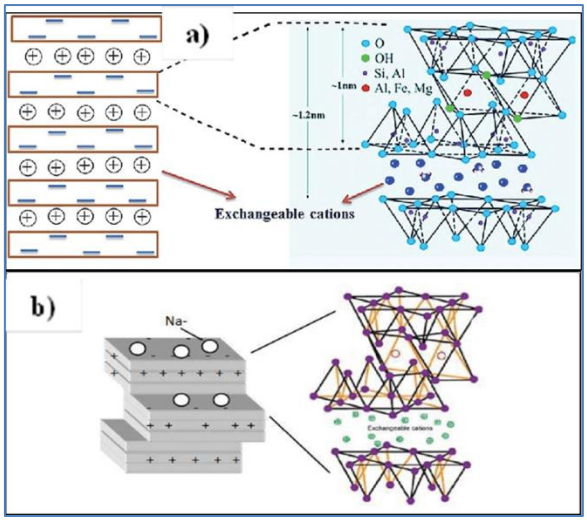

Figure 3: A diagrammatic sketch of the structure of bentonite clay (a) (Hebbar et al., 2014) and crystalline structure of sodium bentonite with inter lamellar water layer (b) (Zaher MS et al., 2018).

2.3.3. Properties of Bentonite Clays

A). CEC of Bentonite Clays

The CEC of clay minerals may be defined as the quantity of cations available for exchange at a given pH (Muurinen, 2011). The use of bentonite as an inorganic compound adsorbent for example such as heavy metal ions is because of having a cation exchange capacity and hydrophilic property on the surface. Bentonite has a surface chemical complex and arises from its ability to form a water gel thixotropic, high water absorption, high surface area, the layered structure and the ability of the cation exchange high. Mineralogical composition and particle size can affect the value of the CEC, for example, the maximum value of CEC found in North Aceh Bentonite obtained of 79.09 meq /100 g with particle size of 250 meshes (Rihayat et al., 2018).

B). Swelling properties

Clay swelling is a result of the increase in interlayer spacing in clay particles. Clay swelling occurs when the clay is exposed to aqueous solutions having a brine concentration below the critical salt concentration (Magzoub et al., 2020). Bentonite is commonly chosen to be the clay backfill material because of its favorable physical and chemical properties including low

permeability and high swelling capacity (Daniels et al., 2017). Both sodium (Na) and calcium (Ca) bentonites have been considered for use within Europe, although a greater emphasis has been placed on Na-bentonites. Comparing the two, Marcial and co-workers (Marcial et al., 2002) studied the compression characteristics, observing that the Ca-bentonite still had a larger void ratio and suggesting that the reduced compression was related to the larger diameter of the divalent Ca^{2+} cation. Na-bentonite contained an increased number of smaller pores than the Ca-bentonite, suggesting that the Na-bentonite had a higher hydration and swelling capacity (Harrington et al., 2020).

2.3.4. Properties of Sodium Bentonite

A) Physical Properties

Sodium bentonite is most widely known for its ability to swell. It can absorb nearly 5 times its weight in water and at full saturation may occupy a volume 12 to 15 times its dry bulk. The high water absorption capacity of bentonite also makes it very plastic and resistant to fracturing or cracking. Interestingly, bentonite can be hydrated and dried an infinite number of times without losing its original swelling capacity. It can similarly be frozen and thawed repeatedly without losing its ability to swell. Because the platelets are uniformly broad and flat, sodium bentonite has an exceptionally high surface area of 600 to 800 square meters per gram. Less than 10 grams of bentonite, if fully dispersed, could cover a football field. It is a combination of these physical properties that make sodium bentonite an ideal waterproofing material. A layer of hydrated bentonite provides a dense, low porosity barrier to fluid flow that exhibits a typical hydraulic conductivity of 1×10^{-9} cm/sec (Wei & Gencturk, 2019).

B) Electrochemical Properties

The structure of sodium bentonite gives it some important electrochemical properties. As previously discussed, bentonite platelets naturally possess an overall negative charge as a consequence of having more charge contributed by the negatively charged oxide anions than is contributed by the positively charged cations. This unbalanced negative charge resides mainly in the oxide atoms found in the flat edges of the platelets where positively charged aluminum cations in the octahedral layer may be exposed without a full complement of oxide anions, some localized positive charge (edge charge) is possible (Meneses et al., 2018).

C) Hydration Properties

Research indicates that the hydration process of sodium bentonite is a combination of four primary mechanisms contributing to the swelling properties of sodium bentonite; physical orientation of water molecules, position of oxygen in the tetrahedral sheets, excess electrons on Bentonite surface and the presence of sodium (Wei & Gencturk, 2019).

2.3.5. Application of Bentonite Clay

Bentonite clay is mainly used in structural polymers, ceramic bodies, drilling fluids, in adsorption catalytic processes, animal feed additive, wastewater treatments and biomedical applications. Application of bentonite has been widely used for filler, pellet, drilling mud, a catalyst and as adsorbent. Currently it has also been made into several high value products such as nanomaterial materials, medicines and chemicals. Bentonite is widely used for the treatment of esophagitis, gastritis, and colitis and so on. Bentonite is also used as a raw material for cosmetics because of its decontamination, detoxification, as a moisturizer. In addition, with its chemical adsorption and stability, bentonite has been widely used in food processing industries that are closely related to health and human life (Rihayat et al., 2018).

A). Bentonite as antibacterial agent

Healing properties of bentonite are derived from the crystalline structure of the smectite group, which is composed of two octahedral alumina sheets localized between two tetrahedral silica sheets. This structure is behind the ability to intercalate cationic bioactive agents and undergoes interaction with various toxic species and exchanging in return species such as Fe^{3+}, Cu^{2+}, Al^{3+} Ca^{2+} or Na^{+}, presenting antibacterial activity and providing essential minerals to the body. Furthermore, due to its layered structure, bentonite has wide application for the design of biomaterials providing, thus, the stability of bioactive agents and preventing them from aggregation. Moreover, modified bentonite and intercalated bentonite increased when compared with the unmodified bentonite (Srasra & Bekri-Abbes, 2020).

B). Bentonite as supporting materials for Nanoparticle and Nanocomposite

Na-bentonite nanoclay was excellent filler, binder, intercalation and supporting materials, and substrates for metal/metal oxide NPs due to its large surface area, swelling behaviour, and high adsorption and ion exchange properties. Their adsorption capacities help to attract

contaminants into the open pores and therefore raise the efficiency of the dispersed transition metal oxides NPs such as titanium oxide (TiO_2) (Krishnan & Mahalingam, 2017a), zinc oxide (ZnO), zirconium oxide (ZrO_2), tin oxide (SnO_2), manganese oxide (MnO_2), etc. (Chakraborty et al., 2019) reports that the catalytic activity of these oxides was reinforced when they were supported on a bentonite clay which contain a high specific surface area and low cost. A large number of ion exchange sites available in clays are also beneficial for incorporation of electro-active species and nanoparticles.

2.3.6. Bentonite clay in Ethiopia

Bentonite clay resources are found in Ethiopia within the Afar, and Southern, Nations, Nationalities, and People's Regional States. The Afar Regional State bentonite occurrences are easily accessible, as they are located near the main road. Most occurrences in Afar are located at Warssiso, Hadar, Gewane, and Ledi. The Warssiso (Mille) bentonite deposit is located at 500 Km from Addis Ababa to Semera main roads. Gewane is located 376 Km northeast of Addis Ababa to Semera main road, Gewane bentonite deposit on 15 Km Gewane town. The Previous analysis of Warssiso bentonite indicates it a calcium bentonite (Mammo Ghebre, 2019).

2.4. Nanocomposite

Composites, which are one of the most important materials of modern technology, consist of at least two components comprising a continuous matrix phase and an un continuous reinforcement material to obtain the best features from each component (Ates et al., 2017). Composites are generally divided into three basic classes according to the size of the reinforcement in the structures. These are macro composites, micro composites, and nanocomposites.

Nanocomposites that provide quite outstanding features can be prepared by the application of reinforcement (below 100 nm in size) phase in the composite. Because of the high surface to volume ratio of nanocomposites, interaction between matrix and reinforcement is very high. Despite having a very short history, nanocomposites have been frequently used in many applications due to their superior properties. Applications of nanocomposites have been considerably developed in engineering, plastic, rubber, coating, adhesive, electronic and optic materials. However, this rapid growth has also brought some problems and created severe

environmental problems due to the late decomposition periods of nanocomposites in nature (Sabaruddin et al., 2021).

The most important solution to eliminate these problems is the preparation of nanocomposite components from bio-renewable resources. For this purpose, nanocomposites are obtained from bio-renewable resources by the use of vegetable oils, cellulose, starch (S), lignin, chitin, natural rubber, and proteins to name a few. These nanocomposites are mainly divided into three groups in terms of structural type. These reinforcements are composites obtained from bio-renewable sources, composites that their matrix is originated from bio-renewable sources, and composites that have both reinforcement and matrix component obtained from bio-renewable sources (Ates et al., 2020; Omanovi et al., 2020).

Nanocomposites represent new alternative way to overcome current limitations of microcomposites and monolithics and are becoming materials of the future. The main advantages of nanocomposites over other composite materials are: high surface/volume ratio allows small filler size and distance between fillers; better mechanical properties- high ductility without strength loss, scratch resistance; improved optical properties (light transmission depends on particle size). Disadvantages of nanocomposite application are mostly toughness and impact performance associated with nanoparticle incorporation to the bulk-matrix of composite; Insufficient understanding between formulation/property/structure relationships, need for simpler particle exfoliation and dispersion and cost-effectiveness.

Nanocomposite materials are divided into three groups by their matrix materials: metal matrix nanocomposites (MMNC), ceramic matrix nanocomposites (CMNC) and polymer matrix nanocomposites (PMNC) (Omanovi et al., 2020)

In recent years, synthesis of Ag nanocomposite has become an emerging technique, due to its antimicrobial and strong cytotoxic activities. Also, Ag nanocomposite is less toxic to humans (Kukushkina et al., 2021; Nasrollahzadeh et al., 2019). Ag nanoparticles are extensively used in other areas such as dental filling, wound dressing, water treatment, and textile fabrics. However, the ionic form of Ag is toxic to most microorganisms; it can damage the mammalian cells if loaded at high concentrations. To overcome these problems, Ag nanoparticles are frequently used to make nanocomposites. A broad spectrum of materials including metal

oxides e.g., copper oxide (CuO), zinc oxide (ZnO) (Lungu et al., 2016), and titanium oxide (TiO_2) (Muflikhun et al., 2019), nanoparticles have been used as supporting material for Ag nanoparticles. The combination of Ag/TiO_2 nanocomposite has proven to be a promising antibacterial material and shows low toxic in nature. TiO_2 nanoparticles are one of the most commonly used materials for photocatalytic antibacterial applications due to its low-cost, chemical stability, and nontoxic to humans(Wu et al., 2010). TiO_2 is a wide semiconductor with the band gap of 3.26 eV for anatase. However, Ag/TiO_2 nanoparticles possess large surface area and high reactivity than the corresponding bulk materials. Therefore, Ag/TiO_2 displays stronger biocompatibility properties and antibacterial activity. On the other hand, Ag/TiO_2 has the tendency to aggregate when it is used as individual components which result in the release of nanoparticles into the environment during the treatment process (Krishnan & Mahalingam, 2017a).

2.4.1. Silver / Bentonite nanocomposite

In order to utilize the nanoparticle as an antibacterial agent, it must be applied on the substrates such as graphite, zeolite, carbon nanotubes, and clays or polymer materials. Clays are excellent and expandable aluminum silicate material. Clays such as bentonite, montmorillonite (MMT), kaolinite, halloysites, and palygorskite are commonly used supporting substrates for nanoparticles (Dutta & Wang, 2019; Krishnan & Mahalingam, 2017a). The unique properties of silver NPs (or its composites) and its supportive materials such as clay, ceramics, charcoal, silica beads, cotton fabric, filter paper, cellulose gels, alginate beads and polyurethane sponge have provided great opportunity to revolutionize the water disinfection systems which have achieved 99 to 100% of deactivation of bacteria (Bhardwaj et al., 2021).

It is interesting to note that Bentonite share a number of characteristics such as the antimicrobial potency, active site type, high adsorption capacity, ionic exchange capacity, surface acidity, large surface area and thermal stability. Bentonite offers several advantages over other supports. Indeed, Bentonite is a naturally sourced product and quite abundant in nature; it is a cheap, ecofriendly, stable and selective catalyst. Furthermore, Bentonite can be used to develop new materials with a microporous structure involving new catalytic sites by cation incorporation (Aznárez et al., 2015).

2.4.2. Zinc oxide/Bentonite nanocomposite

There are challenges in the large-scale utilization of nanoparticles such as ZnO in water treatment due to difficulty in their separation and recovery after treatment. In addition, the use of metal oxides nanoparticles for water treatment has some disadvantages, namely: (1) higher colloidal stability in aqueous solution, (2) agglomeration of the nanomaterials at high concentrations, and (3) difficulty in separating and recovering the nanomaterial after use (Lei et al., 2017). However, steps have been adopted in order to overcome these shortcomings. These include doping and co-doping of metal oxide nanomaterials and immobilization of nanomaterials on suitable matrices (Darvishi Cheshmeh Soltani et al., 2016). This suitable substrate could function as support in order to overcome the difficulties involved in post-separation and recovery. Moreover, the support of nanosized semiconductor materials on matrices could help to enhance their activity when compared with ordinary nanomaterials. In this respect, various clay matrices such as kaolinite, montmorillonite, and bentonite have been successfully employed as support. An immobilizing and anchoring nanosized ZnO nanoparticle on the surface of clay minerals provide more active surface sites, reduces the agglomeration of the nanoparticles, and prevents the release of nanoparticles into the environment. Clay nanocomposites have become major components of clay with metallic nanoparticles used in recent research findings in tackling environmental pollutants. Since, ZnO nanoparticles are cheap, non-toxic, and capable of removing emerging contaminants, and given the fact that rural communities are affected by contaminants from wastewater, cheaper and environmentally friendly methods for the wastewater treatment need to be adopted for water and wastewater treatment.

It has been demonstrated that using nanoparticles alone is dangerous, because their sizes can affect human health and the environment. To overcome this problem, hybrid processes were introduced by combining nanoparticles with other environmentally friendly materials, such as inert and stable materials to utilize nanoparticles' full properties in wide-range applications. Moreover, introducing nanoparticles with other substrates/fillers would result in composites with novel and enhanced properties that cannot be achieved by the individual components (Pouraboulghasem et al., 2016).

2.4.3. Synthesis and Characterization of Nanocomposite

The nanocomposites synthesis method is crucial for improving the performance. Moreover, synthesis methods resulting in the assembly of uniformly distributed particles and consistent shapes are necessary to enhance the linearity and therefore the detection limits of the nanosensors, amongst other performance parameters (Munonde & Nomngongo, 2020). There are two common approaches for the synthesis of nanocomposite, namely top down and bottom up methods (Gregorczyk & Knez, 2016). Common top down methods involve mechanical methods such as; mechanical grinding, high energy ball milling, mechanical alloying, reactive milling and lithography (Munonde & Nomngongo, 2020). Common bottom up methods include chemical methods such as; hydrothermal, co-precipitation, microemulsion, sol-gel, chemical-vapor deposition, electrodeposition, and colloidal dispersion.

Biological Synthesis

Biological synthesis of nanoparticles is a green chemistry approach that interconnects nanotechnology and biotechnology. However, despite the stability, biological nanoparticles are not monodispersed and the rate of synthesis is slow. The concentration of synthesized macromolecules or components involved in the nucleation of particles varies with time and prolongs the nucleation period, which causes the polydispersity of nanoparticles and subsequent decreased rate of synthesis. In order to overcome these problems, several methods, such as microbial cultivation methods and the extraction techniques, have to be optimized, and a combinatorial approach, such as photo biological methods, may be used. Cellular, biochemical, and molecular mechanisms that mediate the synthesis of biological nanoparticles should be studied in detail to increase the rate of synthesis and improve the properties of the nanoparticles. Owing to the rich biodiversity of plants and microbes, the potential as biological materials for nanoparticle synthesis is yet to be fully explored (Bandeira et al., 2020; Jadoun et al., 2021)

The nanocomposites characterized by XRD, XPS, SEM, TEM, EDX, FT-IR, and UV-Vis spectroscopy techniques to see the crystalline size, morphology, surface composition, functional groups, and optical band gap of the nanocomposites. TEM, EDX, and XPS were wont to analyze the chemical elemental composition by observing the behavior and oxidation states (Garavand et al., 2022).

2.5. Application of Ag and ZnO based Nanocomposite

Chemical, physical and biological properties of Ag NPs have boosted their commercial and scientific applications for biomedical, textile, food, environmental, pharmacological and other industries (Azizi-Lalabadi et al., 2021). A most current application of Ag NPs relates to the preservation of drinking water or milk from microbial contamination. In 1954, Ag NPs were recorded in the US as antimicrobial substances (Nowack et al., 2011). These days, Ag NPs as bacteriostatic materials have high application due to the increasing resistance of microorganisms to the antibiotics developed throughout the 20th century (Eckhardt et al., 2013). In fact, the microorganisms which are resistant to other antimicrobial agents are unexpectedly sensitive to Ag NPs (Roig, 2018a). Ag NPs have a supreme stability at high temperatures unlike antibiotics (Nowack et al., 2011). Despite using Ag NPs for an extended time, people are concerned about the toxicological impacts of those particles. Therefore, applying a safe method to incorporate Ag NPs into nanomaterials is very important (Azizi-Lalabadi et al., 2021). Generally Ag and ZnO based nanocomposites have different activity like antibacterial activity, catalytic activity, photocatalytic activity, and also used in waste water treatments (Bel Hadjltaief et al., 2018; *Krishnan2017.Pdf*, n.d.; Motshekga et al., 2013; Weldegebrieal, 2020).

A). **Antibacterial Activity**

Antibacterial activity is defined as the action by which bacterial growth is inhibited or destroyed. Bacteria are classified into Gram positive and Gram negative depending on whether they give positive or negative result on Gram's stain test. That is, while those which retain the initial pink color of crystal violet stain, by virtue of their thick peptidoglycan layer in their cell walls are named Gram positive, those that are decolorized and are stained red with carbol fuchsin or saffranin owing to their relatively thinner peptidoglycan layer in their cell walls are Gram negative. Antibacterial activity can be measured by activity index (AI) which is obtained by dividing the inhibition zone of the sample to that of the positive control, both measured in millimeters. Zone of inhibition or clearance zone is the area where there is no growth of any bacteria observed due to the antibacterial action of the applied test nanocrystals suspended in appropriate solvent such as dimethyl sulfoxide, which doesn't kill bacteria itself.

Standard antibiotics such as ampicillin, chloramphenicol are used as positive control against which the inhibition zone of test solutions are compared (Weldegebrieal, 2020).

A lot of nanocomposite work has been reported for antibacterial activity but they have some limitations that need further study. For instance Ag/TiO_2/bentonite nanocomposite has enhanced antibacterial activity than pristine Na-bent against Gram-positive (*S. aureus*) and Gram-negative (*E. coli*) bacteria. But In vitro studies showed that Ag/TiO_2/bent nanocomposite exhibited nontoxic effect only at low concentrations (0.25–50 mg/mL) against HEK 293 cell (Krishnan & Mahalingam, 2017a).

Both ZnO and Ag nanoparticles have antibacterial activity, but the antibacterial activity of Ag nanoparticles is higher than that of ZnO nanoparticles while the cost of ZnO nanoparticles is lower than that of Ag nanoparticles (Hou et al., 2018; Santhosh et al., 2016). As a result, the mixture of ZnO and Ag nanoparticles are often used as an alternate (Cerrón-Calle et al., 2019; Chelli & Golder, 2018). Ag/ZnO nanocomposites are often synthesized by several different methods including hydrothermal method, photoreduction, and microwave-assisted synthesis method (Liu et al., 2015). It was reported that the antibacterial activity of Ag/ZnO nanocomposites were higher than that of ZnO nanoparticles. (Motshekga et al., 2013) synthesize composites of silver-zinc oxide nanoparticles supported on bentonite clay by the microwave-assisted synthesis method for use of antibacterial with particle sizes ranging from 9-70 nm. The antibacterial activities of the composites were evaluated against Gram-negative *Escherichia coli* bacteria and Gram-positive *Enterococcus faecalis* bacteria by the disk diffusion method. And they conclude that both composites of Ag-clay and ZnO-clay showed good antibacterial activity against bacteria, but a better antibacterial activity was observed with Ag/ZnO-clay composite. In order to enhance the antibacterial activity of nanocomposite this study proposed an innovative attempt synthesis of Ag/ZnO /bentonite nanocomposites.

2.7. Research Gap

As mentioned in the above literature review section, many research studies have investigated on finding of antibacterial agents. So, as a solution may finding are reported a different nanoparticles and nanocomposites, but still using nanoparticles have its own limitation related to toxicity and others. Similarly using nanocomposite as a solution has its own short coming on final activity, especially related with agglomeration. In the same manner previously, few

studies have reported about Ag/ZnO/bent/chitosan and Ag/ZnO/bentonite NCs synthesizeed by microwave method, but it is been reported that this methods may cause inefficient and non-uniform reaction condition. On otherhand, several reserearch groups have developed a one-step synthesis of montmorillonite (Mt)-polymer, Ag/Mt, Ag/bentonite and Ag/TiO_2/MMT hetrostructure by various methods of synthesis at low temperature but the particle size were not uniform. Further more, among these NCs have not been widely studied, may be due to the particle size distribution and stablize the particle is extremly difficult and does not provide sufficient usage for biological application (Becker et al., 2015; Deák et al., 2015; Wu et al., 2010). After careful considration of the benefit and drawback of the previousely reported materials, the cost-effective, facile, and green synthesis of Ag/ZnO/Bentonite NCs exhibited remarkable activity toward both tested bacterial strain. Even though there were many researcher reported on Ag and ZnO and some other Composite materials, to our knowledge the combination of three species as Ag, ZnO and Bentonite clay synthesized by green methods have not been reported yet.

CHAPTER THREE
MATERIALS AND METHODS

3.1. Materials and Chemicals

Raw Bentonite was collected from Mille (Warssiso) (Elevation of 518 m above sea level, weather: 27 °C, Wind: W at 4.45 km/h, 46 % Humidity, Latitude: 11° 25' 18" N, Longitude: 40° 45' 46" E. 500 km from Addis Ababa), woreda of Awsi Rasu (Administrative Zone 1), located in Afar Region, north-eastern Ethiopia.

The plant *Hagenia abyssinica* used as a reducing and capping agents in synthesis of NPs and NCs were collected from Adele town, Amigna woreda (Elevation: 2,475 m,weather: 13 °C, Wind: SW at 6 km/hr, 65% Humidity, Latitude 7°47'26" N, longitude 39°54'26" E. 241km from Addis Ababa) East Arsi Zone, Oromia regional state, Southeastern Ethiopia. All reagents were analytical grade and purchased from Addis Ababa, Ethiopia (YESHADAM TRADING PLC, PARACHEM INDUSTRY & TRADING PLC and ET WISDOM IMPORT & EXPORT PLC) local market and used without any further purification. $AgNO_3$ (99.98%) used as the silver precursor, zinc acetate dihydrate ($Zn(CH_3COO)_2 \cdot 2H_2O$ 99.9%), Sodium hydroxide (NaOH), and distilled water were used. The bacterial strains, Gram-negative (*Escherichia coli*) ATCC 25922 and Gram-positive (*Staphylococcus aureus*) ATCC 25923 bacteria used for checking antibacterial activity were taken from American type Culture Collection (ATCC) found in Adama Public Health Research and Referral Laboratory Center.

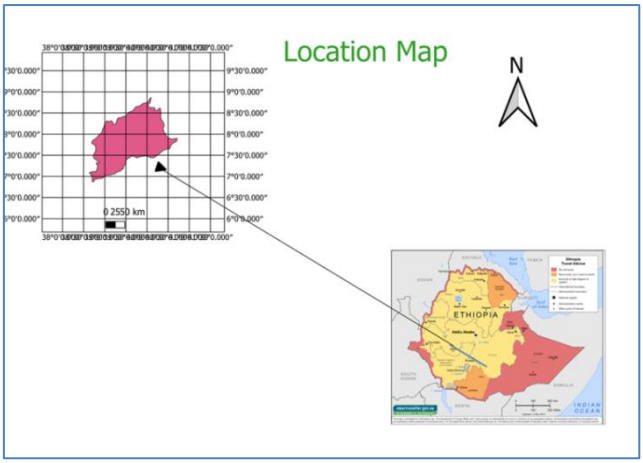

Figure 4: Map of Ethiopia plant collection site

3.2. Experimental procedure

3.2.1. Purification of bentonite

The collected natural bentonite were dried in air and crushed to particle size < 250 μm using a mortar and pestle. To remove quartz, carbonates, calcites, and iron-hydroxide, the grounded bentonite was then dispersed in distilled water (100 g/ 1L) at room temperature and clay fraction was recovered with a homogenizer (1000 rpm) for 1 hr. This process was repeated four times, in order to obtain samples in a pure form. The suspensions were allowed standing for 24 hr to settle the impurities. The supernatant was decanted and any bottoms settled in the flask were discarded. The suspension was centrifuged at 3000 rpm for 20 min, dried in an oven at 60 ˚C, ground, sieved using a 63 μm mesh, and stored in tightly closed plastic bottles for characterizations and use in the experiments (Gong et al., 2016).

3.2.2. Activation of bentonite clay by Sodium Carbonate (Na_2CO_3)

Activation of the purified bentonite was carried out using a previous procedures by (Magzoub et al., 2020; Shah et al., 2013) with slight modification. 100 g of purified bentonite powder was dispersed into 1 L distilled water to form a suspension. Then, 5 g of $Na_2CO_3.10\ H_2O$ was added to the suspension to obtain a stable aqueous dispersion. The suspension was stirred slowly and boiled for 1 hr. The suspension was allowed to cool to room temperature and diluted with 1 L of distilled water, and allowed to stand for 24 hr. The supernatant was decanted and any bottoms settled in the flask were discarded. The Na-bentonite suspension was centrifuged at 3000 rpm for 20 min then dried in an oven at 60 ˚C for 12 hr and ground to obtain activated bentonite powder for further experiments.

3.2.3. Collection of *Hagenia Abyssinica* Plant Leaves and Preparation of its Powder

The collected plant leaf samples were washed three times with tap water followed by distilled water to remove extraneous matter. The cleaned leaves were completely dried at room temperature in open air and under shadow for about two weeks (15 days) to remove any remaining moisture content from the leaves. The dried leaves was crushed by using an electrical grinding machine (grinding machine) to produce a fine powder followed by packing in a brown bottle to protect the effect of light.

3.2.4. Preparation of Aqueous Plant Leaf Extract

For preparing plant extract, 25 g of the powdered leaves of *Hagenia abyssinica* was taken in a 1000 ml of conical flask containing 400 ml of disttiled water. The flask was then covered with

aluminum foil; to prevent the effect of light. After that, a contents of the flask were shaken using a magnetic stirrer for 30 minutes and allowed to warm at 50 °C for 1 hr on a magnetic stirrer; then it was allowed to cool down to room temperature overnight. The prepared solution was filtered through Whatsman No.1 filter paper to obtain a clear solution. The filtrate will be stored at 4 °C until required (Murthy et al., 2020).

Figure 5: Process in plant leaf extracts preparation

3.2.5. Preliminary Phytochemical Screening of *H. Abyssinica* Plant Leaf Extract

The presence of phytochemical like alkaloids, reducing sugars, flavonoids, phenolic compounds, tannins, Phlobatannins, Terpinoides, and Saponins in *H. abyssinica* plant leaf extract was evaluated using standard testing methods (Shaikh & Patil, 2020).

Table 1: Qualitative Tests for Phytochemical Screening of *H. abyssinica* Plant leaf extract

Test	Procedure	Observations (Positive Test)	References
Detection of alkaloids			
Wagner's test	10 mL of plant extract filtrate + 2 drops of Wagner's reagent (Iodine in potassium iodide) in a test tube	A brown/reddish precipitate	(Shaikh & Patil, 2020; V. Singh & Kumar, 2017)
Detection of Reducing sugars			
Benedict's test	0.5 mL filtrate + 0.5 mL Benedict's reagent + Boiled for 2 min.	Green/yellow/red colour	(V. Singh & Kumar, 2017)
Detection of Flavonoids			

Alkaline reagent test	1mL extract + 2mL of 2% NaOH solution (+ few drops dil. HCl)	An intense yellow colour, becomes colorless on addition of diluted acid	(Gul et al., 2017; V. Singh & Kumar, 2017)
Detection of Phenolic compounds			
Ferric chloride test	5 mL of extract aqueous solution + 7 drops of 5% ferric chloride solution	Dark green/bluish black colour	(Shaikh & Patil, 2020)
Detection of Tannins			
Braymer's test	1 mL filtrated + 3 mL distilled water + 3 drops 10% Ferric chloride solution	Blue-green colour	(V. Singh & Kumar, 2017)
Detection of Phlobatannins			
HCl test	2 mL aq. extract + 2 mL 1% HCl (boiled)	A red precipitate	(Auwal et al., 2014)
Detection of Terpinoides			
	2 mL chloroform + 5 mL plant extract, (evaporated on water bath) + 3 mL conc. H_2SO4 (boiled on water bath)	A grey coloured solution	(Gul et al., 2017)
Detection of Saponins			
Frothing test	3 mL of plant extract was dissolved in 5 mL of distilled water and the mixture was shaken vigorously.	The formation of stable persistent froth	(Auwal et al., 2014)

Note: Reagents/Solutions Composition (Shaikh & Patil, 2020).

Wagner's reagent: 1.27 gm iodine + 2 gm potassium iodide + distilled water to make final volume 100 mL.

Benedict's reagent: Solution A: 173 gm sodium citrate + 100 gm sodium carbonate + 800 mL water, dissolve & boil to make solution clear Solution B: 17.3 gm of copper sulphate dissolved in 100 mL distilled water working solution: Mix solution A and solution B

3.2.6. Synthesis of Silver Nanoparticles (Ag NPs)

A 0.2 M concentration aqueous $AgNO_3$ solution was prepared and stored in brown bottle.100 mL of plant leaf extract was mixed with 100 mL of 0.2 M $AgNO_3$ solution (1:1) by maintaining the temperature of about 50 °C for 2 hr. The color change was checked periodically after 30 min of duration. Then the mixture has been incubated at room temperature for 24 hr and the solution was centrifuged for 15 min at 3000 rpm. The obtained Ag suspension was washed by deionized water and ethanol to remove any impurities. Then after, the NPs were allowed to dry and ground so as to be used for further analysis (Murthy et al., 2020).

3.2.7. Synthesis of Zinc Oxide Nanoparticles (ZnO NPs)

100 mL *H. abyssinica* leaf extract was added drop-wise to 100 mL Zinc acetate aqueous solution of 0.2 M concentration and the mixture was vigorously stirred at 80 °C for 30 min through observing color change. The solution was continuously stirred for 3 hr at 80 °C through adjusting the pH of the solution at 12 by 1 M of NaOH solution. Then, the solution was cooled and centrifuged at 3000 rpm for 20 min to separate the precipitates. The precipitates were washed several times with double distilled water and dried at room temperature. The Solid powders were ground using an agate mortar and placed in a furnace at 450 °C for 3 hr for calcination (Golmohammadi et al., 2020).

3.2.8. Synthesis of Ag/Bentonite Nanocomposites

2.2 g of Na-activated Bentonite were suspend in distilled water and stirred for 30 min. Then, 100 mL of 0.2 M concentration of a silver nitrate solution, prepared by dissolving the required amount of $AgNO_3$ in deionized water were added. 100 ml of plant leaf extract were mixed to the solution (1:1) slowly dropwise with constant stirring by maintaining the temperature of about 50 °C. After 3 hr, the dark brown-colored mixture was made to settle down overnight.

The settled nanocomposites were collected and then washed with deionized water and ethanol for 4 times to remove the bio residues. Furthermore, the washed material was dried in a hot air oven at 80 °C for 12 h to obtain the powdered Ag-clay material. Finally, the powder was characterized and stored until was required (Abdelkrim et al., 2020; Hariram et al., 2021).

3.2.9. Synthesis of ZnO/Bentonite Nanocomposite

2.2 g of Na-activated Bentonite were suspend in deionized water and stirred for 30 min. Then, 100 ml of 0.2 M Zn $(CH_3COO)_2 \cdot 2H_2O$ were added and vigorously stirred. 100 mL aqueous extract of H. abyssinica was added drop wise under vigorous stirring on magnetic stirrer for 30 min at room temperature. The color change was observed from white to light brown. After 30 min, the mixtures were transferred to a heated and stirring continued at 80 °C for 30 min at pH 12 adjusted by 1M NaOH solution. The obtained light brown precipitations were centrifuged at 3000 rpm for 20 min. The particles precipitated at the bottom of the container was filtered, washed with double distilled water and ethanol. Then the samples were dried at room temperature, calcined at 550 ˚C for 1 hr and stored in glass bottle till required (Kassem, 2015).

3.2.10. Synthesis of Ag/ZnO/Bentonite nanocomposite

Ag/ZnO/Bentonite nanocomposite were synthesised from ZnO/Bentonite synthesized in the above section and $AgNO_3$ solution. 2.2 gm of ZnO/Bentonite was suspended in distilled water for 30 min at room temperature. Then, 100 mL of 0.2 M of a silver nitrate solution was added. 100 mL of plant leaf extract was mixed to the solution (1:1) slowly dropwise with constant stirring by maintaining the temperature of about 50 °C. After 3 hr, the mixture was made to settle down overnight. The settled nanocomposites were collected, centrifuged at 3000 rpm for 20 min and then washed with deionized water and ethanol 4 times to remove the bio residues. Furthermore, the washed material was dried in a hot air oven at 80 °C to obtain the powdered Ag/ZnO/Bentonite NCs. Finally, the powder was characterized and stored until it required (Asamoah et al., 2020; Krishnan & Mahalingam, 2017a).

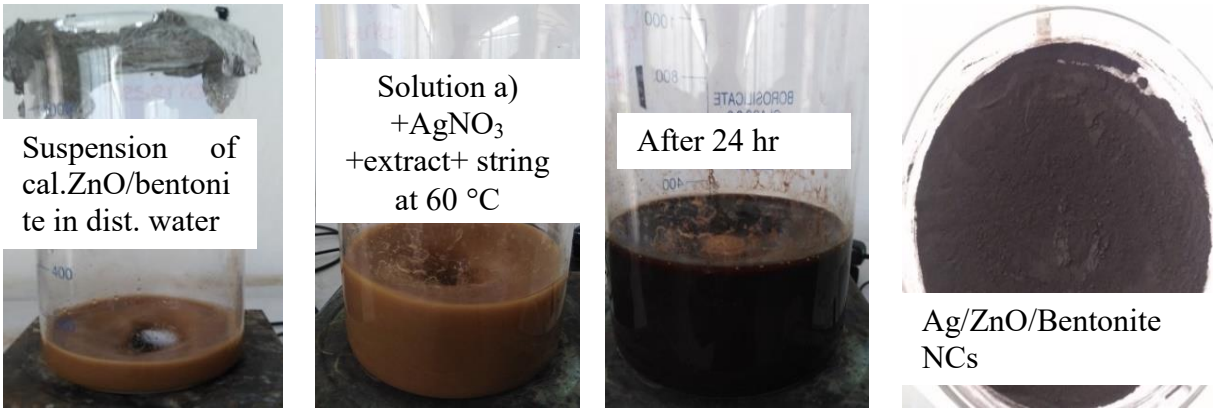

Figure 6: The scheme representation of green synthesis of Ag/ZnO/Bentonite NCs

3.3. Characterization

Different characterization techniques were performed to know the crystalline structure, optical properties, various phyto-chemical constituents involved in the reduction and stabilization and morphology of synthesized nanoparticles and nanocomposite. The detail procedures are mentioned below for each technique.

A). X-ray Diffraction (XRD)

The XRD analysis used to study the crystalline structure of the purifed bentonite (PB), Sodium-activated bentonite (Na-AB), synthesized nanoparticles and nanocomposite samples. For all samples their Powder was used in analysis. XRD works by irradiating a material with incident X-rays and then measuring the intensities and scattering angles of the X-rays that leave the material. The XRD analysis (2θ scan) was performed using an X-ray diffractometry (XRD700, Shimadzu Co., Japan). The diffraction data were recorded within a range of 2θ from 10° to 80° for Ag and ZnO NPs and from 5° to 80° for PB, Na-AB and NCs. The diffraction data were recorded at 40 kV and current of 30 mA in continuous scan mode with scan rate 3 (deg/ min) by using CuKα radiation with a wavelength of 1.5406 Å (Asamoah et al., 2020). The average crystallite sizes (D) of the powders were calculated by using Debye-Scherrer's formula, $D = 0.9\ \lambda / \beta \cos\theta$, Where, λ is the X-ray wavelength, θ is Bragg's diffraction angle, and β is the Full width at half maximum (FWHM) of the diffraction line at half of the maximum intensity.

B). **UV–Vis diffused reflectance (UV–Vis DRS) Spectroscopy**

Diffuse reflectance spectra were obtained in a spectrophotometer model (UV3600plus, Shimadzu, Japan), with a coupled integration sphere. The spectra were obtained for powder samples in the wavelength range of 200–800 nm. The absorption values were re-plotted using OriginPro 8. The reference was a 100% reflectance sample.

Kubelka-Munk function

The original idea to use the DR spectra recorded from semiconducting nanostructures to calculate the Eg was proposed by Kubelka-Munk theory in 1931 (Landi et al., 2022). Originally, the theory describes the behavior of light travelling inside a light scattering sample and based on two differential equations (Abdullahi et al., 2016; Pouraboulghasem et al., 2016):

$$-di = -(S + K) + Sjdx$$

$$dj = -(S + K)jdx + Sidx \quad \ldots\ldots\ldots\ldots\ldots\ldots (1)$$

Here i and j are the intensities of light travelling inside the sample towards its unilluminated and illuminated surfaces, respectively; dx is the differential part along the light path; S and K are the scattering and absorption coefficients, respectively. The Kubelka-Munk theory holds for a particle size that is comparable or smaller than the wavelength of incident light and DR no longer permits the secondary contributions of reflection, refraction, and diffraction.

When the thickness of sample is in the relevant limitation then it has no influence on the reflectance. Hence, the Kubelka-Munk equation at any wavelength (Milosevic & Berets, 2002), can be written as

$$\frac{K}{S} = \frac{(1-R)2}{2R} \equiv \mathrm{F}(R) \quad \ldots\ldots\ldots\ldots\ldots\ldots\ldots\ldots\ldots\ldots\ldots\ldots (2)$$

Where R is the diffuse reflectance and F (R) is called the Kubelka-Munk function. In the parabolic band structure, the Eg and absorption coefficient are related through the well-known Tauc relation (Abdel-Galil et al., 2020). The Tauc relation for a direct band gap material is given by the expression

$\alpha h\upsilon = A\ (h\upsilon - Eg)$ …… (3)

Where α is linear absorption coefficient, υ is light frequency, and A is the proportionality constant. The power of the parenthesis, n is taken equal to the 2 for direct band gap materials. When incident radiation scatters in a perfectly diffuse manner, the absorption coefficient K becomes equal to 2α. In this case, considering the scattering coefficient S as constant with respect to wavelength, the Kubelka-Munk function is proportional to the absorption coefficient α (Klier, 1972), applying eq. (2) we obtain the relation:

$[F\ (R)\ h\upsilon]^{2} = A\ (h\upsilon - Eg)$ …… (4).

C). Fourier transform infrared (FT-IR) Spectroscopy

Fourier transform infrared (FT-IR) spectroscopy helps to ascertain the identity of various phyto-chemical constituents involved in the reduction and stabilization of the nanoparticles and nanocomposites. FT-IR spectrum for dry powders of NPs and NCs were obtained using Perkin Elmer FT-IR Spectrophotometer Frontier using the technique of Attenuated Total Reflectance (ATR) in the range of 4000–400 cm^{-1} (Jamdagni et al., 2016). The values were re-plotted using OriginPro 8.

D). Morphological and Composition Characterization

Scanning electron microscopy with energy-dispersive x-ray spectroscopy (SEM-EDX-EVO18 model with low vacuum facility and ALTO1000Cryo attachment) and transmission electron microscope with high-resolution (JEOLJEM2100HRTEM) were used for understanding morphological and structural features of Ag and ZnO NPs. Selected area electron diffraction (SAED) also performed to confirm the crystal structure of ZnO NPs. Particle size and SAED image was also computed by using imageJ and Microsoft paint software.

3.4. Antibacterial Test

The antibacterial activity of *H. abyssinica* leaf powder, purified bentonite, Na Bentonite, Ag N Ps, ZnO NPs, Ag/bentonite, ZnO/bentonite and Ag/ZnO/bentonite nanocomposite were

investigated against Gram-negative bacteria *Escherichia coli (E. coli)* ATCC 25922 and Gram-positive bacteria *Staphylococcus aureus* (*S. aureus*) ATCC 25923 using disk diffusion and Broth dilution method in Adama Public Health Research and Referral Laboratory Center (APHRRLC).

3.4.1. Disk Diffusion Methods

A). Media Preparation

Muller Hinton Agar and Sheep Blood Agar Media were prepared by dissolving, 38 g of Muller Hinton powder and 50 mL of Sheep Blood in1L of distilled water separately and then sterilized by autoclave at 121 °C and 15 pound pressure for 20 min. After cooling, about 20 mL of medium are added aseptically to sterilized Petri dishes. Then the Petri dishes were labeled and incubate until they solidify. The pH of the medium is generally maintained around the physiological pH of 7.4.

B). Bacterial cultures, Serial Dilution and inhibition zone testing of Synthesised Samples

Bacterial cultures were maintained on Blood agar at 37 °C. Bacterial strains were taken from ATCC and grown aerobically on Blood Agar for 24 h at 37 °C and 0% CO_2. Bacterial suspension was prepared by taking it from blood agar and dissolving in sterile normal saline until the concentration of bacterial suspensions were achieved to1×10^8 colony forming units (CFU) mL^{-1} by comparison with the 0.5 McFarland Standard. 100 μL of 24 hr standardized culture of test bacteria was first evenly spread onto the surface of the Muller-Hinton agar plates using sterile cotton swabs. A sterile swab is used to inoculate the surface of the media in Petri dishes with making three rotations with an angle of 60° to ensure a homogeneous growth. The plates were then turned upside down. 6 mm diameter of filter paper was prepared and placed in different areas of the disc. The antibiotic Contrimoxazole was used as the positive control, and DMSO solvent was used as the negative control.

20 mg of each prepared samples were dissolved in 1 mL DMSO (20 mg mL^{-1}). From 20 mg mL^{-1} concentration of each sample, 10 mg mL^{-1}, 5 mg mL^{-1} and 2.5 mg mL^{-1} were diluted serially for PB, Na-AB, ZnO NPs and ZnO/Bentonite NCS and 5 mg mL^{-1}, 2.5 mg mL^{-1} , and 1.25 mg mL^{-1} were serially diluted from10 mg mL^{-1} for Ag NPs, Ag/Bentonite and Ag/ZnO/Bentonite NCs. 6 mm diameter disc were saturated with 20 μL of each concentration and 25 μg of Contrimoxazole (positive control) and placed on a plate covered with lids and

incubated at 37 °C and 0% CO_2 for 24 hr (Shao et al., 2015). The diameter was measured from the area around the disc where no bacterial growth has been observed, called the inhibition zone. All antibacterial tests were carried out in triplicate and the averages were reported. This diameter can be compared to the critical diameters of antibiotics Contrimoxazole and digital images were captured (Dadi et al., 2019).

3.4.2. Determination of the Minimum Inhibitory Concentration (MIC) and Minimum Bactericidal Concentration (MBC)

Ag/ZnO/Bentonite nanocomposites were tested for bactericidal effect using both the microbial culture selected for the study. The lowest concentration of material that inhibits the growth of an organism was defined as the minimum inhibitory concentration (MIC) (Gupta & Kumar, 2018). The serial dilution method was employed to determine the MIC of the Ag/ZnO/Bentonite nanocomposite. Each of the 10 test tubes was filled with 2 mL of the liquid Muller Hinton Agar medium. In the test tubes number 1, 2 mL solution containing 20 $mgmL^{-1}$ of nanocomposite that had been sonicated at room temperature was added and mixed thoroughly with the culture medium. The concentration of nanocomposites in test tube 1 becomes 10 $mgmL^{-1}$. Then, 2 ml of the content of test tube number 1 was added to test tube number 2 and mixed completely. This process was performed serially to test tube number 11. Consequently, 2 ml content of test tube number 11 was discarded. Finally, 0.2 mL of standard microbial suspensions *Escherichia coli* (ATCC 25922) and *Staphylococcus aureus* (ATCC 25923) containing 1×10^8 $CFUmL^{-1}$ microorganism were added to test tubes number 1 to 10, and the test tubes were incubated at 35 °C for 24 hr. Then, the microbial growth was studied by turbidity observation. The experiments also included a positive control (test tube containing nanoparticles and Muller Hinton Agar medium, devoid of inoculum) and a negative control (test tube containing inoculum and Muller Hinton Agar medium, devoid of nanocomposites). The negative controls indicated the microbial growth profile in the absence of nanocomposites. All the experiments were carried out in triplicate. The minimum bactericidal concentration (MBC), i.e., the lowest concentration of nanoparticles that kills 99.9% of the bacteria was also determined from the batch culture studies. For growth inhibitory concentration (MIC) the presence of viable microorganisms was tested and the lowest concentration causing bactericidal effect was reported as MBC (Chikezie, 2017). To experiments for bactericidal effect, from each test tube (Specially, negative and positive test

tubes) was inoculated on Muller Hinton Agar and incubated at 35 °C for 24 hr. The nanoparticles concentration illustrating bactericidal effect was picked out based on absence of colonies on the agar plate.

3.5. Statistical Data Analysis

Data in the current study (antibacterial activity data) were analyzed by Microsoft Excel 2010 software. The means of three replications and standard error (± SE) were also calculated for all the results obtained. Differences between means were considered significant at P-values < 0.05.

3.6. Software for Data Analysis

OriginPro 8, ImageJ, Microsoft paint, QJIS and Excel software were used to analysis the data

CHAPTER FOUR
RESULTS AND DISCUSSION

4.1. Bentonite purification and Na_2CO_3 Activation of purified Bentonite

Impurities limit the application of low-grade bentonite, resulting in a large waste of resources. A simple physical method composed of grinding, dispersion and centrifugation was adopted to purify a low-grade bentonite from Afar, Ethiopia. So, this experiment was to increase the montmorillonite content of the bentonite. A suitable amount of dispersant can change the surface potential of minerals and enlarge the flottability and stability differences between montmorillonite and impurities, which is important for their separation by aqueous dispersion. Centrifugal speed is also critical as too low speed decreases the purity level of the purified bentonite and too high speed lowers the yield of montmorillonite (Gong et al., 2016). The activation process also confirmed from X-ray diffraction patterns of the purified and Na_2CO_3 activated bentonite samples. The Na-montmorillonite obtained by soda activation at 5 g Na_2CO_3/100 g bentonite has a lower d_{001} spacing (~12.6 A˚) than the original Ca-montmorillonite (15 A˚) (Fig. 9), suggesting that the Na^+ ions replaced Ca^{2+} ions in the montmorillonite interlayer (Shah et al., 2013).

4.2. Observation Result

4.2.1. Results of Phytochemical Screening of Aqueous *Hagenia abyssinica* Plant Leaf Extract

The presence of tannins, phenolic compounds and different glycosides were confirmed during the screening of phytoconstituents of *H. abyssinica* extract. The details are given in fig.7 and table 2. Bioactive compounds such as polyphenols act as ligand and bind to metal ions and reduce to form nanoparticles. These ligands also act as particle size controllers as reported by the earlier researcher (Anbu et al., 2019).

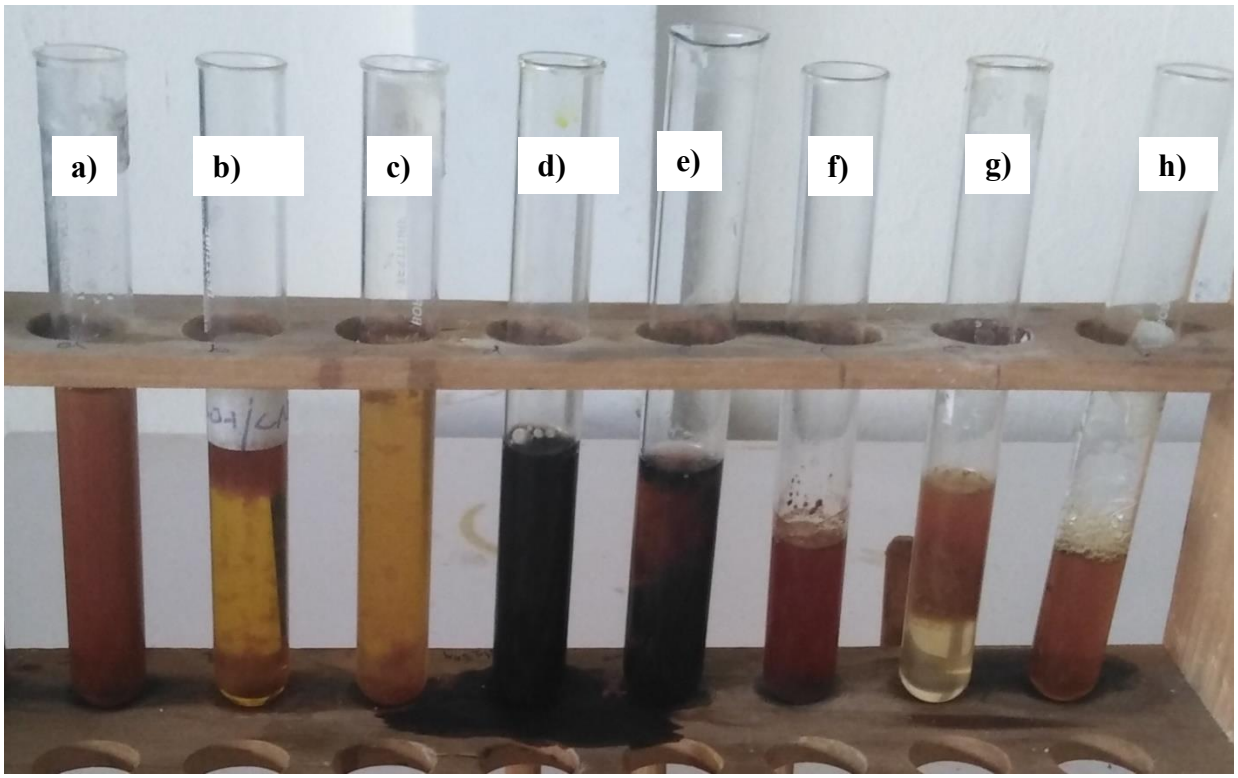

Figure 7: Results of Qualitative Tests for Phytochemical Screening

Where: a, b, c, d, e, f, g and h are test for alkaloids, reducing sugars, flavonoids, phenols, tannins, Phlobatannins, terpinoides and Saponins respectively.

Primary components of *H. abyssinica* extract are Alkaloids, reducing sugars, flavonoids, phenols, tannins, Saponins, and terpinoides. Phenolic compounds contain hydroxyl and carboxylic groups which have very high tendency to bind metal ions. Metal ions in solution interact with polyphenolic compound and help in the nucleation and formation of NPs.

Formation of nanoparticles is believed to be due to the combinational effect of bioactive compounds of plant extract (Roy et al., 2019).

Table 2: Phytochemicals result of the *H. abyssinica* plant leaves aqueous extracts

Serial No	Test /Reagent	Phytoconstituents	Observation	Result
a	Wagner's reagent	Alkaloids	A reddish-brown precipitate	+
b	Benedict's reagent	Reducing sugars	Yellow colour	+
c	Alkaline reagent test	Flavonoids	An intense yellow colour, becomes colorless on addition of diluted acid	+
d	Ferric chloride test	Phenols	Bluish black colour	+
e	Braymer's test	Tannins	Blue-green colour	+
f	HCl test	Phlobatannins	A red colour	-
g		Terpinoides	A grey coloured solution	+
h	Frothing test	Saponins	The formation of stable persistent froth	+

Where; + = the presence of phytochemical constituents, - = the absence of phytochemical constituents.

4.2.2. Synthesis of NPs and NCs

Synthesized of Ag NPs was accompanied with a distinct color change. At the beginning, the color of the mixture of plant extract and the aqueous solution of $AgNO_3$ was yellow (Appendix Fig. A 2a). However, after 3 h of moderate stirring at 50 °C, the color of the mixture first turned to light brown, brown, and finally brown-reddish (Appendix Fig. 2A b). This color change was considered one of the indications of successful synthesis of AgNPs.

The color change in the aqueous solution could be due to the surface excitation of the plasmon resonance phenomenon of silver metal (Shameli et al., 2014). In the same manner in the synthesis of ZnO NPs, the color of solution changed after 1 hr indicating the formation of colloidal ZnO suspensions. Formation of light yellow precipitate after heating the solution mixture confirms the formation of Zinc hydroxide. More over the formations of ZnO NPs was confirmed by formation of white powder after calcination of that hydroxide at 450 °C.

Commercial ZnO is white in color whereas synthesized powder may have different color depending on the synthesis method employed. For example, ZnO nano powder synthesized using plant extract may assume the color of the extract. Additionally, in nature it may exist in yellow or red color because of the presence of impurities such as manganese (Parihar et al., 2018) . It is thermo chromic compound, turning to yellow when heated and white again when cooled. Owing to oxygen vacancies or Zn interstitials, ZnO is naturally n-type direct band gap semiconductor with bulk band gap value of 3.37 eV at room temperature (RT) (Ciolan & Motrescu, 2022). However, this value may be different when its size is reduced to the nano-scale and when doped with other elements. Reduction in particles size widens its band gap as a result of quantum confinement effect.

The formation of dark brown-colored, light brown and deep dark brown mixture after synthesis and settling for 24 hr confirms the formation of Ag/Bentonite, ZnO/Bentonite and Ag/ZnO/Bentonite nanocomposite respectively and confirmed further by characterization techniques.

4.3. Analysis of Characterizations Result

4.3.1. UV-visible diffuse reflectance (UV-Vis - DRS) spectra and Bandgap Analysis

As shown from fig 8. synthesised Ag and ZnO NPs shows maximum absorption peaks at 313 and 311 nm respectively. Those absorption peaks was due to the strong surface plasmon resonance (SPR) band, these peaks depends on the particle size and shape of NPs (Krishnan & Mahalingam, 2017b). After modification, Ag/Bentonite NCs, and ZnO/Bentonite NCs shows maximum absorption peaks at 313.7, and 316 nm respectively. Whereas Ag/ZnO/Bentonite NCs shows two maximum absorption peaks at 318 and 372.7 nm due to existence of both Ag and ZnO NPs in the composite. This finding agreed with most of earlier report. For example, Ghamsari et al., 2017 reported the absorbance peak of ZnO nanoparticles

was between 310 nm and 360 nm (Ghamsari et al., 2017). Also shift in peak to higher wavelength from 311 nm to 316 nm after mixed with Na-Bentonite, in synthesis of ZnO NPs and ZnO/Bentonite NCs were associated with the formation of nanocomposites which was agreed with earlier report (Hakimi et al., 2018).

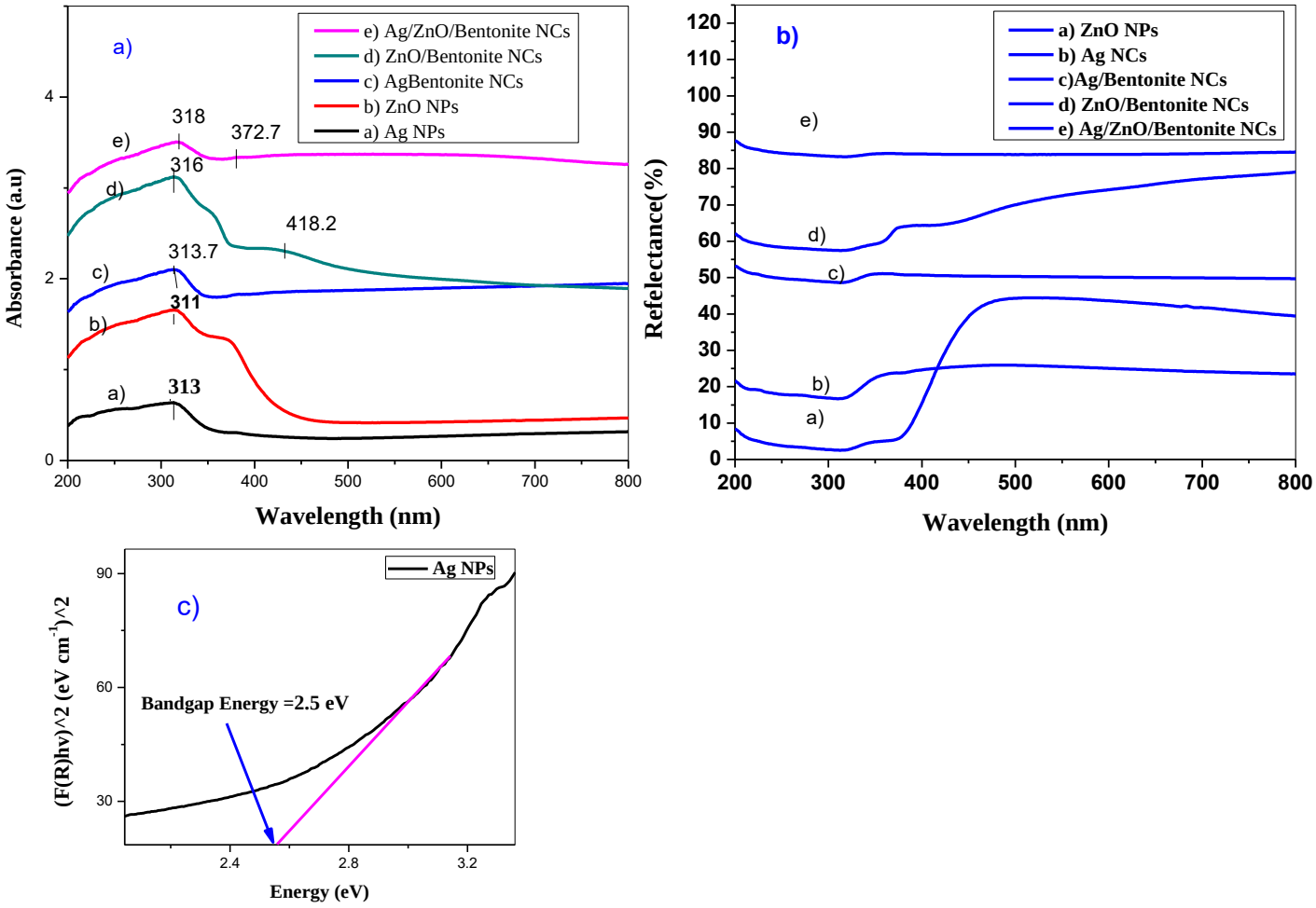

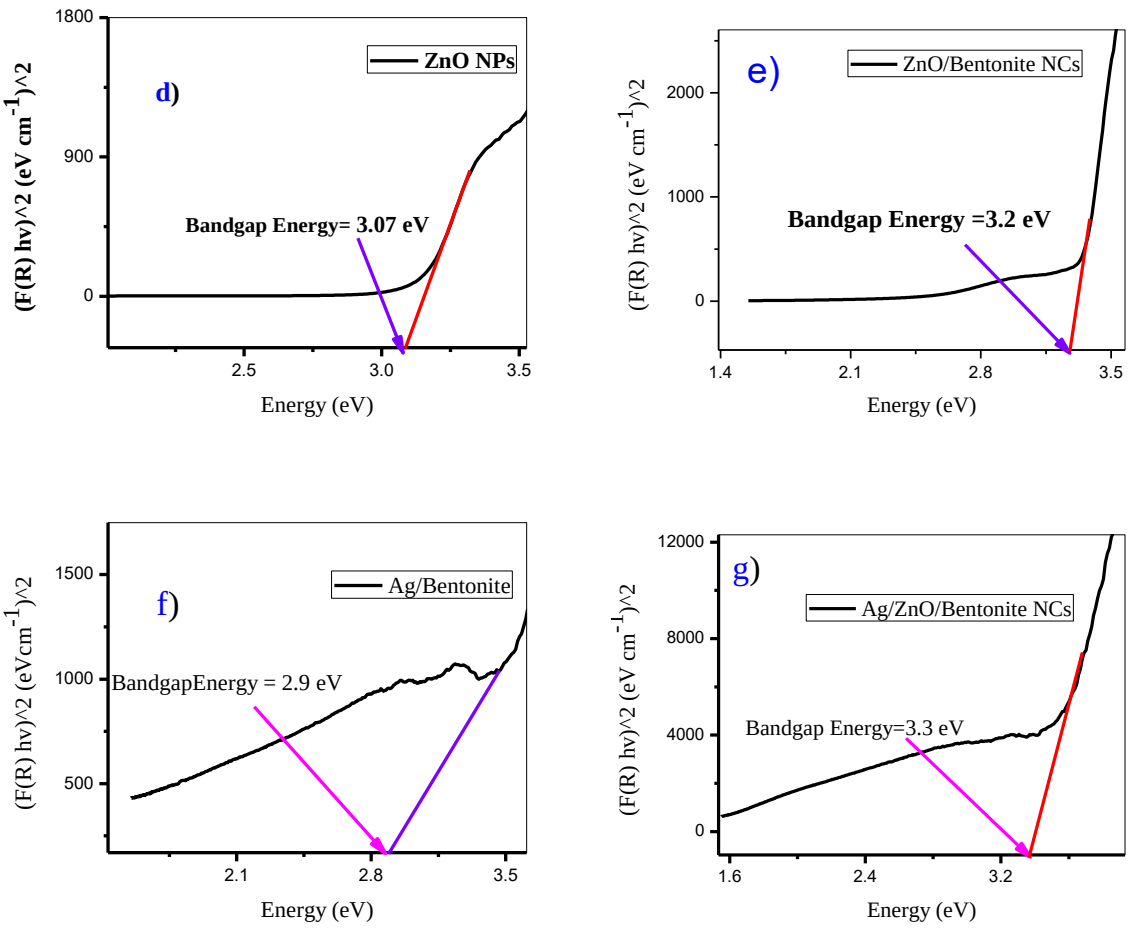

Figure 8: UV-Visible absorbance, UV-Visible diffused reflectance spectrum and Band gap of synthesized samples

Diffuse reflectance spectra (DR) is used to present a simple method for the determination of band gap of the synthesized NPs and NCs. The idea was originated from Kubelka-Munk theory which describes the behavior of light travelling inside a light scattering sample. The optical direct band gap energies of those samples were calculated by plotting the square of the Kubelka- Munk $[F(R\alpha)h\upsilon\ ]^n$ versus energy in eV, by extending the straight line from the straight segment of the graph touching the E axis. The bandgap energy, Eg of Ag NPs, ZnO NPs, Ag/Bentonite NCs, ZnO/Bentonite NCs and Ag/ZnO/Bentonite NCs was found to be 2.5, 3.07, 2.9, 3.2, and 3.3 eV respectively as shown in Fig.8. The nanocomposites are having larger band gap energy than that corresponding bulk material due to Ag, ZnO NPs involved in nanocomposite formation.

The measurement of diffuse reflection (DR) with a UV-Vis spectrophotometer is a standard method to determine the optical properties of powder nanomaterials (Us et al., 2016). Because of the confinement of the electrons and holes, the band gap energy increases between the valence band and the conduction band with decreasing the particle size. This is because the electron hole pairs are now much closer together and the Coulombic interaction between them can no longer be neglected giving an overall higher kinetic energy. This increase in bandgap can be observed experimentally by the blue-shift in the absorption spectrum of synthesized nanocomposite. A larger bandgap means that more energy is required to excite an electron from the valance band to the conduction band and hence light of a higher frequency and lower wavelength would be absorbed (M. Singh et al., 2018).

4.3.2. X - ray Diffraction (XRD) Result Analysis

A). Analysis of XRD Results of Bentonite

XRD patterns of Purified Bentonite (PB) and Sodium-activated Bentonite (Na-AB) samples are exhibited in Fig.9. Fig. 9 shows the basal reflections at the 2θ positions, of 6.24 (for PB), 6.9 (for Na-AB), 15.6 (for PB), 15.9 (for Na-AB), 19.8, 26.4, 29.4, 34.5, and 61.4°. According to the crystal data sheet JCPDS 02–0037, they correspond to basal reflections d(001), d(003), d(100), d(400), d(330), d(105) and d(300), respectively, those agreed with earlier report (Colín-Luna et al., 2018).

The d_{001}, d_{100}, d_{104}, and d_{061} diffractions of the main montmorillonite (MMT) component of PB and Na-AB are seen at 6.24 (for PB), 6.9 (for Na-AB), 15.6 (for PB), 15.9 (for Na-AB), 19.8, 34.5, and 61.4° with the distances of ~14 (for PB), 12.8 (for Na-AB), 5.67(for PB), 5.56 (for Na-AB), 4.48, 2.59, and 1.51 Å, respectively (Fig.9 and Table 3). The peaks originating from the nonclay components (dolomite (D) and quartz (Q)) are observed at 26.4 and 29.4° with the d_{400} and d_{330} values of 3.37 and 3.04 Å, respectively. It may be concluded from the comparison of the intensities of the d_{001} peak of PB, (Na-AB) and the diffractions of the nonclay components that the main component of bentonite is montmorillonite and the quartz and dolomite fractions are small which agree with other report (Caglar et al., 2009).

The PB power diffraction patterns revealed that this bentonite is in the family of smectite having similar reflection from (001) plan with inter-planar distances (d_{001}) value of 14 Å. This

shows that the natural bentonite is in calcium form (El Miz et al., 2017). The larger d_{001} distance of PB (~14 Å) than that of Na-montmorillonite (12.8 Å) may be explained as the PB was calcium-rich bentonite (Caglar et al., 2009). The Na-montmorillonite obtained by soda activation at 5 g Na_2CO_3/100 g bentonite has a lower d_{001} spacing (~12.8 A˚) than the original Ca-montmorillonite (14 A˚) (Table 3), suggesting that the Na^+ ions replaced Ca^{2+} ions in the montmorillonite interlayer. This finding agreed with early report (Shah et al., 2013). So, comparative XRD diagram of PB and of sodium exchanged bentonite actually confirms a good exchange of calcium by sodium by comparison of the lines with the (001) peak. A shift in the position of the (001) line from 14.1 Å to 12.8 Å, shows that the exchange between calcium and sodium was take place.

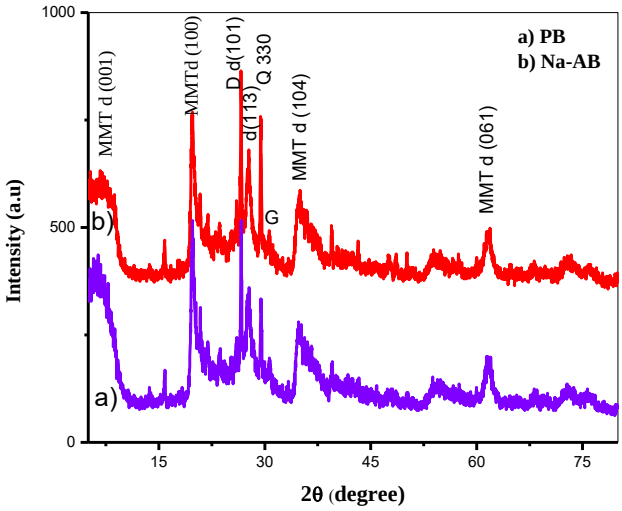

Figure 9: XRD Patterns of a) PB (Purified Bentonite) and b) Na-AB (Na- activated Bentonite)

Where, MMT: Montmorillonite, D: Dolomite, Q: quartz and G: Gypsum

Table 3: Results of Interlayer spacing and composition of PB and Na-AB

PB				Na-AB			
2θ (°)	Miller index (hkl)	d-space (Å)	Indication	2θ (°)	Miller index (hkl)	d-space (Å)	Indication
6.24	(001)	14.15281	MMT	6.9	(001)	12.80047	MMT
15.6	(003)	5.675841	MMT	15.9	(003)	5.569418	MMT

19.8	(100)	4.480335	MMT	19.8	(100)	4.480335	MMT
26.4	(400)	3.373318	D	26.4	(400)	3.373318	D
29.4	(330)	3.03557	Q	29.4	(330)	3.03557	Q
34.5	(105)	2.597612	MMT	34.5	(105)	2.597612	MMT
61.4	(300)	1.508786	MMT	61.7	(300)	1.502168	MMT

B). Analysis of XRD Results of Synthesized Nanoparticles and nanocomposites

XRD analysis was carried out to further confirm the crystal structure of the NPs and NCs. The diffraction pattern of the Ag NPs shown sharp peaks at 2θ = 38.20° (111), 43.21° (200), 64.56° (220), and 77.48° (311) indicating that the Ag NPs were well crystallized (Fig. 10). Furthermore, the diffraction peaks of the Ag NPs were in accordance with the reports of the face center cubic structure (Thi Lan Huong & Nguyen, 2019). The diffraction results were in good agreement with the data of JCPD fileno.00-004-7383 (Fm3m) (Murthy et al., 2020). There was no peak of impurity, confirming that the synthesized Ag NPs were purely silver metal. The crystallite average size of Ag NPs was calculated from the three strongest intense peak corresponding to (111), (220), and (311) crystal planes using the Debye–Scherer equation (1) (Holzwarth & Gibson, 2011), and obtained 8.14 nm. This small particle size confirms the high potential reduction and stabilization of plant extract.

$$D=K\lambda/\beta Cos\theta \qquad \text{.....equation (1)}$$

where λ is the X-ray wavelength coming from Cu-Kα (1.540560 Å), β is the full width at half maxima of the diffraction peak in radians, θ is the Braggs' angle in degrees, and K is the shape factor and its value is equal to 0.9.

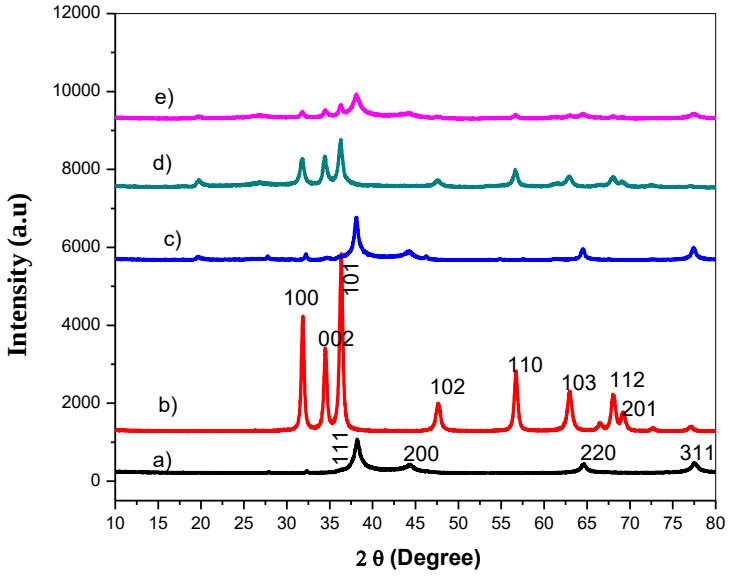

Figure 10: XRD patters of synthesized a) Ag NPs, b) ZnO NPs, c) Ag/Bentonite NCs, d) ZnO/Bentonite NCs and e) Ag /ZnO/Bentonite NCs

The XRD pattern of synthesized ZnO NPs also clearly indicates crystalline structure for the synthesized nanoparticles (Fig.10 b). The sharp diffraction peaks were observed at 2θ values 31.9°, 34.5°, 36.3°, 47.6°, 56.6°, 62.9°, 66.5°, 68° and 69.1° These peaks are indexed as of (100), (002), (101), (102), (110), (103), (200), (112) and (201) diffraction lattice planes respectively which confirm the hexagonal wurtzite structure for the synthesized nanoparticles, which in close agreement with the previous findings (Fakhari et al., 2019). All the peaks observed were coordinated with the hexagonal phase (wurtzite structure) in comparison with the data from JCPDS card No.36-1451. The XRD pattern of the ZnO NPs is in accord with the zincite diffraction in the hexagonal phase (primitive) and hexagonal wurtzite phase of ZnO with lattice constants around a=b=0.325nm, c = 0.521nm, c/a=1.61 and space group of C^4_{6v} or $P6_3mc$.This data is in well agreement with the Joint Committee on Powder Diffraction Standards (JCPDS) card no 36-1451 (Dinesh et al., 2014). It also confirms the synthesized nano-powder was free of impurities as it does not contain any characteristics XRD peaks other than ZnO peaks. The FWHM results revealed d(100) = 2.806 Å, d(002) = 2.60 Å, and d(101) = 2.487 Å, with sharp and intense peaks which closest to early findings (Madhumitha et al.,

2019). The crystallite average size of ZnO NPs was calculated from three strong peaks (31.8°, 34.5° and 36.3°) and estimated to 18.1 nm.

From XRD patters of ZnO/Bentonite NCs, Ag-Bentonite NCs, and Ag/ZnO/Bentonite NCs (Fig. 10 c-e), the Bentonite characteristic peaks are shown at 2θ values of 6.9, 19.8 and 27.7° and the prominent ZnO peaks observed at 2θ of 31.7°, 34.3°, 36.3°, 47.5°, 56.7°, 62.9° and 68.01 are attributed to (100), (002), (1 0 1), (102), (110), (103), (112) and (201) planes, respectively (fig. 10). After making composite of bentonite with ZnO NPs the reduction of the peaks as well as forming of new peaks above 2θ of 30° are probably due to the formation of ZnO/Bentonite NCs (Chakraborty et al., 2019). XRD pattern of ZnO-bentonite NCs, the left hand peaks (below 2θ of 30°) are strongly shows the bentonite character and right hand peaks (above 2θ of 30°) are strongly show the ZnO character. So, from XRD pattern (fig. 10), the synthesized ZnO-bentonite NCs were composed of ZnO and bentonite phases. The bentonite characteristics peaks intensity are lower than that of activated bentonite, this might be due to the intercalation of ZnO into the interlayers of bentonite, which changed the structure of host materials.

Table 4: Calculations of average particle sizes of Na-AB and Synthesized NPs Samples

Sample	Strong Peak position (2θ (°))	d(Å)	FWHM (°)	β(rad)	D(nm)	Average D (nm)	(hkl)
Ag NPs	38.2	2.3527	0.8496	0.0148	8.83	8.14	(111)
	64.5	1.4423	0.7714	0.0157	6.88		(220)
	77.4	1.2308	0.9000	0.0134	8.71		(311)
ZnO NPs	31.8	2.8057	0.3900	0.0068	19.15	18.1	(100)
	34.5	2.5965	0.4162	0.0072	17.8		(002)
	36.3	2.4697	0.4272	0.0074	17.3		(101)
Na-AB	19.72	4.49833	0.4548	0.0079	17.97	37.6	(100)
	26.6138	3.34670	0.1624	0.0028	49.7		(400)
	29.4131	3.03425	0.1772	0.0031	45.3		(330)

Where; Ag NPs = Silver Nanoparticle, ZnO NPs = Zinc Oxide Nanoparticle, Na-AB = Sodium-activated Bentonite and D = Crystal size, d = d-space and , FWHM = Full width at half maximum

The XRD pattern of Ag/Bentonite and Ag/ZnO/Bentonite nanocomposites were illustrated in fig. 10(c and e). Bentonite characteristic peaks are shown at 2θ values of 6.9, 19.8 and 27.7° and at 6.9, 19.6 and 26.6° for Ag/Bentonite and Ag/ZnO/Bentonite respectively. The peaks are evident in all patterns, which are also consistent with other reported works (Motshekga et al., 2015).

Table 5: Calculations of average particle sizes of and Synthesized NCs Samples

Samples		Strong Peak position (2θ (°))	d(Å)	FWHM (°)	β(rad)	D(nm)	Average D(nm)	(hkl)
Ag/Bentonite	For Ag	38.1 64.4 77.3	2.3595 1.4439 1.2322	0.6150 0.5222 0.5585	0.0107 0.0091 0.0097	12.2 12.86 11.1	12	(111) (220) (311)
ZnO/Bentonite	For ZnO	31.8 34.4 36.3	2.8120 2.6004 2.4743	0.5662 0.5436 0.5816	0.0098 0.0094 0.0101	13.5 13.9 12.9	13	(100) (002) (101)
Ag/ZnO/Bentonite	For Ag	38.1 64.5 77.4	2.35756 1.44353 1.23201	1.1271 0.8167 0.9600	0.01967 0.01425 0.01675	6.9 8.6 6.7	7.4	(111) (220) (311)
	For ZnO	31.8 34.5 36.3	2.81077 2.59565 2.46968	0.6100 0.6893 0.7775	0.01065 0.01203 0.01357	6.7 11.4 10.1	9.4	(100) (002) (101)

After nanoparticles of Ag and ZnO were intercalated in the clay, additional peaks are observed corresponding to the formation Ag and ZnO in the composites. These peaks were reflected at 2θ = 38° for Ag which can be attributed to the (111) crystallographic planes of the face-

centred cubic (fcc) silver crystals (Dupraz et al., 2015), and at 2θ = 32, 34 and 36° corresponding to (100), (002) and (101), which reflect the presence of wurtzite phase of ZnO (Hashim et al., 2019). The presence of the diffraction patterns of Ag, ZnO and bentonite confirms that the prepared composites are composed of these three species.

XRD pattern have also been used to calculate the average crystalline sizes (D) of samples with the help of Scherrer equation (equation (1). The calculated D values of Ag NPs, ZnO NPs and Na-AB were 8.14, 18.1 and 37.6 nm respectively. The D values in NCs decreased due to intercalation of NPs into Na-Bentonites. Hence, the intercalation process causes structural changes in Na-Bentonite samples. It may be due to the presence of strong electrostatics attraction and hydrogen bonding forces in between Na-bentonite and intercalate NPs (Krishnan & Mahalingam, 2017a).

4.3.3. Fourier Transforms Infrared (FT-IR) Results Analysis

FT-IR measurements were carried out to identify the major functional groups in the Plant leaf extract, green synthesized Ag NPs, ZnO NPs, Ag/Bentonite, ZnO/Bentonite, and Ag/ZnO/Ben tonite NCs using plant leaf extract. That was to identify possible involvement of plant leaf extract in the synthesis and stabilization of NPs and NCs.

Table 6: FT-IR Profile of the *H.abyssinica* plant Leaf Extract

Peak values (cm^{-1})	Functional group	Class
3400	-OH	Alcohol
2930	-C-H (Stretch)	Alkane
2845	C-H	Alkane
2260	C≡N	nitrile
2072	C≡C stretching	Alkyne
1628	C=C	Alkene(conjugated)
1359	C-O	Alcohol
1010	C-O (strech)	Alcohols

The peak observed at 3400 cm^{-1} is typical of –OH (alcohol) while, 2930 and 2845 cm^{-1} can be said to be C-H (stretch) for alkanes. The peak at 2260 cm^{-1} indicates the presence of nitrile

group. Also, the peak at 1628 cm^{-1} (C=C) is that of conjugated alkenes. The signal at 1359 (C-O) is that of alcohol and 1010 cm^{-1} (C-O stretch) is typical of alcohols also. (Table 6 and Fig. 10) The FTIR analysis revealed the presence of two basic functional group; C=O and O-H which indicate the presence of alcohol, phenol or esters. The O-H (Alcohol/ Phenol) group was observed in the leaf extract with wavelengths of 3400 cm^{-1}. The peaks between the range of 1000 – 1500 cm^{-1} are present in the extract is due to the presence of the C-O bond. This band may either be an alcohol, ester, ether or anhydride. The presence of secondary amine was also detected at 1628 cm^{-1} for the extract. Tannins and flavonoid are simple phenolic compounds that serve as defense against pathogens and herbivores (S. Kumar et al., 2020).

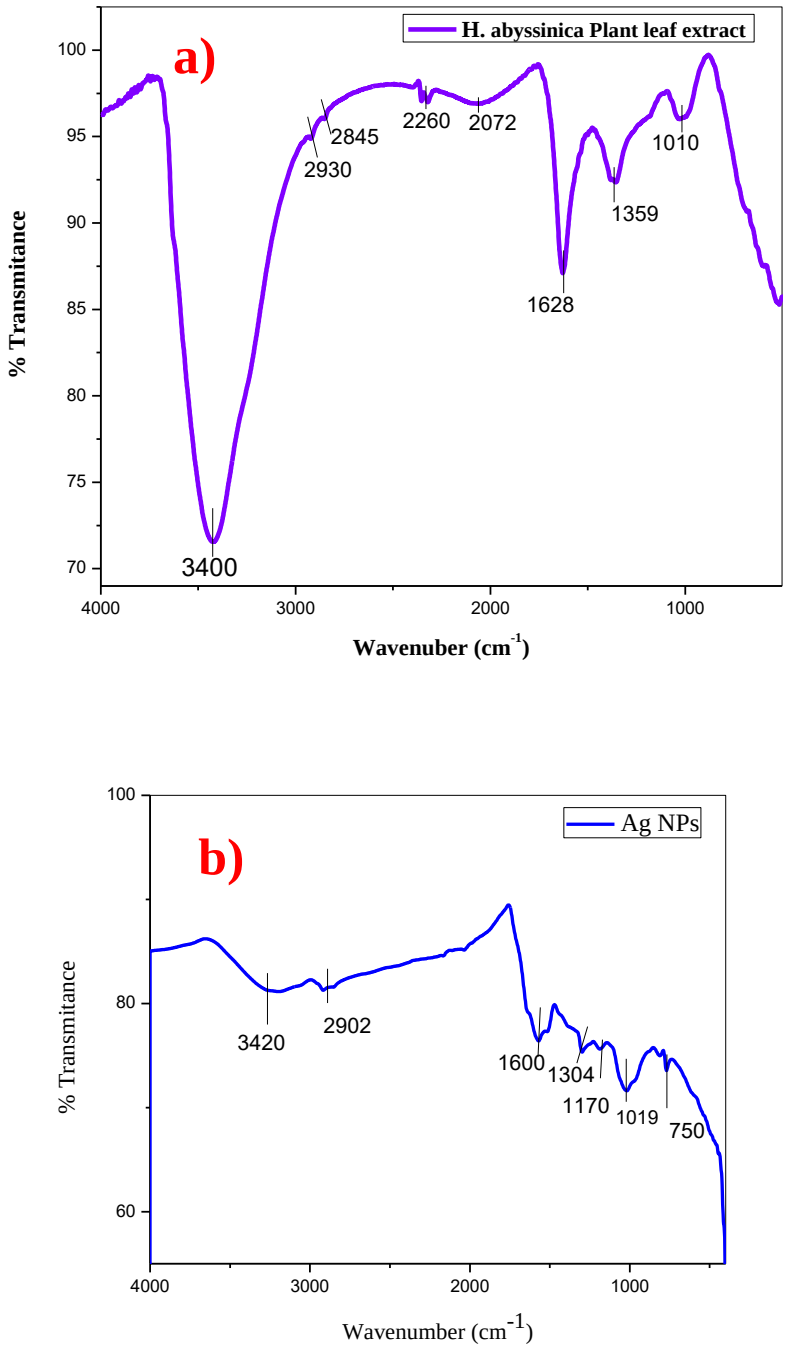

Figure 11: FT-IR spectra of *H. abyssinica* plant leaf extract (a) and Ag NPs (b)

FT-IR was used to characterize the biomolecules that were responsible for reducing Ag^{+} ions and capping the biosynthesized AgNPs. Fig.11b shows the absorption bands of the biosynthesized Ag NPs in the range of 400-4000 cm^{-1}. A band at 3420 cm^{-1} is assigned to the

stretching vibration of the hydroxyl (-OH) group in plant powder. A band at 2902 cm^{-1} arises from the sp^3 bond of aromatic C-H bending for the plant powder. A potent peak at 1600 cm^{-1} is due to C=O bond adsorption of double carbonyl group in ketone. The bands at 1304 cm^{-1} are because of C=C double bonds. The peaks at 1170 and 1014 cm^{-1} are assigned to the absorption of C–O and C–O–C bonds, respectively. These results demonstrate that many organic constituents of plant powders were adsorbed on the surface of biosynthesized Ag NPs. In addition to this, the FTIR spectrum of Ag NPs shows peaks corresponding to the band at 750 cm^{-1} which is possibly due to the interaction of Ag with protein molecules of extract.

Fig. 12 shows the FT-IR absorption bands of the biosynthesized ZnO NPs (calcined at 450 °C for 1 hour) in the range of 400-4000 cm^{-1}. From the fig. 12, it is observed that the bands are at 3405 cm^{-1}, 2350 cm^{-1}, 2169 cm^{-1}, 1989 cm^{-1}, 1439 cm^{-1}, 1000 cm^{-1}, 881 cm^{-1} and 526 cm^{-1}. The broad peaks around 3405 cm^{-1}corresponds to H-bonded or OH stretch bond vibration of polyphenols and flavonoids. Also they were due to the water adsorption on the surface of zinc oxide nanoparticles. The peaks at 2350 cm^{-1} corresponds to N-H stretching or the C=O stretching vibrations (Awwad et al., 2014). The band which appeared at 2169 cm^{-1} is due to C=C stretching (Dobrucka & Długaszewska, 2016). C=C=C stretching were observable at 1989 cm^{-1} .The band at 1439 cm^{-1} were attributed to the C-C stretching of aromatic ring (Suresh et al., 2018). The band at 1000 cm^{-1} is assigned to the absorption of C-O (stretch). The bands at 881 cm^{-1} were due to C=C bending of alkene. The peak in the region between 400 and 600 cm^{-1} is allotted to Zn–O (Yuvakkumar et al., 2015). So, the band located near 600 cm^{-1} is assigned to Zn-O stretching vibration (S. P. Rajendran & Sengodan, 2017). FTIR analyses confirmed the presence of natural phenolic antioxidant compounds and hence offer favorable effects for the synthesis of ZnO NPs.

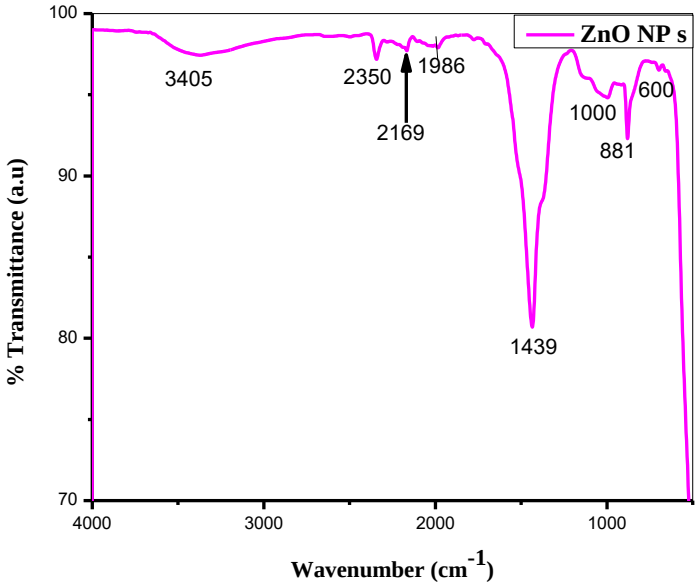

Figure 12: FT-IR spectra of synthesized ZnO nanoparticles

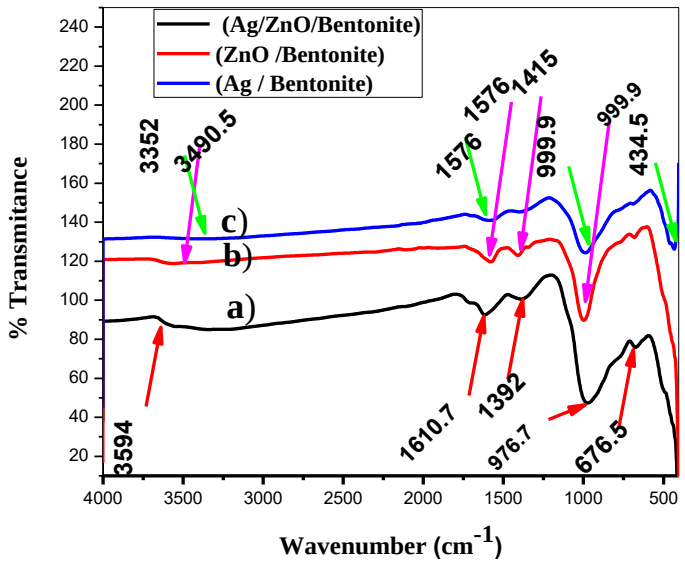

Figure 13: FT-IR spectra of synthesized a) Ag/Bentonite, b) ZnO/Bentonite and c) Ag/ZnO/Bentonite nanocomposites using *H. abyssinica* plant leaf extract

The FT-IR spectra of Ag/Bentonite, ZnO/bentonite and Ag/ZnO/Bentonite nanocomposite were displayed in Fig.13 a-c. The bands of nanocomposites at around 3490-3590 cm^{-1} can be assigned as the stretching vibration absorption peaks of O–H, 1576-1610 cm^{-1} was attributed to C=O and C=C bending mode of vibrations. The band at 1392-1415 cm^{-1} suggests the presence of C-C stretching vibration, 1000 cm^{-1} was attributed to the stretching vibration absorption peaks of Al–O and Si–O. The Al–O–Si deformation and Zn–O stretching vibration were shown at the range of 420-520 cm^{-1} and 476 cm^{-1} is due to Zn–O stretching vibration (Chakraborty et al., 2019; Kassem, 2015).This results relived the involvement of plant extract in the formation of nanocomposites and the spectra may suggest a certain interaction between the clay and the nanoparticles.

4.3.4. Scanning Electron Microscopy -Energy dispersive X-ray spectroscopy (SEM-EDX) of ZnO NPs

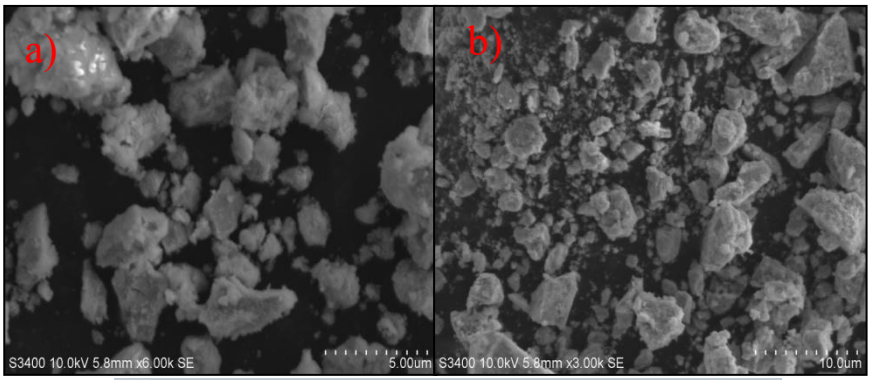

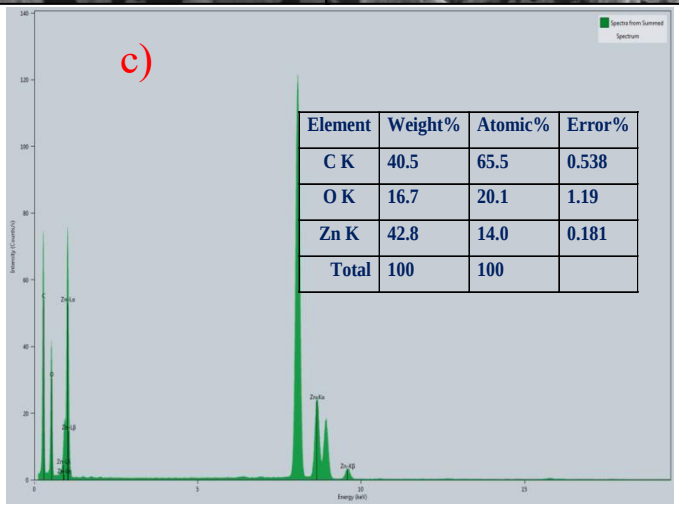

Element	Weight%	Atomic%	Error%
C K	40.5	65.5	0.538
O K	16.7	20.1	1.19
Zn K	42.8	14.0	0.181
Total	100	100	

Figure 14: SEM-EDS spectrum of ZnO NPs

SEM image showed in Fig. 16 a and b from this image, it is evident that the morphology of ZnO NPs is hexagonal, rod-shaped or spherical at different nanometer scales. Analysis of EDX was confirmed the presence of elemental Zn and O signal of the ZnO NPs (Fig. 14 c). It is also possibly believed that the presence of C is basically from the capped bioactive compounds.

4.3.5. Transmission electron microscopic (TEM) images and SAED

Transmission electron microscopic (TEM) study was carried out to obtain information about the internal structure (size and morphology) of the biosynthesized Ag and ZnO nanoparticles as shown in Fig. 15. From the TEM image, it is clear that the morphology of ZnO NPs is hexagonal, rod-shaped or spherical at different nanometer scales and the size ranges between 5 - 35 nm. The average diameter of ZnO nanoparticles was found to be around 18.5 nm which best fit with XRD results.

The TEM micrographs which exhibited very finely grained Ag NPs with spherical, cylindrical, as well as hexagonal shapes are presented in fig.15 (S1). All these particles with varying sizes from 3 nm to 20 nm with an average particle size of 10.8 nm, which best fit with XRD results, as determined by imageJ Software are as shown in fig.15 (S2).

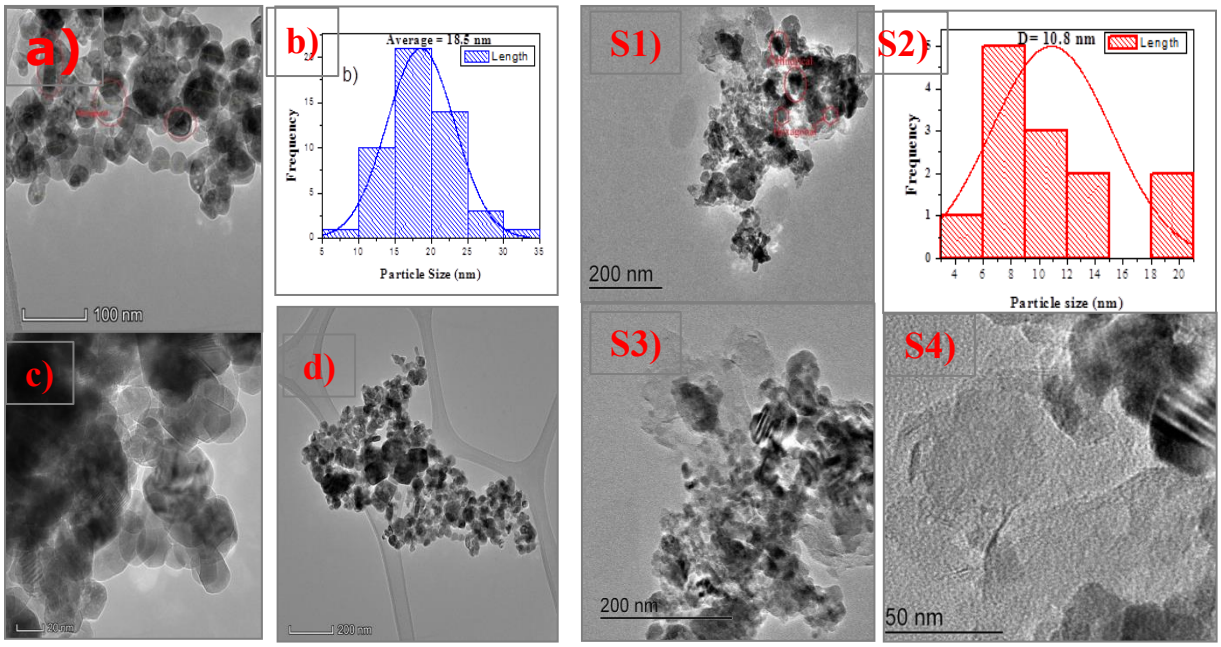

Figure 15: TEM images of ZnO NPs (a, c and d) and Ag NPs (S1, S3 and S4) at different scale, and histogram show size distribution of ZnO NPs (b) and Ag NPs (S2) obtained from TEM images

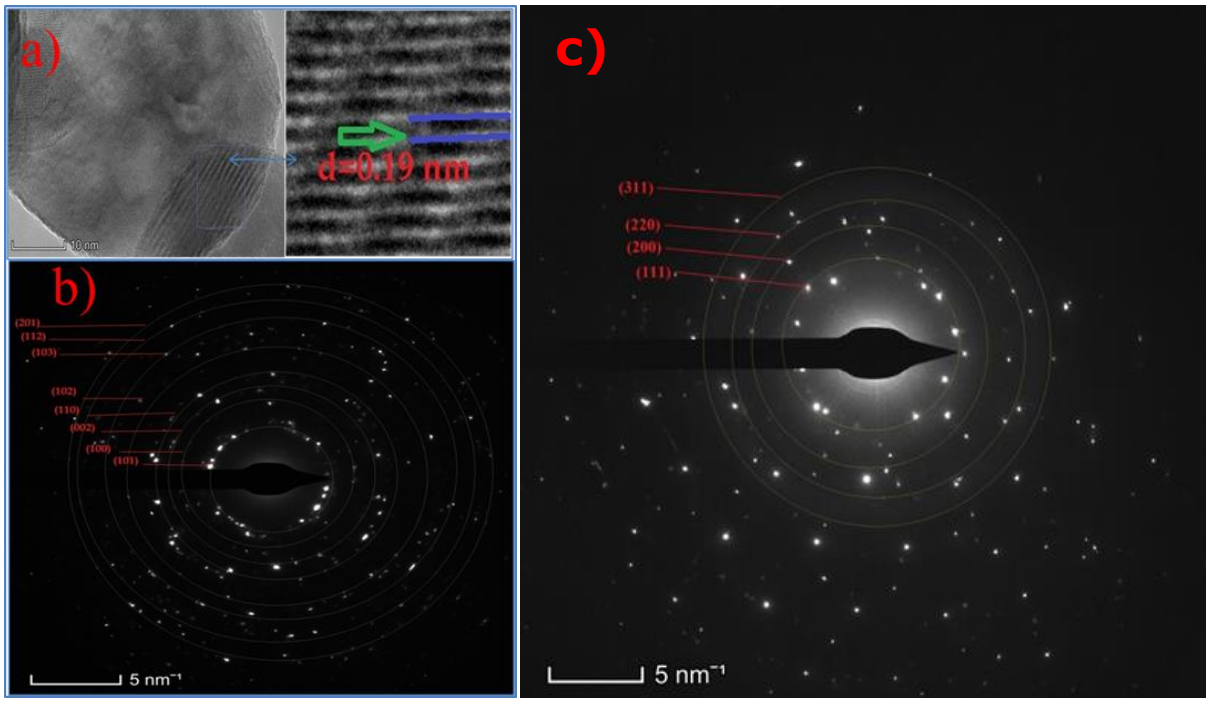

Figure 16: HRTEM of ZnO NPs (a), SAED pattern of ZnO NPs (1 to 8 spots) (b) and Ag NPs (1 to 4 spots) (c) with crystal planes

HRTEM shows the crystalline structure of single ZnO nanoparticle, with visible lattice fringes. A lattice spacing of 0.19 nm was calculated, corresponding to the plane family (102) of hexagonal (wurtzite) ZnO (Fig.18 a). Additionally, Fig. 16 b shows selected area electron diffraction (SAED) pattern and the results are consistent with the XRD diffractogram.

The SAED pattern of ZnO NPs (fig. 16 b) contained eight bright ring (small spots making up a ring) each corresponding to specific crystal planes. The d-spacing values for all the spots depicted in the SAED pattern of ZnO NPs (fig.18) are presented in table 7. Each spot on the SAED pattern corresponds to specific set of lattice planes. The XRD pattern of ZnO NPs presented earlier in fig.8, revealed 8 major peaks corresponding to (101), (100), (002), (110). (102), (103), (112), and (201) planes of hexagonal phase (wurtzite structure) of pure ZnO NPs (JCPDS card No.36-1451 ($P6_3mc$)). The d-spacing values of the derived diffraction planes from spot 1 to spot 8; d_{101}ZnO =2.47 Å, d_{100} ZnO =2.80 Å, d_{002} ZnO =2.59 Å and d_{110} ZnO =1.62 Å, d_{102} ZnO = 1.90 Å, d_{103} ZnO =1.47, d_{112} ZnO= 1.37 Å and d_{201} ZnO = 1.36 Å are in good agreement with XRD diffraction pattern of ZnO NPs.

Table 7.The d-spacing values for ZnO NPs and Ag NPs from their SAED pattern

NPs	1/2r (nm^{-1})	1/r (nm^{-1})	r (nm)	d-spacing(Å)	(hkl)
ZnO	8.096	4.048	0.247	2.47	(101)
	7.14	3.57	0.28	2.80	(100)
	7.72	3.86	0.259	2.59	(002)
	12.34	6.17	0.162	1.62	(110)
	10.52	5.26	0.190	1.90	(102)
	13.6	6.80	0.147	1.47	(103)
	13.62	6.81	0.37	1.37	(112)
	14.7	7.35	0.136	1.36	(201)
Ag	8.65	4.33	0.231	2.31	(111)
	9.52	4.76	0.210	2.10	(200)
	13.07	6.53	0.153	1.53	(220)
	16.66	8.33	0.120	1.20	(311)

4.4. Antibacterial Activity Analysis

4.4.1. Disk Diffusion Methods

NB: The corresponding concentration of A to D, and X_n abbreviations are illustrated in table 8 and 9.

The antibacterial activity of the prepared NPs and NCs was tested at APHRRLC against Gram- negative *Escherichia coli (E. coli)* ATCC 25922 and Gram-positive *Staphylococcus aureus (S. aureus)* ATCC 25923 bacteria through the disk diffusion method. Contrimoxazole (25 μg) antibiotics and DMSO was used as positive and negative control respectively. The standard Contrimoxazole (at 25 μg) has the antibacterial activities within the range of 18.3 ± 0.3 to 23.7 ± 0.3 and 20.7 ± 0.3 to 24.3± 0.3 for *E. coli* ATCC 25922 and *S. aureus* ATCC 25923 respectively. DMSO has no activity (6 mm) on both tested bacterial strain and it was used as solvent in samples serial dilution.

Figure 17-21 illustrates photographs of the antibacterial tests results of synthesised samples and the details are summarized in Table (8 and 9). The presence of an inhibition zone indicates the antibacterial effect of the NPs and NCs. The results reveal that purified bentonite (denoted with "X_6" in (Fig. 19)) and Na- bentonite (denoted with "X_7") does not exhibit any antibacterial effect. While the Plant powder (denoted with "X_8") has an effect as shown by the inhibition zone and the results were more pronounced on Gram-positive bacteria *(S. aureus)*. *H. abyssinica* plant leaf powder showed significant antibacterial activities ($P < 0.05$) against both tested bacterial strain. The maximum inhibition zone of plant powder toward *S. aureus* was 10 mm at 20 mg/mL and minimum 8.3 mm at 2.5 mg/mL. Whereas 9 mm at 20 mg/mL and 7.3 ± 0.3 mm at 2.5 mg/mL were the Maximum and minimum values respectively toward *E. coli* (detail in Table 9).

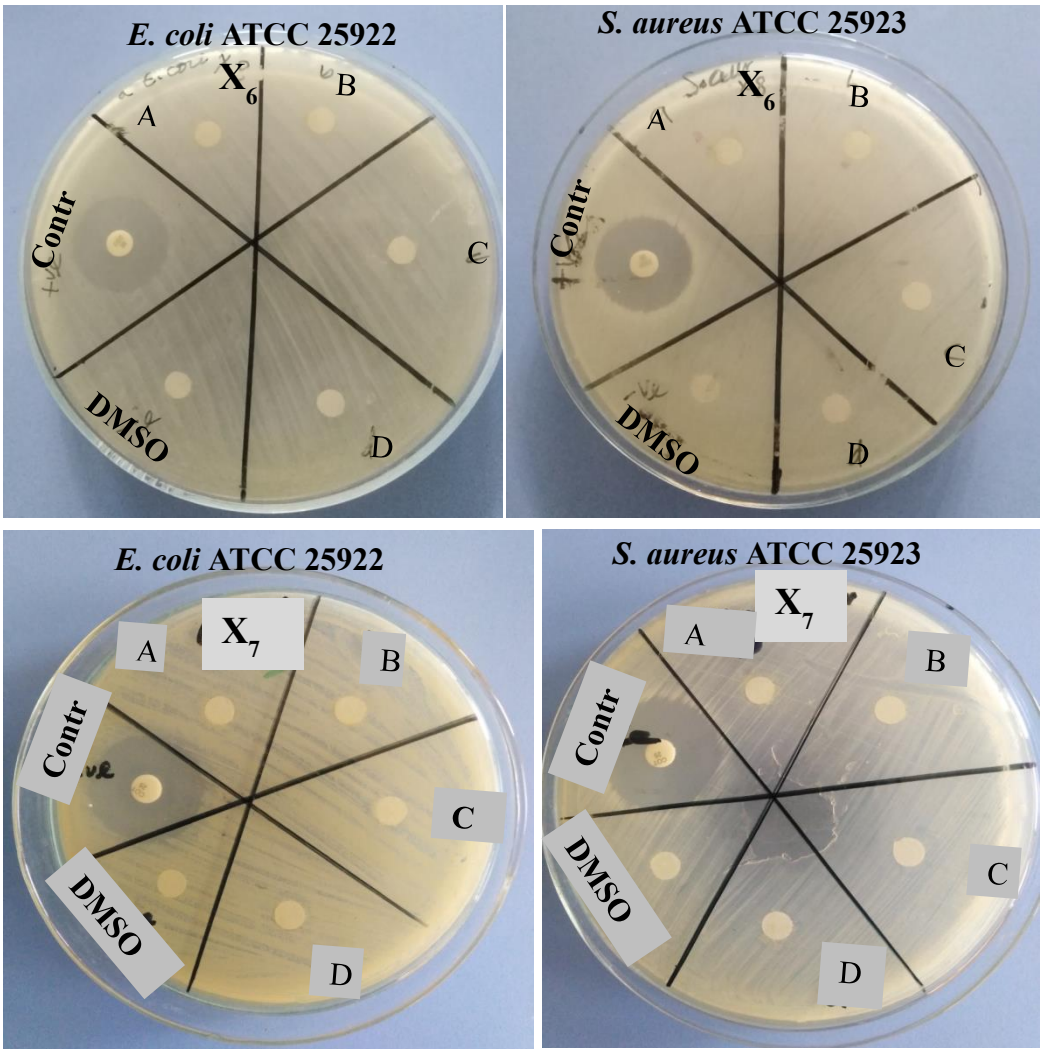

Figure 17: Photographs of antibacterial activities of X_6 (PB) and X_7 (Na-AB)

The antibacterial effect of plant powder can be attributed to the large number of different chemical compounds such as (phenolic compounds and its derivative compounds, the esters of weak acid, fatty acid, and others) are presented in plant leaf powder. Tannins and flavonoid are simple phenolic compounds that serve as defense against pathogens and herbivores. The antioxidant property of phenolic compounds is attributed to the free radical scavenging capacity, donating hydrogen atom, electrons or chelate metal cations (Minatel et al., 2017). Thus chemical components can affect multiple target sites against the bacterial cells (Gonelimali et al., 2018). *E. coli* bacteria are more resistance against *H. abyssinica* plant leaf powder than *S. aureus* due to Gram–negative bacteria have a thin peptidoglycan layer with an

additional outer membrane consisting of lipopolysaccharide. This additional membrane means that there is also an extra membrane layer termed periplasm, which makes it resistance than Gram-positive, which contain a thick layer of peptidoglycan in their cell walls (Slavin et al., 2017).

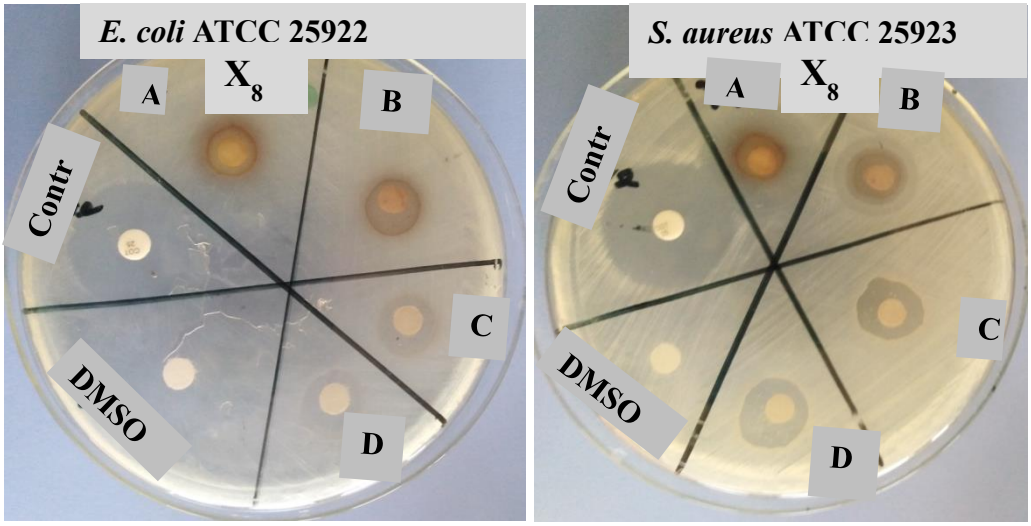

Figure 18: Photographs of antibacterial activities of X_8 (*H. abyssinica* Plant leaf extract)

The antibacterial activity of the synthesized Ag NPs was investigated against *E. coli* ATCC 25922 and *S. aureus* ATCC 25923. The viable disc diffusion method was performed to assess the antibacterial properties of Ag NPs at various concentrations (10, 5, 2.5 and 1.25 mg/mL) (denoted with "X_1"). The growth result of *E. coli* ATCC 25922 and *S. aureus* ATCC 25923 that were exposed to various concentrations of Ag NPs are shown in Fig. 19 and Table 8. The results show that Ag NPs exhibited significant antibacterial activities against both bacteria even for the lowest concentration at 1.25 mg/mL.

The antibacterial of Ag NPs (denoted with "X1") was displayed in Fig. 21. It's inhibition zone was between 10.3 ± 0.3 to 11.6 ± 0.3 mm and 11.3 ± 0.3 to 14.3 ± 0.3 mm for *E. coli* ATCC 25922 and *S. aureus* ATCC 25923 at 1.25 mg/mL to 10 mg/mL respectively the detail was described in table 8. Those results show *S. aureus* ATCC 25923 bacteria were more sensitive toward Ag NPs. This is due to bacterial structure as mentioned above. The result relieved that the effect was dose-dependent. Because the result shows as Ag NPs concentration increases from 1.25 mg/mL to 10 mg/mL the activity also increased (Table 8).

The reasons behind Ag NPs activities toward those bacteria are due to having the ability to penetrate bacterial cell walls, changing the structure of cell membranes and even leading to cell death. The strong antimicrobial action of Ag NPs is related to their nanoscale size and unique properties (Kukushkina et al., 2021). Their efficacy is not only to their nanoscale size but also to their reactivity towards bacteria DNA or amino acids. They can increase the permeability of cell membranes, produce reactive oxygen species, and interrupt replication of deoxyribonucleic acid by releasing silver ions (Yin et al., 2020) and as a concentration of this NPs increase the Ag ions released to the bacterial cell also increase. Current results also confirm as the antibacterial activity of Ag NPs are dose dependent. This suggests that the inhibition zone increased as concentration of Ag NPs (Table 7).

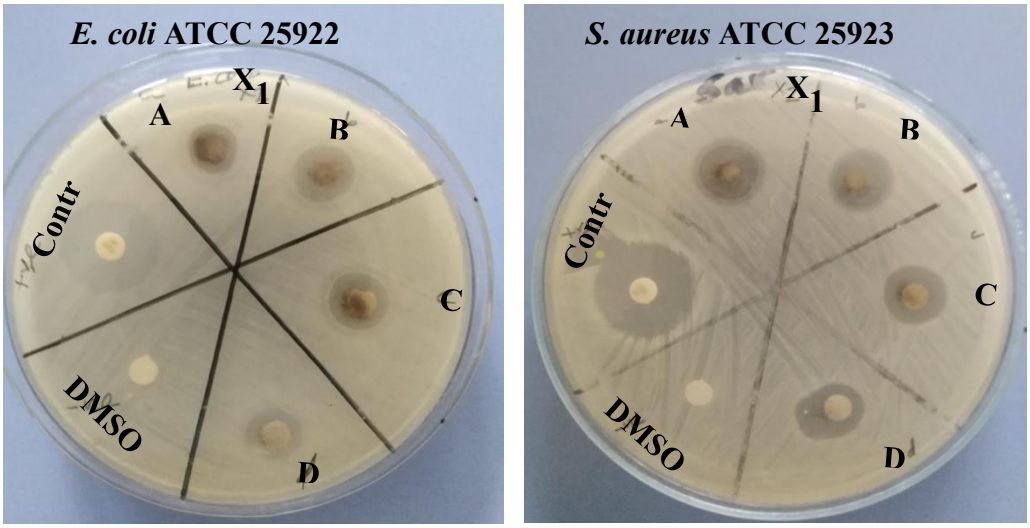

Figure 19: Photographs of antibacterial activities of X_1 (Ag NPs)

The antibacterial activity of ZnO nanoparticles was evaluated by measuring the zone of inhibition against the test organisms. The sizes of the zones of growth inhibition are presented in Table 8. The results indicated that ZnO nanoparticles showed effective antibacterial activity against both tested strains, but its activities were less than Ag NPs. Generally, the results showed that that the inhibitory effect of ZnO increased with increasing of concentration ($P < 0.05$).

In Table 8 zone of inhibition for standard Contrimoxazole (denoted with "Contr"), DMSO and 0.2 M of ZnO NPs (denoted with "X_4") against both Gram-negative (*E. coli* ATCC 25922)

and Gram-positive (*S. aureus* ATCC 25923) are shown. There photograph also shown on Fig. 17. There inhibition zones are 20.3 ± 0.3 mm, 6 mm and 10.3 ± 0.3 mm at 20 mg/mL, 10 ± 0 at10 mg/mL, 7.6 ± 0.3 mm at 5 mg/mL and 6.3 ± 0.3 mm at 2.5 mg/mL respectively for Contrimoxazole, DMSO and ZnO NPs (with different dosage) against *E. coli* ATCC 25922. Whereas 21.3 ± 0.3 mm, 6 mm and 11 ± 0.6 mm at 20 mg/mL, 10.3 ± 0.3 at10 mg/mL, 8± 0 mm at 5 mg/mL and 7 ± 0.6 mm at 2.5 mg/mL respectively against *S. aureus* ATCC 25923. A comparison of zone inhibition values shows a larger zone of inhibition for Gram-positive bacteria (*S. aureus* ATCC 25923) than that of Gram- negative (*E. coli* ATCC 25922) bacterial strain toward standard and different dosage of ZnO NPs. The observed better inhibition zones shows that the synthesized ZnO NPs disrupt the membrane with high rates of surface oxygen species generation and finally cause the death of pathogens (Suresh et al., 2018).

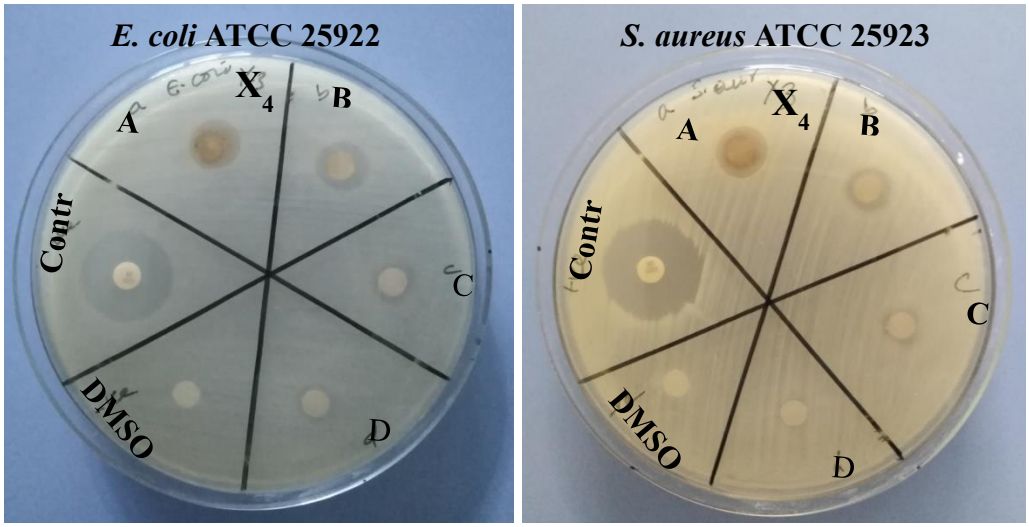

Figure 20: Photographs of antibacterial activities of X_4 (ZnO NPs)

ZnO shows good antibacterial property on both gram-positive and gram-negative bacteria. But, the results more pronounced against gram-positive this is might be due to the bacterial structure mentioned above.

There are different mechanisms for NPs to be an antibacterial. Those mechanisms include the release of antimicrobial ions (Espitia et al., 2012), the interaction of NPs with microorganisms (Lin et al., 2018), and the formation of ROS by the effect of light radiation(Jalal et al., 2010). Espitia et al., 2012 reported, the release antimicrobial ion/solubility of metal oxides is

dependent on different factors such as the concentration of metal oxides, time of interaction, and the nature of microorganisms (Espitia et al., 2012).

ZnO nanoparticles cause disruption of bacterial membranes probably by the production of reactive oxygen species, such as superoxide and hydroxyl radicals. Moreover, ZnO nanoparticles have positive zeta potential at their surface. This depends on the nature of the surface of different bacteria. Moreover, the antibacterial activity is reported to be dependent on the concentration of ZnO nanoparticles and the impact of the type of surfactant used (Dobrucka & Długaszewska, 2016).

Composites of Ag/Bentonite (denoted with "X_2") and ZnO/Bentonite (denoted with "X_5") show good antibacterial property, which confirm that they can also be used alone for antibacterial activity. The inhibition zone results of Ag/Bentonite (denoted with "X_2") was 14 ± 0 mm at 10 mg/mL, 13.3 ± 0.7 at 5 mg/mL, 13 ± 0.6 mm at 2.5 mg/mL and 12 ± 0 mm at 1.25 mg/mL against *E. coli* ATCC 25922 and 14.7 ± 0 mm at 10 mg/mL, 13.7 ± 0.3 at 5 mg/mL, 13.3 ± 0.3 mm at 2.5 mg/mL and 12.3 ± 0.3 mm at 1.25 mg/mL against *S. aureus* ATCC 25923. Similarly, ZnO/bentonite NCs (denoted with "X_5") show good antibacterial activities than ZnO NPs towards both tested bacterial strain (detail in Table 9).

The inhibition zone results indicate that both composites perform much better in inhibiting bacterial growth than Ag and ZnO NPs. The bactericidal effect of Ag and ZnO nanoparticles in the composites can be explained by their nano-scale exceptional properties. Both bulk materials of Ag and ZnO possess bactericidal properties. But at nano-scale, their nanoparticles exhibits more pronounced bacterial effects towards a broad range of microorganisms. Their small size allows for better penetration and interaction with the bacteria, disrupting the cell membrane, and hence their effectiveness as bactericidal material is increased compared to their bulk material (Motshekga et al., 2013). Furthermore, a combination of the two composites (Ag/ZnO/Bentonite, denoted "X_3") results in an excellent antibacterial activity. The antibacterial activity was more pronounced against the Gram-positive (*S. aureus* ATCC 25923) than the Gram-negative (*E. coli* ATCC 25922) (Table 8). The inhibition zone results of Ag/ZnO/Bentonite NCs (denoted with "X_3") was 14.3 ± 0.3 mm at 10 mg/mL, 13.7 ± 0.3 at 5 mg/mL, 13.3 ± 0.3 mm at 2.5 mg/mL and 12.3 ± 0.3 mm at 1.25 mg/mL against *E. coli* ATCC

25922 and 17 ± 0 mm at 10 mg/mL, 16.3 ± 0.3 at 5 mg/mL, 15.3 ± 0.3 mm at 2.5 mg/mL and 14.3 ± 0.3 mm at 1.25 mg/mL against *S. aureus* ATCC 25923.

The main objective of combining these three nanoparticles: Ag NPs, ZnO NPs, and Na-Bent to develop composite with the better antibacterial to target both the Gram-negative (*E. coli*) and Gram-positive (*S. aureus*) bacteria. The results obtained suggest that the composite can be used as an effective antibacterial material in this application. The enhanced antibacterial activity of the composites can be attributed to chemical and physical properties of the nanoparticles together with the large surface area of the Na-AB. This means that a large amount of nanoparticles were highly dispersed per unit area of the bentonite surfaces, thus, maximizing antibacterial activity. In such combinations, nanoparticles are largely attached on bentonite surfaces which ensure uniform dispersion, as unsupported nanoparticles tend to agglomerate and hence reducing their final properties (Motshekga et al., 2015) .

There are a number of factors that could influence the results of the disc diffusion assay. Firstly, the diameter of the zones is affected by the rate of diffusion of the antimicrobial compound and thus may not exactly represent the potency of the Sample's antimicrobial activity. Where studies of Sample's are concerned, the disc preparation technique could present with another problem wherein the Samples was not properly and evenly impregnated into the paper discs. Another important factor is the standardization of the inoculum size to 0.5McFarland turbidity. This inoculum size is important to ensure confluent or almost confluent lawn growth as a smaller inoculum size (such that single colonies are seen) may produce falsely large inhibition zones while a bigger inoculum size (thick bacterial lawn) may produce falsely smaller zones instead (Razmavar et al., 2014).

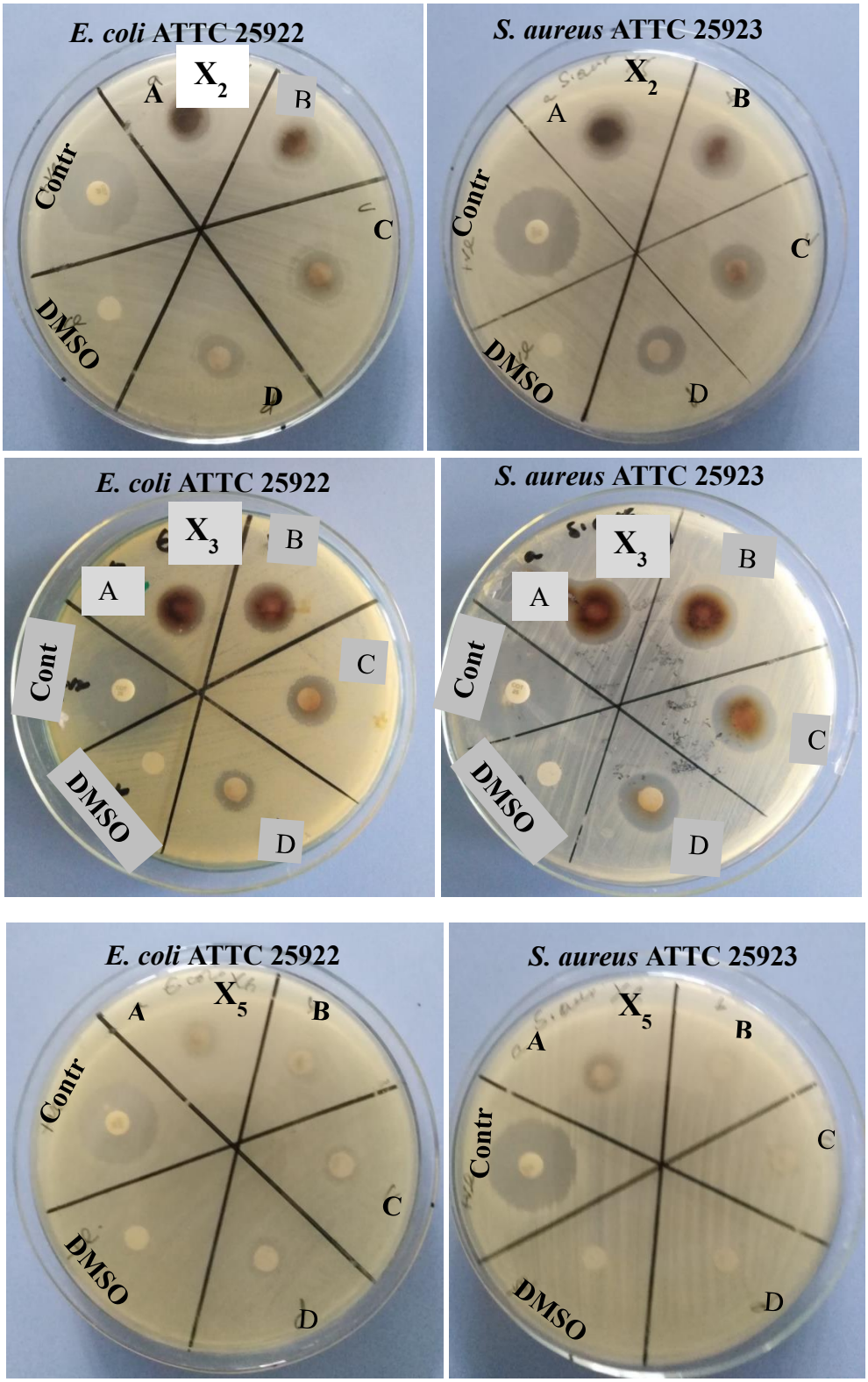

Figure 21: Photographs of antibacterial activities of X_2, X_3 and X_5

Where; X_2 (Ag/Bentonite NCs), X_3 (Ag/ZnO/Bentonite NCs) and X_5 (ZnO/Bentonite NCs)

Table 8: Results of dilution and zone of clearance in mm for synthesised Ag NPs and Ag-based NCs

Types of NPs/NCs and Organism			Dilution Results, Means of three replications and Standard error (±SE) of Inhibition zones in mm					
S. No	Types of NPs/ NCs	Types of Organism	10 mg/mL (A)	5 mg/mL (B)	2.5 mg/mL(C)	1.25 mg/mL (D)	Contrimoxazole (+ve)	DMSO (-ve)
1	X_1	E. coli	11.6 ± 0.3	11.3 ± 0.3	11 ± 0.6	10.3 ± 0.3	20	6
		S. aureus	14.3 ± 0.3	13.3 ± 0.3	13 ± 0.3	11.3 ± 0.3	21.3±0.3	6
2	X_2	E. coli	14	13.3 ± 0.3	13 ± 0.6	12	20	6
		S. aureus	14.7 ± 0.3	13.7 ± 0.3	13.3 ± 0.3	12.3 ± 0.3	21.3±0.3	6
3	X_3	E. coli	14.3 ± 0.3	13.7 ± 0.3	13.3 ± 0.3	12.3 ± 0.3	23.7±0.3	6
		S. aureus	17	16.3 ± 0.3	15.3 ± 0.3	14.3 ± 0.3	24.3±0.3	6

Where; X_1, X_2, and X_3 are Ag NPs, Ag/Bentonite NCs, and Ag/ZnO/Bentonite NCs respectively.

Table 9: Results of dilution and zone of clearance in mm for synthesised ZnO NPs and ZnO-based NCs

Types of NPs/NCs and Organism			Dilution Results, Means of three replications and Standard error (±SE) of Inhibition zones in mm					
S. No	Types of NPs/ NCs	Types of Organism	20 mg/mL (A)	10 mg/mL (B)	5 mg/mL (C)	2.5 mg/mL (D)	Contrim oxazole (25µg) (+ve)	DMSO (-ve)
1	X_4	E. coli	10.3 ± 0.3	10	7.6±0.3	6.3±0.3	20.3±0.3	6
		S. aureus	11 ± 0.6	10.3 ± 0.3	8	7± 0.6	21.3±0.3	6
2	X_5	E. coli	12	10.6±0.3	8.3±0.3	6.6 ± 0.7	20	6
		S. aureus	12.3 ±0.3	11.3±0.3	8.6 ± 0.3	7 ± 0.6	22.3±0.3	6
3	X_6	E. coli	6	6	6	6	20	6
		S. aureus	6	6	6	6	22	6
4	X_7	E. coli	6	6	6	6	22.3±0.3	6
		S. aureus	6	6	6	6	22.7±0.3	6
5	X_8	E. coli	9	8.7 ± 0.3	8.3 ± 0.3	7.3 ± 0.3	22.7±0.3	6
		S. aureus	10	9	8.7	8.3	23.7±0.3	6

Where, X_4, X_5, X_6, X_7, X_8, are ZnO NPs, ZnO/Bentonite NCs, purified bentonite (PB), Na-AB, and Plant powder respectively.

To know the statistical significance of the data P-values were calculated for all tests. Fig.22 also confirms the significance of the data obtained in antibacterial study of synthesised nanomaterials. As p-values less than 0.05 ($P < 0.05$) in all data, the data was statistically significant and acceptable. The P value is defined as the probability under the assumption of no effect or no difference (null hypothesis), of obtaining a result equal to or more extreme than what was actually observed. The P stands for probability and measures how likely it is that any observed difference between groups is due to chance. Being a

probability, P can take any value between 0 and Values close to 0 indicate that the observed difference is unlikely to be due to chance, whereas a P value close to 1 suggests no difference between the groups other than due to chance.

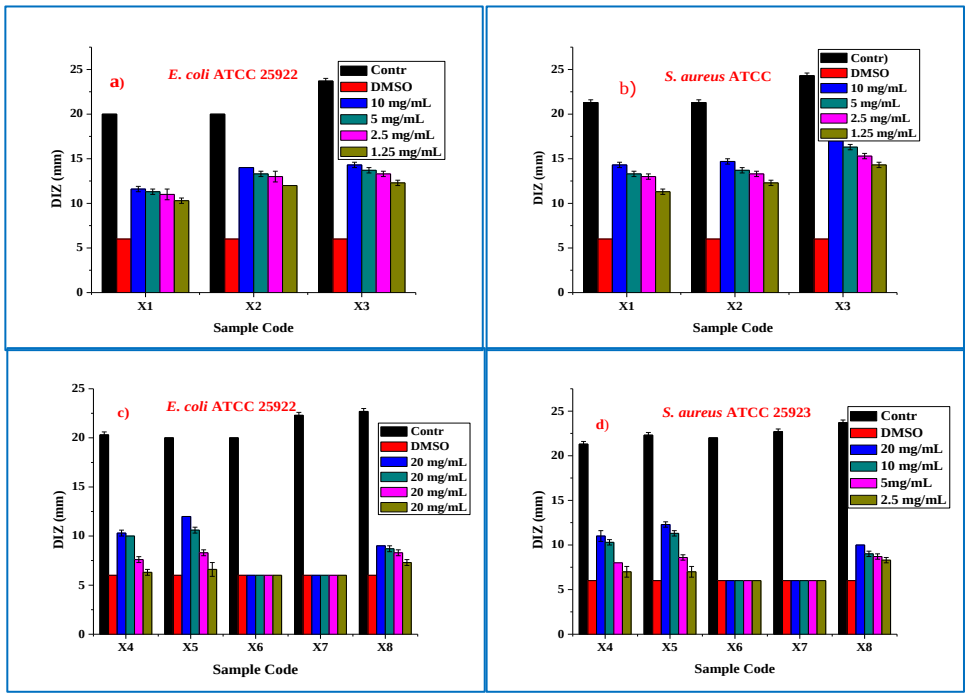

Figure 22: Diameter of Zone of inhibition of synthesized NPs and NCs at different concentration against *E. coli* and *S. aureus* bacterial strain

Were: X_1, X_2, X_3, X_4, X_5,X_6,X_7,X_8 and DIZ are Ag NPs, Ag/Bentonite NCs, Ag/ZnO/Bentonite NCs, ZnO NPs, ZnO/Bentonite NCs, purified bentonite (PB), Na-AB, Plant powder and diametr of inhbtion zone respectively.

4.4.2. Minimum Inhibitory Concentration (MIC) and minimum bactericidal concentration (MBC) of Ag/ZnO/Bentonite Nanocomposites

The results of the antibacterial effects of Ag/ZnO/Bentonite nanocomposites against selected bacterial via the MIC and the MBC are summarized in Table 10. The bactericidal effect of nanocomposites is dependent on the concentration of nanocomposites and the initial bacterial concentration. In this study, the initial bacterial concentration was 1×10^{8} CFU mL^{-1}. In this work, Ag/ZnO/Bentonite nanocomposite showed better antibacterial activities against both *Staphylococcus aureus* (ATCC 25923) and *Escherichia coli* (ATCC 25922) when it was compared with the components of the composite, especially for *Staphylococcus aureus* (ATCC 25923). The sensitivity of *S. aureus* toward this nanocomposite than *E. coli* is due to Gram–negative bacteria has a thin peptidoglycan layer with an additional outer membrane consisting of lipopolysaccharide. This additional membrane means that there is also an extra membrane layer termed periplasm, which makes it resistance than Gram-positive (Slavin et al., 2017).

The MIC observed for Ag/ZnO/Bentonite nanocomposites were 156.25 μgmL^{-1} and 78.125 μgmL^{-1} for *Escherichia coli* ATCC 25922 and *Staphylococcus aureus* ATCC 25923 respectively. The MBC observed for Ag/ZnO/Bentonite nanocomposites were 312.5 μgmL^{-1} and 156.25 μgmL^{-1} for *Escherichia coli* ATCC 25922 and *Staphylococcus aureus* ATCC 25923 respectively. The results observed that the *Staphylococcus aureus* were most sensitivity against Ag/ZnO/Bentonite nanocomposites.

Table 10: MIC (μgmL^{-1}) and MBC (μgmL^{-1}) of Ag/ZnO/Bentonite nanocomposites for *E. coli* and *S. aureus* bacterial strain

Bacterial strain	Strain no	MIC (μgmL^{-1})	MBC(μgmL^{-1})
E. coli	ATCC 25922	156.25	312.5
S. aureus	ATCC 25923	78.125	156.25

CHAPTER 5
CONCLUSIONS AND RECOMMENDATIONS

5.1. CONCLUSIONS

The Ag/ZnO/Bentonite nanocomposites were synthesized by a rapid and facile green method. The characterization results also confirmed the formation of Ag/ZnO/Bentonite NCs. The presence of phytoconstituents such as polyphenols and tannins played roles as reducing and capping agents during the formation of nanocomposites was confirmed by FT-IR analysis. UV-Vis-DRS, XRD, and SEM also confirm the formation of the nanocomposites. Ag/ZnO/Bentonite nanocomposites have higher antibacterial activity than as synthesized Ag NPs, ZnO NPs, Ag/Bentonite nanocomposites, and ZnO/Bentonite nanocomposites. Therefore, Ag/ZnO/Bentonite nanocomposites result in a promising antibacterial material which is effective against both Gram-negative and Gram-positive bacteria. The excellent antibacterial activity of Ag/ZnO/Bentonite nanocomposites provides another dimension to expand the application of the material.

5.2. RECOMMENDATIONS

The following is recommended for the extension of this work:

1. Surface Raman scattering and surface plasmon effects should be studied in nanohybrid nanoparticles for further applications in optoelectronics and sensors.
2. Advance study should be carried out on proper isolation of compounds acting as the reducing agents in each plant extract considered in this study.
3. Toxicity testing of the synthesized nanocomposites should also be carried out.
4. Leaching tests of nanocomposites should also be carried out to use them in other applications like waste water treatments.

REFERENCE

Abdel-Galil, A., Atta, A., & Balboul, M. R. (2020). Effect of Low-Energy Oxygen Ion Beam Treatment on the Structural and Physical Properties of ZnO Thin Films. *Surface Review and Letters*, *27*(12). https://doi.org/10.1142/S0218625X20500195

Abdelkrim, S., Mokhtar, A., Djelad, A., Bennabi, F., Souna, A., Bengueddach, A., & Sassi, M. (2020). Chitosan/Ag-Bentonite Nanocomposites: Preparation, Characterization, Swelling and Biological Properties. *Journal of Inorganic and Organometallic Polymers and Materials*, *30*(3), 831–840. https://doi.org/10.1007/s10904-019-01219-8

Abdullahi, S. S., Güner, S., Koseoglu, Y., Musa, I. M., Adamu, B. I., & Abdulhamid, and M. I. (2016). Simple Method For The Determınatıon of Band Gap of a Nanopowdered Sample Usıng Kubelka Munk Theory. *Journal of the Nigerian Association of Mathematical Physics*, *35*(August), 241–246. https://www.researchgate.net/publication/305810656

Abed, S., Bakhsheshi-Rad, H. R., Yaghoubi, H., Ning, L., Sadeghianmaryan, A., & Chen, X. (2020). Antibacterial activities of zeolite/silver-graphene oxide nanocomposite in bone implants. *Materials Technology*, *00*(00), 1–10. https://doi.org/10.1080/10667857.2020.1786784

Aguiar, K. L. N. P., Pereira, K. A. B., Mendes, M. S. L., Pedroni, L. G., Oliveira, P. F., & Mansur, C. R. E. (2020). Study of the modification of bentonite for the formation of nanocomposite hydrogels with potential applicability in conformance control. *Journal of Petroleum Science and Engineering*, *195*, 107600. https://doi.org/10.1016/j.petrol.2020.107600

Ahmed, S., Ahmad, M., Swami, B. L., & Ikram, S. (2016). A review on plants extract mediated synthesis of silver nanoparticles for antimicrobial applications: A green expertise. *Journal of Advanced Research*, *7*(1), 17–28. https://doi.org/10.1016/j.jare.2015.02.007

Ajitha, B., Kumar Reddy, Y. A., Reddy, P. S., Jeon, H. J., & Ahn, C. W. (2016). Role of capping agents in controlling silver nanoparticles size, antibacterial activity and potential application as optical hydrogen peroxide sensor. *RSC Advances*, *6*(42), 36171–36179. https://doi.org/10.1039/c6ra03766f

Al-Hammood, A. A., Frayyeh, Q. J., & Abbas, W. A. (2021a). Raw bentonite as

supplementary cementitious material - A review. *Journal of Physics: Conference Series*, *1795*(1). https://doi.org/10.1088/1742-6596/1795/1/012018

Al-Hammood, A. A., Frayyeh, Q. J., & Abbas, W. A. (2021b). Raw bentonite as supplementary cementitious material - A review. *Journal of Physics: Conference Series*, *1795*(1), 206–213. https://doi.org/10.1088/1742-6596/1795/1/012018

Alarcon, E. I. (2015). Nanoparticles | Nanoparticle Applications. In *Springer International Publishing*. https://www.understandingnano.com/nanoparticles.html

Alavi, M., & Varma, R. S. (2021). Phytosynthesis and modification of metal and metal oxide nanoparticles/nanocomposites for antibacterial and anticancer activities: Recent advances. *Sustainable Chemistry and Pharmacy*, *21*(August 2020), 100412. https://doi.org/10.1016/j.scp.2021.100412

Alemayehu, T. (2021). Prevalence of multidrug-resistant bacteria in Ethiopia: a systematic review and meta-analysis. *Journal of Global Antimicrobial Resistance*, *26*, 133–139. https://doi.org/10.1016/j.jgar.2021.05.017

Anbu, P., Gopinath, S. C. B., Yun, H. S., & Lee, C. G. (2019). Temperature-dependent green biosynthesis and characterization of silver nanoparticles using balloon flower plants and their antibacterial potential. *Journal of Molecular Structure*, *1177*, 302–309. https://doi.org/10.1016/j.molstruc.2018.09.075

Araújo, C. M., das Virgens Santana, M., do Nascimento Cavalcante, A., Nunes, L. C. C., Bertolino, L. C., de Sousa Brito, C. A. R., Barreto, H. M., & Eiras, C. (2020). Cashew-gum-based silver nanoparticles and palygorskite as green nanocomposites for antibacterial applications. *Materials Science and Engineering C*, *115*(April), 110927. https://doi.org/10.1016/j.msec.2020.110927

Asad, M. A. (2013). Suitability of Bentonite Clay: An Analytical Approach. *Earth Sciences*, *2*(3), 88. https://doi.org/10.11648/j.earth.20130203.13

Asamoah, R. B., Yaya, A., Nbelayim, P., Annan, E., & Onwona-Agyeman, B. (2020). Development and characterization of clay-nanocomposites for water purification. *Materials*, *13*(17). https://doi.org/10.3390/MA13173793

Ates, B., Koytepe, S., Balcioglu, S., Ulu, A., & Gurses, C. (2017). Biomedical applications of hybrid polymer composite materials. In *Hybrid Polymer Composite Materials: Applications*. Elsevier Ltd. https://doi.org/10.1016/B978-0-08-100785-3.00012-7

Ates, B., Koytepe, S., Ulu, A., Gurses, C., & Thakur, V. K. (2020). Chemistry, structures, and advanced applications of nanocomposites from biorenewable resources. *Chemical Reviews*, *120*(17), 9304–9362. https://doi.org/10.1021/acs.chemrev.9b00553

Auwal, M. S., Saka, S., Mairiga, I. A., Sanda, K. A., Shuaibu, A., & Ibrahim, A. (2014). Preliminary phytochemical and elemental analysis of aqueous and fractionated pod extracts of Acacia nilotica (Thorn mimosa). *Veterinary Research Forum : An International Quarterly Journal*, *5*(2), 95–100.

Awwad, A. M., Albiss, B., & Ahmad, A. L. (2014). Green synthesis, characterization and optical properties of zinc oxide nanosheets using Olea europea leaf extract. *Advanced Materials Letters*, *5*(9), 520–524. https://doi.org/10.5185/amlett.2014.5575

Ayukekbong, J. A., Ntemgwa, M., & Atabe, A. N. (2017). The threat of antimicrobial resistance in developing countries: Causes and control strategies. *Antimicrobial Resistance and Infection Control*, *6*(1), 1–8. https://doi.org/10.1186/s13756-017-0208-x

Azizi-Lalabadi, M., Garavand, F., & Jafari, S. M. (2021). Incorporation of silver nanoparticles into active antimicrobial nanocomposites: Release behavior, analyzing techniques, applications and safety issues. In *Advances in Colloid and Interface Science* (Vol. 293). Elsevier B.V. https://doi.org/10.1016/j.cis.2021.102440

Aznárez, A., Gil, A., & Korili, S. A. (2015). Performance of palladium and platinum supported on alumina pillared clays in the catalytic combustion of propene. *RSC Advances*, *5*(100), 82296–82309. https://doi.org/10.1039/c5ra15675k

Bagheri, M., Jafari, S. M., & Eikani, M. H. (2019). Development of ternary nanoadsorbent composites of graphene oxide, activated carbon, and zero-valent iron nanoparticles for food applications. *Food Science and Nutrition*, *7*(9), 2827–2835. https://doi.org/10.1002/fsn3.1080

Bandeira, M., Giovanela, M., Roesch-Ely, M., Devine, D. M., & da Silva Crespo, J. (2020). Green synthesis of zinc oxide nanoparticles: A review of the synthesis methodology and mechanism of formation. *Sustainable Chemistry and Pharmacy*, *15*, 1–36. https://doi.org/10.1016/j.scp.2020.100223

https://www.researchgate.net/publication/269107473_What_is_governance/link/548173090cf22525dcb61443/download%0Ahttp://www.econ.upf.edu/~reynal/Civil wars_12December2010.pdf%0Ahttps://think-

asia.org/handle/11540/8282%0Ahttps://www.jstor.org/stable/41857625

Bel Hadjltaief, H., Ben Ameur, S., Da Costa, P., Ben Zina, M., & Elena Galvez, M. (2018). Photocatalytic decolorization of cationic and anionic dyes over ZnO nanoparticle immobilized on natural Tunisian clay. *Applied Clay Science*, *152*(November), 148–157. https://doi.org/10.1016/j.clay.2017.11.008

Bhardwaj, A. K., Sundaram, S., Yadav, K. K., & Srivastav, A. L. (2021). An overview of silver nano-particles as promising materials for water disinfection. *Environmental Technology and Innovation*, *23*, 101721. https://doi.org/10.1016/j.eti.2021.101721

Caglar, B., Afsin, B., Tabak, A., & Eren, E. (2009). Characterization of the cation-exchanged bentonites by XRPD, ATR, DTA/TG analyses and BET measurement. *Chemical Engineering Journal*, *149*(1–3), 242–248. https://doi.org/10.1016/j.cej.2008.10.028

Cândido, E. de S., de Barros, E., Cardoso, M. H., & Franco, O. L. (2019). Bacterial cross-resistance to anti-infective compounds. Is it a real problem? *Current Opinion in Pharmacology*, *48*, 76–81. https://doi.org/10.1016/j.coph.2019.05.004

Cerrón-Calle, G. A., Aranda-Aguirre, A. J., Luyo, C., Garcia-Segura, S., & Alarcón, H. (2019). Photoelectrocatalytic decolorization of azo dyes with nano-composite oxide layers of ZnO nanorods decorated with Ag nanoparticles. *Chemosphere*, *219*, 296–304. https://doi.org/10.1016/j.chemosphere.2018.12.003

Chakraborty, T., Chakraborty, A., Shukla, M., & Chattopadhyay, T. (2019). ZnO–Bentonite nanocomposite: an efficient catalyst for discharge of dyes, phenol and Cr(VI) from water. *Journal of Coordination Chemistry*, *72*(1), 53–68. https://doi.org/10.1080/00958972.2018.1560429

Chaudhuri, S. K., & Malodia, L. (2017). Biosynthesis of zinc oxide nanoparticles using leaf extract of calotropis gigantea: Characterization and its evaluation on tree seedling growth in nursery stage. *Applied Nanoscience (Switzerland)*, *7*(8), 501–512. https://doi.org/10.1007/s13204-017-0586-7

Chelli, V. R., & Golder, A. K. (2018). Ag-doping on ZnO support mediated by bio-analytes rich in ascorbic acid for photocatalytic degradation of dipyrone drug. *Chemosphere*, *208*, 149–158. https://doi.org/10.1016/j.chemosphere.2018.05.158

Chen, L., Zhao, Y., Bai, H., Ai, Z., Chen, P., Hu, Y., Song, S., & Komarneni, S. (2020). Role of Montmorillonite, Kaolinite, or Illite in Pyrite Flotation: Differences in Clay Behavior

Based on Their Structures. *Langmuir*, *36*(36), 10860–10867. https://doi.org/10.1021/acs.langmuir.0c02073

Chikezie, I. O. (2017). Determination of minimum inhibitory concentration (MIC) and minimum bactericidal concentration (MBC) using a novel dilution tube method. *African Journal of Microbiology Research*, *11*(23), 977–980. https://doi.org/10.5897/ajmr2017.8545

Ciolan, M. A., & Motrescu, I. (2022). Pulsed Laser Ablation: A Facile and Low-Temperature Fabrication of Highly Oriented n-Type Zinc Oxide Thin Films. *Applied Sciences (Switzerland)*, *12*(2). https://doi.org/10.3390/app12020917

Colín-Luna, J. A., Zamora-Rodea, E. G., González-Brambila, M. M., Barrera-Calva, E., Rosas-Cedillo, R., Medina-Mendoza, A. K., & García-Martínez, J. C. (2018). Biodiesel production using immobilized lipase supported on a zirconium-pillared clay. Effect of the immobilization method. *International Journal of Chemical Reactor Engineering*, *16*(11). https://doi.org/10.1515/ijcre-2017-0260

Dadi, R., Azouani, R., Traore, M., Mielcarek, C., & Kanaev, A. (2019). Antibacterial activity of ZnO and CuO nanoparticles against gram positive and gram negative strains. *Materials Science and Engineering C*, *104*(July), 109968. https://doi.org/10.1016/j.msec.2019.109968

Daniels, K. A., Harrington, J. F., Zihms, S. G., & Wiseall, A. C. (2017). Bentonite permeability at elevated temperature. *Geosciences (Switzerland)*, *7*(1), 1–24. https://doi.org/10.3390/geosciences7010003

Darvishi Cheshmeh Soltani, R., Jorfi, S., Ramezani, H., & Purfadakari, S. (2016). Ultrasonically induced ZnO-biosilica nanocomposite for degradation of a textile dye in aqueous phase. *Ultrasonics Sonochemistry*, *28*, 69–78. https://doi.org/10.1016/j.ultsonch.2015.07.002

Dawadi, S., Katuwal, S., Gupta, A., Lamichhane, U., Thapa, R., Jaisi, S., Lamichhane, G., Bhattarai, D. P., & Parajuli, N. (2021). Current Research on Silver Nanoparticles: Synthesis, Characterization, and Applications. *Journal of Nanomaterials*, *2021*. https://doi.org/10.1155/2021/6687290

de Dicastillo, C. L., Vidal, C. P., Falcó, I., Sánchez, G., Márquez, P., & Escrig, J. (2020). Antimicrobial bilayer nanocomposites based on the incorporation of as-synthetized

hollow zinc oxide nanotubes. *Nanomaterials*, *10*(3). https://doi.org/10.3390/nano10030503

Deák, Á., Janovák, L., Tallósy, S. P., Bitó, T., Sebok, D., Buzás, N., Pálinkó, I., & Dékány, I. (2015). Spherical LDH-Ag°-montmorillonite heterocoagulated system with a pH-dependent sol-gel structure for controlled accessibility of AgNPs immobilized on the clay lamellae. *Langmuir*, *31*(6), 2019–2027. https://doi.org/10.1021/la504096t

Díez-Pascual, A. M., & Luceño-Sánchez, J. A. (2021). Antibacterial activity of polymer nanocomposites incorporating graphene and its derivatives: A state of art. *Polymers*, *13*(13). https://doi.org/10.3390/polym13132105

Dinesh, V. P., Biji, P., Ashok, A., Dhara, S. K., Kamruddin, M., Tyagi, A. K., & Raj, B. (2014). Plasmon-mediated, highly enhanced photocatalytic degradation of industrial textile dyes using hybrid ZnO@Ag core-shell nanorods. *RSC Advances*, *4*(103), 58930–58940. https://doi.org/10.1039/c4ra09405k

Dobrucka, R., & Długaszewska, J. (2016). Biosynthesis and antibacterial activity of ZnO nanoparticles using Trifolium pratense flower extract. *Saudi Journal of Biological Sciences*, *23*(4), 517–523. https://doi.org/10.1016/j.sjbs.2015.05.016

Duffy, L. L., Osmond-McLeod, M. J., Judy, J., & King, T. (2018). Investigation into the antibacterial activity of silver, zinc oxide and copper oxide nanoparticles against poultry-relevant isolates of Salmonella and Campylobacter. *Food Control*, *92*, 293–300. https://doi.org/10.1016/j.foodcont.2018.05.008

Dupraz, M., Beutier, G., Rodney, D., Mordehai, D., & Verdier, M. (2015). Signature of dislocations and stacking faults of face-centred cubic nanocrystals in coherent X-ray diffraction patterns: A numerical study. *Journal of Applied Crystallography*, *48*, 621–644. https://doi.org/10.1107/S1600576715005324

Dutta, P., & Wang, B. (2019). Zeolite-supported silver as antimicrobial agents. *Coordination Chemistry Reviews*, *383*, 1–29. https://doi.org/10.1016/j.ccr.2018.12.014

Eckhardt, S., Brunetto, P. S., Gagnon, J., Priebe, M., Giese, B., & Fromm, K. M. (2013). Nanobio silver: Its interactions with peptides and bacteria, and its uses in medicine. *Chemical Reviews*, *113*(7), 4708–4754. https://doi.org/10.1021/cr300288v

El Miz, M., Akichoh, H., Berraaouan, D., Salhi, S., & Tahani, A. (2017). Chemical and Physical Characterization of Moroccan Bentonite Taken from Nador (North of Morocco).

American Journal of Chemistry, *2017*(4), 105–112. https://doi.org/10.5923/j.chemistry.20170704.01

Espitia, P. J. P., Soares, N. de F. F., Coimbra, J. S. dos R., de Andrade, N. J., Cruz, R. S., & Medeiros, E. A. A. (2012). Zinc Oxide Nanoparticles: Synthesis, Antimicrobial Activity and Food Packaging Applications. *Food and Bioprocess Technology*, *5*(5), 1447–1464. https://doi.org/10.1007/s11947-012-0797-6

Fakhari, S., Jamzad, M., & Kabiri Fard, H. (2019). Green synthesis of zinc oxide nanoparticles: a comparison. *Green Chemistry Letters and Reviews*, *12*(1), 19–24. https://doi.org/10.1080/17518253.2018.1547925

Farzana, R., Shamsuzzaman, S. M., & Mamun, K. Z. (2013). Isolation and molecular characterization of New Delhi metallo-beta-lactamase-1 producing superbug in Bangladesh. *Journal of Infection in Developing Countries*, *7*(3), 161–168. https://doi.org/10.3855/jidc.2493

Franci, G., Falanga, A., Galdiero, S., Palomba, L., Rai, M., Morelli, G., & Galdiero, M. (2015). Silver nanoparticles as potential antibacterial agents. *Molecules*, *20*(5), 8856–8874. https://doi.org/10.3390/molecules20058856

Fytianos, G., Rahdar, A., & Kyzas, G. Z. (2020). Nanomaterials in cosmetics: Recent updates. *Nanomaterials*, *10*(5), 1–16. https://doi.org/10.3390/nano10050979

Garavand, F., Cacciotti, I., Vahedikia, N., Rehman, A., Tarhan, Ö., Akbari-Alavijeh, S., Shaddel, R., Rashidinejad, A., Nejatian, M., Jafarzadeh, S., Azizi-Lalabadi, M., Khoshnoudi-Nia, S., & Jafari, S. M. (2022). A comprehensive review on the nanocomposites loaded with chitosan nanoparticles for food packaging. *Critical Reviews in Food Science and Nutrition*, *62*(5), 1383–1416. https://doi.org/10.1080/10408398.2020.1843133

Ghamsari, M. S., Alamdari, S., Han, W., & Park, H. H. (2017). Impact of nanostructured thin ZnO film in ultraviolet protection. *International Journal of Nanomedicine*, *12*, 207–216. https://doi.org/10.2147/IJN.S118637

Gharpure, S., Akash, A., & Ankamwar, B. (2019). A Review on Antimicrobial Properties of Metal Nanoparticles. *Journal of Nanoscience and Nanotechnology*, *20*(6), 3303–3339. https://doi.org/10.1166/jnn.2020.17677

Golmohammadi, M., Honarmand, M., & Ghanbari, S. (2020). A green approach to synthesis

of ZnO nanoparticles using jujube fruit extract and their application in photocatalytic degradation of organic dyes. *Spectrochimica Acta - Part A: Molecular and Biomolecular Spectroscopy*, *229*, 117961. https://doi.org/10.1016/j.saa.2019.117961

Gonelimali, F. D., Lin, J., Miao, W., Xuan, J., Charles, F., Chen, M., & Hatab, S. R. (2018). Antimicrobial properties and mechanism of action of some plant extracts against food pathogens and spoilage microorganisms. *Frontiers in Microbiology*, *9*(JUL), 1–9. https://doi.org/10.3389/fmicb.2018.01639

Gong, Z., Liao, L., Lv, G., & Wang, X. (2016). A simple method for physical purification of bentonite. *Applied Clay Science*, *119*, 294–300. https://doi.org/10.1016/j.clay.2015.10.031

Gregorczyk, K., & Knez, M. (2016). Hybrid nanomaterials through molecular and atomic layer deposition: Top down, bottom up, and in-between approaches to new materials. In *Progress in Materials Science* (Vol. 75, pp. 1–37). Elsevier Ltd. https://doi.org/10.1016/j.pmatsci.2015.06.004

Gul, R., Jan, S. U., Faridullah, S., Sherani, S., & Jahan, N. (2017). Preliminary Phytochemical Screening, Quantitative Analysis of Alkaloids, and Antioxidant Activity of Crude Plant Extracts from Ephedra intermedia Indigenous to Balochistan. *Scientific World Journal*, *2017*(Figure 1). https://doi.org/10.1155/2017/5873648

Gupta, M., & Kumar, A. (2018). Comparison of Minimum Inhibitory Concentration (MIC) value of statin drugs: A Systematic Review. *Anti-Infective Agents*, *17*(1), 4–19. https://doi.org/10.2174/2211352516666180629124433

Hakimi, B., Ghorbanpour, M., & Feizi, A. (2018). ZnO / bentonite Nanocomposites Prepared with Solid-state Ion Exchange as Photocatalysts. *Journal of Ultrafine Grained and Nanostructured Materials*, *51*(2), 139–146. https://doi.org/10.22059/JUFGNSM.2018.02.05

Hamad, A., Khashan, K. S., & Hadi, A. (2020). Silver Nanoparticles and Silver Ions as Potential Antibacterial Agents. *Journal of Inorganic and Organometallic Polymers and Materials*, *30*(12), 4811–4828. https://doi.org/10.1007/s10904-020-01744-x

Hariram, M., Ganesan, V., Muthuramkumar, S., & Vivekanandhan, S. (2021). *Functionalization of kaolin clay with silver nanoparticles by Murraya koenigii fruit extract-mediated bioreduction process for antimicrobial applications (a) (b) (c) (d) (*

e) (f) (g). 505–513.

Harrington, J. F., Daniels, K. A., Wiseall, A. C., & Sellin, P. (2020). Bentonite homogenisation during the closure of void spaces. *International Journal of Rock Mechanics and Mining Sciences*, *136*(October), 104535. https://doi.org/10.1016/j.ijrmms.2020.104535

Hashim, F. S., Alkaim, A. F., Mahdi, S. M., & Omran Alkhayatt, A. H. (2019). Photocatalytic degradation of GRL dye from aqueous solutions in the presence of ZnO/Fe2O3 nanocomposites. *Composites Communications*, *16*(September), 111–116. https://doi.org/10.1016/j.coco.2019.09.008

Hebbar, R. S., Isloor, A. M., & Ismail, A. F. (2014). Preparation and evaluation of heavy metal rejection properties of polyetherimide/porous activated bentonite clay nanocomposite membrane. *RSC Advances*, *4*(88), 47240–47248. https://doi.org/10.1039/c4ra09018g

Holzwarth, U., & Gibson, N. (2011). The Scherrer equation versus the "Debye-Scherrer equation." *Nature Nanotechnology*, *6*(9), 534. https://doi.org/10.1038/nnano.2011.145

Hou, J., Wu, Y., Li, X., Wei, B., Li, S., & Wang, X. (2018). Toxic effects of different types of zinc oxide nanoparticles on algae, plants, invertebrates, vertebrates and microorganisms. In *Chemosphere* (Vol. 193, pp. 852–860). Elsevier Ltd. https://doi.org/10.1016/j.chemosphere.2017.11.077

Jadoun, S., Arif, R., Jangid, N. K., & Meena, R. K. (2021). Green synthesis of nanoparticles using plant extracts: a review. *Environmental Chemistry Letters*, *19*(1), 355–374. https://doi.org/10.1007/s10311-020-01074-x

Jalal, R., Goharshadi, E. K., Abareshi, M., Moosavi, M., Yousefi, A., & Nancarrow, P. (2010). ZnO nanofluids: Green synthesis, characterization, and antibacterial activity. *Materials Chemistry and Physics*, *121*(1–2), 198–201. https://doi.org/10.1016/j.matchemphys.2010.01.020

Jamdagni, P., Khatri, P., & Rana, J. S. (2016). Green synthesis of zinc oxide nanoparticles using flower extract of Nyctanthes arbor-tristis and their antifungal activity. *Journal of King Saud University - Science*. https://doi.org/10.1016/j.jksus.2016.10.002

Jamkhande, P. G., Ghule, N. W., Bamer, A. H., & Kalaskar, M. G. (2019). Metal nanoparticles synthesis: An overview on methods of preparation, advantages and disadvantages, and applications. *Journal of Drug Delivery Science and Technology*,

53(July), 101174. https://doi.org/10.1016/j.jddst.2019.101174

Kassem, M. (2015). Performance evaluation of natural bentonite loaded with zinc oxide for the photocatalytic degradation of methyl red. *Revue Roumaine de Chimie*, *60*(10), 957–963.

Katas, H., Moden, N. Z., Lim, C. S., Celesistinus, T., Chan, J. Y., Ganasan, P., & Suleman Ismail Abdalla, S. (2018). Biosynthesis and Potential Applications of Silver and Gold Nanoparticles and Their Chitosan-Based Nanocomposites in Nanomedicine. *Journal of Nanotechnology*, *2018*. https://doi.org/10.1155/2018/4290705

Kifle, Z. D., Debeb, S. G., & Belayneh, Y. M. (2021). In Vitro α -Amylase and α -Glucosidase Inhibitory and Antioxidant Activities of the Crude Extract and Solvent Fractions of Hagenia abyssinica Leaves. *BioMed Research International*, *2021*. https://doi.org/10.1155/2021/6652777

Kifle, Z. D., Kidanu, B. B., Tadesse, T. Y., Belachew, T. F., & Atnafie, S. A. (2021). Evaluation of in Vivo Antidiarrheal Activity of Solvent Fractions of Hagenia abyssinica (Rosaceae) in Swiss Albino Mice. *Evidence-Based Complementary and Alternative Medicine*, *2021*. https://doi.org/10.1155/2021/8828331

Klier, K. (1972). Absorption and Scattering in Plane Parallel Turbid Media. *J Opt Soc Am*, *62*(7), 882–885. https://doi.org/10.1364/JOSA.62.000882

Konwar, R., & Ahmed, A. B. (2016). Nanoparticle: an Overview of Preparation, Characterization and Application. *International Research Journal of Pharmacy*, *4*(4), 47–57. https://doi.org/10.7897/2230-8407.04408

Krishnan, B., & Mahalingam, S. (2017a). Ag/TiO2/bentonite nanocomposite for biological applications: Synthesis, characterization, antibacterial and cytotoxic investigations. *Advanced Powder Technology*, *28*(9), 2265–2280. https://doi.org/10.1016/j.apt.2017.06.007

Krishnan, B., & Mahalingam, S. (2017b). Improved surface morphology of silver/copper oxide/bentonite nanocomposite using aliphatic ammonium based ionic liquid for enhanced biological activities. *Journal of Molecular Liquids*, *241*, 1044–1058. https://doi.org/10.1016/j.molliq.2017.06.104

krishnan2017.pdf. (n.d.).

Kukushkina, E. A., Hossain, S. I., Sportelli, M. C., Ditaranto, N., Picca, R. A., & Cioffi, N.

(2021). Ag-based synergistic antimicrobial composites. A critical review. *Nanomaterials*, *11*(7). https://doi.org/10.3390/nano11071687

Kumar, A., & Lingfa, P. (2020). Sodium bentonite and kaolin clays: Comparative study on their FT-IR, XRF, and XRD. *Materials Today: Proceedings*, *22*(xxxx), 737–742. https://doi.org/10.1016/j.matpr.2019.10.037

Kumar, S., Abedin, M. M., Singh, A. K., & Das, S. (2020). Role of Phenolic Compounds in Plant-Defensive Mechanisms. *Plant Phenolics in Sustainable Agriculture*, 517–532. https://doi.org/10.1007/978-981-15-4890-1_22

Landi, S., Segundo, I. R., Freitas, E., Vasilevskiy, M., Carneiro, J., & Tavares, C. J. (2022). Use and misuse of the Kubelka-Munk function to obtain the band gap energy from diffuse reflectance measurements. *Solid State Communications*, *341*(October 2021), 1–7. https://doi.org/10.1016/j.ssc.2021.114573

Lei, C., Pi, M., Jiang, C., Cheng, B., & Yu, J. (2017). Synthesis of hierarchical porous zinc oxide (ZnO) microspheres with highly efficient adsorption of Congo red. In *Journal of Colloid and Interface Science* (Vol. 490). https://doi.org/10.1016/j.jcis.2016.11.049

Lin, H., Yang, M., Tang, H., & Pan, F. (2018). Effect of minor Sc on the microstructure and mechanical properties of AZ91 Magnesium Alloy. *Progress in Natural Science: Materials International*, *28*(1), 66–73. https://doi.org/10.1016/j.pnsc.2018.01.006

Lungu, M. V., Vasile, E., Lucaci, M., Pătroi, D., Mihăilescu, N., Grigore, F., Marinescu, V., Brătulescu, A., Mitrea, S., Sobetkii, A., Sobetkii, A. A., Popa, M., & Chifiriuc, M. C. (2016). Investigation of optical, structural, morphological and antimicrobial properties of carboxymethyl cellulose capped Ag-ZnO nanocomposites prepared by chemical and mechanical methods. *Materials Characterization*, *120*, 69–81. https://doi.org/10.1016/j.matchar.2016.08.022

Madhumitha, G., Fowsiya, J., Gupta, N., Kumar, A., & Singh, M. (2019). Green synthesis, characterization and antifungal and photocatalytic activity of Pithecellobium dulce peel–mediated ZnO nanoparticles. *Journal of Physics and Chemistry of Solids*, *127*, 43–51. https://doi.org/10.1016/j.jpcs.2018.12.005

Magzoub, M. I., Hussein, I. A., Nasser, M. S., Mahmoud, M., Sultan, A. S., & Benamor, A. (2020). An Investigation of the Swelling Kinetics of Bentonite Systems Using Particle Size Analysis. *Journal of Dispersion Science and Technology*, *41*(6), 817–827.

https://doi.org/10.1080/01932691.2019.1612758

Mammo Ghebre, W. (2019). Local Industrial Applications of Bentonite Deposits from Afar-Ethiopia. *Acta Scientific Agriculture*, *3*(10), 85–90. https://doi.org/10.31080/asag.2019.03.0652

Mankad, M., Patil, G., Patel, S., Patel, D., & Patel, A. (2016). Green synthesis of zinc oxide nanoparticles using Azadirachta indica A. Juss. leaves extract and its antibacterial activity against Xanthomonas orzyae pv. oryzae. *Annals of Phytomedicine : An International Journal*, *5*(2), 76–86. https://doi.org/10.21276/ap.2016.5.2.9

Marcial, D., Delage, P., & Cui, Y. J. (2002). On the high stress compression of bentonites. *Canadian Geotechnical Journal*, *39*(4), 812–820. https://doi.org/10.1139/t02-019

Meneses, X. B., Rillera, A. S., Dahonog, L. A., & Tapia, A. K. G. (2018). Conduction in polyaniline-emeraldine salt/bentonite composites using impedance spectroscopy. *Key Engineering Materials*, *775 KEM*, 63–67. https://doi.org/10.4028/www.scientific.net/KEM.775.63

Milosevic, M., & Berets, S. L. (2002). A review of FT-IR diffuse reflection sampling considerations. *Applied Spectroscopy Reviews*, *37*(4), 347–364. https://doi.org/10.1081/ASR-120016081

Minatel, I. O., Borges, C. V., Borges, C. V., Alonzo, H., Hector, G., Gomez, G., Chen, C. O., Chen, C. O., Pace, G., & Lima, P. (2017). Phenolic compounds: functional properties, impact of processing and bioavailability, Phenolic Compounds - Biological Activity. *Open Science*, 1–24.

Montero, I. D. A. (n.d.). *Evaluation of the antibacterial activity of an indoor waterborne architectural coating containing Ag / TiO 2 under ...*

Motshekga, S. C., Ray, S. S., Onyango, M. S., & Momba, M. N. B. (2013). Microwave-assisted synthesis, characterization and antibacterial activity of Ag/ZnO nanoparticles supported bentonite clay. *Journal of Hazardous Materials*, *262*, 439–446. https://doi.org/10.1016/j.jhazmat.2013.08.074

Motshekga, S. C., Ray, S. S., Onyango, M. S., & Momba, M. N. B. (2015). Preparation and antibacterial activity of chitosan-based nanocomposites containing bentonite-supported silver and zinc oxide nanoparticles for water disinfection. *Applied Clay Science*, *114*, 330–339. https://doi.org/10.1016/j.clay.2015.06.010

Muflikhun, M. A., Frommelt, M. C., Farman, M., Chua, A. Y., & Santos, G. N. C. (2019). Structures, mechanical properties and antibacterial activity of Ag/TiO 2 nanocomposite materials synthesized via HVPG technique for coating application. *Heliyon*, *5*(4). https://doi.org/10.1016/j.heliyon.2019.e01475

Munonde, T. S., & Nomngongo, P. N. (2020). *Nanocomposites for Electrochemical Sensors and Their Applications on the Detection of Trace Metals in Environmental Water Samples*. https://doi.org/10.3390/s210101

Murthy, H. C. A., Zeleke, T. D., Ravikumar, C. R., Kumar, M. R. A., & Nagaswarupa, H. P. (2020). *Electrochemical properties of biogenic silver nanoparticles synthesized using Hagenia abyssinica (Brace) JF . Gmel . medicinal plant leaf Electrochemical properties of biogenic silver nanoparticles synthesized using Hagenia abyssinica (Brace) JF . Gme*.

Muurinen, A. (2011). Measurements on Cation Exchange Capacity of Bentonite in the Long-Term Test of Buffer Material (LOT). *No POSIVA-WR-11-10. Posiva Oy.*

Nasrollahzadeh, M., Mahmoudi-Gom Yek, S., Motahharifar, N., & Ghafori Gorab, M. (2019). Recent Developments in the Plant-Mediated Green Synthesis of Ag-Based Nanoparticles for Environmental and Catalytic Applications. *Chemical Record*, *19*(12), 2436–2479. https://doi.org/10.1002/tcr.201800202

Nones, J., Riella, H. G., Trentin, A. G., & Nones, J. (2015). Effects of bentonite on different cell types: A brief review. *Applied Clay Science*, *105–106*, 225–230. https://doi.org/10.1016/j.clay.2014.12.036

Nowack, B., Krug, H. F., & Height, M. (2011). Reply to comments on “120 years of nanosilver history: Implications for policy makers.” *Environmental Science and Technology*, *45*(17), 7593–7595. https://doi.org/10.1021/es2017895

Omanovi, E., Badnjevi, A., Kazlagi, A., & Hajlovac, M. (2020). *Omanović-Mikličanin2020_Article_NanocompositesABriefReview.pdf*. 51–59.

Parihar, V., Raja, M., & Paulose, R. (2018). A brief review of structural, electrical and electrochemical properties of zinc oxide nanoparticles. *Reviews on Advanced Materials Science*, *53*(2), 119–130. https://doi.org/10.1515/rams-2018-0009

Pouraboulghasem, H., Ghorbanpour, M., Shayegh, R., & Lotfiman, S. (2016). Synthesis, characterization and antimicrobial activity of alkaline ion-exchanged ZnO/bentonite

nanocomposites. *Journal of Central South University*, *23*(4), 787–792. https://doi.org/10.1007/s11771-016-3124-y

Prasad, R. D., Charmode, N., Shrivastav, O. P., Prasad, S. R., Moghe, A., Samant, A., Sarvalkar, P. D., & Prasad, N. R. (2021). A Review on Concept of Nanotechnology in Veterinary Medicine. *ES Food & Agroforestry*, 28–60. https://doi.org/10.30919/esfaf481

Rajendran, R. K., & Lin, C. C. (2021). Stability and Microbial Toxicity of Silver Nanoparticles under Denitrifying Conditions. *ACS Applied Materials and Interfaces*, *13*(39), 46233–46246. https://doi.org/10.1021/acsami.1c10662

Rajendran, S. P., & Sengodan, K. (2017). *Synthesis and Characterization of Zinc Oxide and Iron Oxide Nanoparticles Using Sesbania grandiflora Leaf Extract as Reducing Agent*. *2017*.

Rane, A. V., Kanny, K., Abitha, V. K., & Thomas, S. (2018). Methods for Synthesis of Nanoparticles and Fabrication of Nanocomposites. In *Synthesis of Inorganic Nanomaterials*. Elsevier Ltd. https://doi.org/10.1016/b978-0-08-101975-7.00005-1

Razmavar, S., Abdulla, M. A., Ismail, S. B., & Hassandarvish, P. (2014). Antibacterial activity of leaf extracts of Baeckea frutescens against methicillin-resistant Staphylococcus aureus. *BioMed Research International*, *2014*. https://doi.org/10.1155/2014/521287

Rihayat, T., Salim, S., Arlina, A., Fona, Z., Jalal, R., Alam, P. N., Zaimahwati, Z., Sami, M., Syarif, J., & Juhan, N. (2018). Determination of CEC value (Cation Exchange Capacity) of Bentonites from North Aceh and Bener Meriah, Aceh Province, Indonesia using three methods. *IOP Conference Series: Materials Science and Engineering*, *334*(1). https://doi.org/10.1088/1757-899X/334/1/012054

Roig, A. (2018a). Nanotechnology Governance: from Risk Regulation to Informal Platforms. *NanoEthics*, *12*(2), 115–121. https://doi.org/10.1007/s11569-018-0321-1

Roig, A. (2018b). Nanotechnology Governance: from Risk Regulation to Informal Platforms. *NanoEthics*, *12*(2), 115–121. https://doi.org/10.1007/s11569-018-0321-1

Roshanfekr Rad, L., & Anbia, M. (2021). Zeolite-based composites for the adsorption of toxic matters from water: A review. *Journal of Environmental Chemical Engineering*, *9*(5), 106088. https://doi.org/10.1016/j.jece.2021.106088

Roy, A., Bulut, O., Some, S., Mandal, A. K., & Yilmaz, M. D. (2019). Green synthesis of silver nanoparticles: Biomolecule-nanoparticle organizations targeting antimicrobial

activity. *RSC Advances*, *9*(5), 2673–2702. https://doi.org/10.1039/c8ra08982e

Sabaruddin, F. A., Tahir, P. M., Sapuan, S. M., Ilyas, R. A., Lee, S. H., Abdan, K., Mazlan, N., Roseley, A. S. M., & Khalil Hps, A. (2021). The effects of unbleached and bleached nanocellulose on the thermal and flammability of polypropylene-reinforced kenaf core hybrid polymer bionanocomposites. *Polymers*, *13*(1), 1–19. https://doi.org/10.3390/polym13010116

Sánchez-López, E., Gomes, D., Esteruelas, G., Bonilla, L., Lopez-Machado, A. L., Galindo, R., Cano, A., Espina, M., Ettcheto, M., Camins, A., Silva, A. M., Durazzo, A., Santini, A., Garcia, M. L., & Souto, E. B. (2020). Metal-based nanoparticles as antimicrobial agents: An overview. *Nanomaterials*, *10*(2), 1–39. https://doi.org/10.3390/nano10020292

Santhosh, C., Velmurugan, V., Jacob, G., Jeong, S. K., Grace, A. N., & Bhatnagar, A. (2016). Role of nanomaterials in water treatment applications: A review. In *Chemical Engineering Journal* (Vol. 306, pp. 1116–1137). Elsevier B.V. https://doi.org/10.1016/j.cej.2016.08.053

Saravanakkumar, D., Sivaranjani, S., Kaviyarasu, K., Ayeshamariam, A., Ravikumar, B., Pandiarajan, S., Veeralakshmi, C., Jayachandran, M., & Maaza, M. (2018). Synthesis and characterization of ZnO-CuO nanocomposites powder by modified perfume spray pyrolysis method and its antimicrobial investigation. *Journal of Semiconductors*, *39*(3). https://doi.org/10.1088/1674-4926/39/3/033001

Shah, L. A., Khattak, N. S., Valenzuela, M. G. S., Manan, A., & Valenzuela Díaz, F. R. (2013). Preparation and characterization of purified Na-activated bentonite from Karak (Pakistan) for pharmaceutical use. *Clay Minerals*, *48*(4), 595–603. https://doi.org/10.1180/claymin.2013.048.4.03

Shaikh, J. R., & Patil, M. (2020). Qualitative tests for preliminary phytochemical screening: An overview. *International Journal of Chemical Studies*, *8*(2), 603–608. https://doi.org/10.22271/chemi.2020.v8.i2i.8834

Shameli, K., Ahmad, M. Bin, Shabanzadeh, P., Al-Mulla, E. A. J., Zamanian, A., Abdollahi, Y., Jazayeri, S. D., Eili, M., Jalilian, F. A., & Haroun, R. Z. (2014). Effect of Curcuma longa tuber powder extract on size of silver nanoparticles prepared by green method. *Research on Chemical Intermediates*, *40*(3), 1313–1325. https://doi.org/10.1007/s11164-013-1040-4

Shao, W., Liu, X., Min, H., Dong, G., Feng, Q., & Zuo, S. (2015). Preparation, characterization, and antibacterial activity of silver nanoparticle-decorated graphene oxide nanocomposite. *ACS Applied Materials and Interfaces*, *7*(12), 6966–6973. https://doi.org/10.1021/acsami.5b00937

Singh, M., Goyal, M., & Devlal, K. (2018). Size and shape effects on the band gap of semiconductor compound nanomaterials. *Journal of Taibah University for Science*, *12*(4), 470–475. https://doi.org/10.1080/16583655.2018.1473946

Singh, V., & Kumar, R. (2017). Study of Phytochemical Analysis and Antioxidant Activity of Allium sativum of Bundelkhand Region. *International Journal of Life-Sciences Scientific Research*, *3*(6), 1451–1458. https://doi.org/10.21276/ijlssr.2017.3.6.4

Slavin, Y. N., Asnis, J., Häfeli, U. O., & Bach, H. (2017). Metal nanoparticles: Understanding the mechanisms behind antibacterial activity. *Journal of Nanobiotechnology*, *15*(1), 1–20. https://doi.org/10.1186/s12951-017-0308-z

Srasra, E., & Bekri-Abbes, I. (2020). Bentonite Clays for Therapeutic Purposes and Biomaterial Design. *Current Pharmaceutical Design*, *26*(6), 642–649. https://doi.org/10.2174/1381612826666200203144034

Suresh, J., Pradheesh, G., Alexramani, V., Sundrarajan, M., & Hong, S. I. (2018). Green synthesis and characterization of zinc oxide nanoparticle using insulin plant (Costus pictus D. Don) and investigation of its antimicrobial as well as anticancer activities. *Advances in Natural Sciences: Nanoscience and Nanotechnology*, *9*(1). https://doi.org/10.1088/2043-6254/aaa6f1

Thi Lan Huong, V., & Nguyen, N. T. (2019). Green synthesis, characterization and antibacterial activity of silver nanoparticles using Sapindus mukorossi fruit pericarp extract. *Materials Today: Proceedings*, *42*(xxxx), 88–93. https://doi.org/10.1016/j.matpr.2020.10.015

Tobaldi, D. M., Piccirillo, C., Pullar, R. C., Gualtieri, A. F., Seabra, M. P., Castro, P. M. L., & Labrincha, J. A. (2014). Silver-modified nano-titania as an antibacterial agent and photocatalyst. *Journal of Physical Chemistry C*, *118*(9), 4751–4766. https://doi.org/10.1021/jp411997k

Us, S., Munk, K., Abdullahi, S. S., Güner, S., Koseoglu, Y., & Murtala, I. (2016). *S ı mple Method For The Determ ı nat ı on of Band Gap of a Nanopowdered Sımpl e Method For*

The Determ ınatıon o f Band Gap of a Nanopowdered Sample Usıng Kubelka Munk Theory. *August*.

Vijayakumar, M., Priya, K., Nancy, F. T., Noorlidah, A., & Ahmed, A. B. A. (2013). Biosynthesis, characterisation and anti-bacterial effect of plant-mediated silver nanoparticles using Artemisia nilagirica. *Industrial Crops and Products*, *41*(1), 235–240. https://doi.org/10.1016/j.indcrop.2012.04.017

Wei, J., & Gencturk, B. (2019). Hydration of ternary Portland cement blends containing metakaolin and sodium bentonite. *Cement and Concrete Research*, *123*(May), 105772. https://doi.org/10.1016/j.cemconres.2019.05.017

Weldegebrieal, G. K. (2020). Synthesis method, antibacterial and photocatalytic activity of ZnO nanoparticles for azo dyes in wastewater treatment: A review. *Inorganic Chemistry Communications*, *120*(July), 108140. https://doi.org/10.1016/j.inoche.2020.108140

Wu, T. S., Wang, K. X., Li, G. D., Sun, S. Y., Sun, J., & Chen, J. S. (2010). Montmorillonite-Supported Ag/TiO2 nanoparticles: An efficient visible-Light bacteria photodegradation material. *ACS Applied Materials and Interfaces*, *2*(2), 544–550. https://doi.org/10.1021/am900743d

Xiao, X., Wu, Z. C., & Chou, K. C. (2011). A multi-label classifier for predicting the subcellular localization of gram-negative bacterial proteins with both single and multiple sites. *PLoS ONE*, *6*(6). https://doi.org/10.1371/journal.pone.0020592

Yin, I. X., Zhang, J., Zhao, I. S., Mei, M. L., Li, Q., & Chu, C. H. (2020). The antibacterial mechanism of silver nanoparticles and its application in dentistry. *International Journal of Nanomedicine*, *15*, 2555–2562. https://doi.org/10.2147/IJN.S246764

Yunusov, K. E., Sarymsakov, A. A., Jalilov, J. Z. o. g. l., & Atakhanov, A. A. o. g. l. (2021). Physicochemical properties and antimicrobial activity of nanocomposite films based on carboxymethylcellulose and silver nanoparticles. *Polymers for Advanced Technologies*, *32*(4), 1822–1830. https://doi.org/10.1002/pat.5223

Yuvakkumar, R., Suresh, J., Saravanakumar, B., Joseph Nathanael, A., Hong, S. I., & Rajendran, V. (2015). Rambutan peels promoted biomimetic synthesis of bioinspired zinc oxide nanochains for biomedical applications. *Spectrochimica Acta - Part A: Molecular and Biomolecular Spectroscopy*, *137*, 250–258. https://doi.org/10.1016/j.saa.2014.08.022

Zaher MS, A., Wahab SM, A., MH, T., & AM, M. (2018). Sorption Characteristics of Iron,

Fluoride and Phosphate from Wastewater of Phosphate Fertilizer Plant using Natural Sodium Bentonite. *Journal of Membrane Science & Technology*, *08*(02). https://doi.org/10.4172/2155-9589.1000186

APPENDIX

Fig B1: Photos show antibacterial test process

PUBLICATION

1) Girma A (2022). A Review on Ag/Bentonite and ZnO/Bentonite Nanocomposite: Synthesis and their Applications.

   Journal of Equity in Science and sustainable Development (JESSD)

   (Accepted)

2) Recent advance and Future Perspective of 2D MXene for Energy storage: mini review

   Journal of Nanoscience and Nanometrology

   (Under Review)